Synthesis and characterization of Lanthanide Aluminotungstates and Rhenium Polyoxometalates: Potential Application in Molecular Information Storage Devices

By

Fang Bian

A dissertation submitted to the graduate Faculty in Chemistry in partial fulfillment of the requirements for the degree of Doctor of Philosophy, The City University of New York

2011

This manuscript has been read and accepted for the Graduate Faculty in Chemistry in satisfaction of the dissertation requirement for the degree of Doctor of Philosophy.

Professor Lynn C. Francesconi

_____

_____ _____

Date **Chair of Examining Committee**

Professor Mahesh K. Lakshman

_____

_____ _____

Date **Executive Officer**

Professor Klaus Grohmann

_____

Professor Charles M. Drain

_____

Professor Harry D. Gafney

_____

Supervisory Committee

The City University of New York

Abstract

Synthesis, speciation, and application of Polyoxometalates: Redox Molecular Information Storage Device Pre-research and Rhenium Chemistry

By

Fang Bian

Adviser: Professor Lynn C. Francesconi

Polyoxometalates (abbreviated as POMs) are metal-oxide clusters with frameworks built from group 5 or 6 transition metals linked by shared oxide ions. The Keggin structure is one of the most famous structural forms of POMs. Keggin anions have a general formula of $[XM_{12}O_{40}]^{n-}$, where X is a p-block atom and M is a transition metal atom such as W or Mo. Upon removal of one MO^{4+} unit from the Keggin anion, the monovacant structure $[XM_{11}O_{39}]^{n-}$ is formed. Those POMs that have lost one or more metal center are called lacunary POMs, which are very nice building blocks for the fabrication of coordination polymers. My research focuses on two facets of POM chemistry: 1) Lanthanide chemistry of aluminum tungstate monovacant Keggin and 2) Rhenium chemistry of aluminum tungstate Keggin and Wells-Dawson POM α_1-$P_2W_{17}O_{61}$.

In lanthanide POM research area, we obtained the following results:

1) The starting material aluminum tungstate monovacant Keggin α-$K_9AlW_{12}O_{39}$ was synthesized. Its single crystal was firstly identified by multinuclear NMR and X-ray crystallography. Its redox properties on the nano-scale solid state were determined by Conducting Electrostatic Force Mode (EFM) probes. It is well known that for POMs, a

number of varies redox states are normally stable and reversible. Thus we estimated that POMs can potentially be used in molecular information storage applications, which we refer to as “redox disk drives”.

2) Eight lanthanide aluminum tungstate Keggin complexes were synthesized. In their molecular structures (identified by multinuclear NMR and X-ray crystallography), each α-$AlW_{11}O_{39}$ is connected by lanthanide (III) cations to form 1D and 2D networks. All $AlW_{11}O_{39}$ Keggin POMs are regularly aligning on a flat plane. Microscopic data also verified that there is layer-by-layer morphology in this series of compounds.

Overall, we postulate that aluminum tungstate Keggin POMs are a very promising materials for making future information storage device because they have several stable redox states and can be reduced by adding voltage in solid state, The Keggin POMs can be regularly aligned on a flat plane,

3) In rhenium chemistry research area, we successfully synthesized rhenium complexes of the $[\alpha_1\text{-}P_2W_{17}O_{61}]^{10-}$ and α-$K_9AlW_{13}O_{39}$. The structure info of $[Re^{V}O(\alpha_1\text{-}P_2W_{17}O_{61})]^{7-}$ was identified by multinuclear NMR and X-ray crystallography. The cyclic-voltammetry of $[Re^{V}O(\alpha_1\text{-}P_2W_{17}O_{61})]^{7-}$ has also been measured and compared to the $[Re^{V}O(\alpha_2\text{-}P_2W_{17}O_{61})]^{7-}$ isomer. A rhenium derivative of α-$K_9AlW_{11}O_{39}$ also has been synthesized. Multinuclear NMR gives structure information. After oxidation in air, this compound can aggregate to form insoluble nanoparticles.

To MY FAMILY

AND

TO MY GRANDFATHER

Acknowledgments

It is my pleasure to thank professors, colleagues and friends who made this research possible.

First of all, I would like to gratefully appreciate my PhD advisor, Professor Lynn Francesconi. She spent a lot of time giving me advice, supervising me solve problems, and taught me a good working style and ways to think. Even though I may not work in chemistry in my future career, a good working style and thinking method will still benefit me a lot.

I want to thank my committee members, Professor Michael Drain, Professor Klaus Grohmann and Professor Harry Gafney for giving me good advice and ideas in my committee meetings. In addition, I want to specially thank Professor Klaus Grohmann help me transfer from City College to Hunter College in 2006, offer me financial aid and help me in teaching. I also want to appreciate my previous advisor Professor Ira Weinstock who encouraged med and introduced polyoxometalate chemistry to me.

I would like to thank my coworkers Dr. Hanying Bai and Dr. Benjamin Burton-Pye. Both of you helped me finish some very important work in this project. I would also like to thank Dr. Louis Todaro, Dr. Jianrong Li, Dr. Matthew Devany and Dr. Jorge Morales helping me handle the characterization work. I acknowledge the following colleagues who gave me much help during my PhD study: Dr. Xiaoping Zhu, Yijia Yang, Anjia Luona, Menglu Shi, Wei Su, Junyi Wang, Amit Aggarwal, Jacopo Samson, Professor Roberto Sanchez-Delgado and Minfeng Fang. I also thank Kristina Fabijanic, Sam Groveman, and Benjamin Reed helping me to improve my dissertation thesis.

I greatly appreciate my coworkers in class teaching, and all CUNY Chinese Students and Scholars Association members.

I would like to give special thanks to Professor Yuh-kang Pan and Dr. Yayin Fang. Without your help and encourage from time to time, I would not have any chance to finish my PhD degree. Thank you.

Fang Bian

March 23, 2011

Table of Contents

Chapter 1. Overview

Chapter 2. Tungstoaluminates Keggin: The Syntheses, Single Crystal Structure and Redox in EFM

List of Figures

Chapter 1

Chapter 2

Chapter 3

Chapter 4

Chapter 5

List of Tables

Chapter 2

Chapter 3

Chapter 4

Chapter 5

Chapter 1 Overview

1.1 Current Information Storage Technology Review

1.1.2 Hard Disk Drive

A hard disk drive is a typical example of a modern information storage device. The development of the hard-drive industry has been very fast during the past 50 years. The growth of data density is about twice as compared to Moore's law for semiconductor technology. [1]

In a typical hard disk drive, information is stored on a disk plate, which can be read and written by a read/write head. The movement of the motor and actuator can easily locate where the information is being stored on the disk plate. The higher the spin speed of the motor, the faster the read/write speed is. The most important parts on a hard drive are the magnetic heads and plates. On the surface of the hard-drive plate, there are billions of small alloy magnets. Currently the size of each magnetic particle is about 10 nm. There are hundreds of magnet particles that form a particular record region. In each record region, the magnetic spin orientations of the magnetic particles are the same. Magnetic orientations of each are either represented by a one or a zero. The size of a record region is around 300 nm or less in width.

The principle of the reading and writing principle is shown on Figure **1-1**. When the hard-drive is writing, the electro-magnet on the magnetic head induces a local magnetic moment on the record region. The local magnetic moment will change the magnetic spin orientations of the magnetic particles in the record region. On the other hand, reading

means that the GMR (Giant magneto-Resistive) sensor on the magnetic head measures the magnetization of the record region.

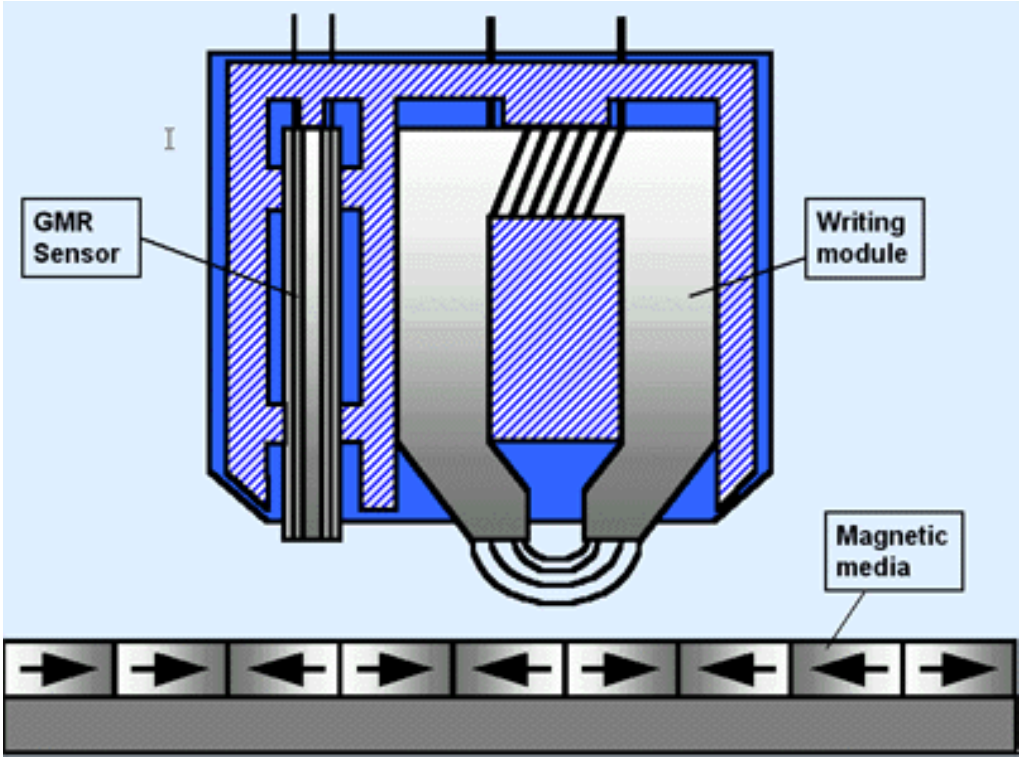

Figure **1-1**: Principle of how hard drive working
(From http://www.spmtips.com/bibliography/data_storage/)

1.1.2 Optical Disc

The optical disc is another important data storage device. The first optical disc, or a compact disc, was originally developed for the music industry in 1982 and is currently still utilized in standard audio media. Later, compact discs became data storage devices for computer.

The structure of optical discs is not complicated. Data is encoded and stored in the form of small pits and bumps (track pitch) in the data layer, which is often made from aluminum or some other metal. The data layer is applied on the surface of a 12mm thick plastic disc and is protected by a film of lacquer.

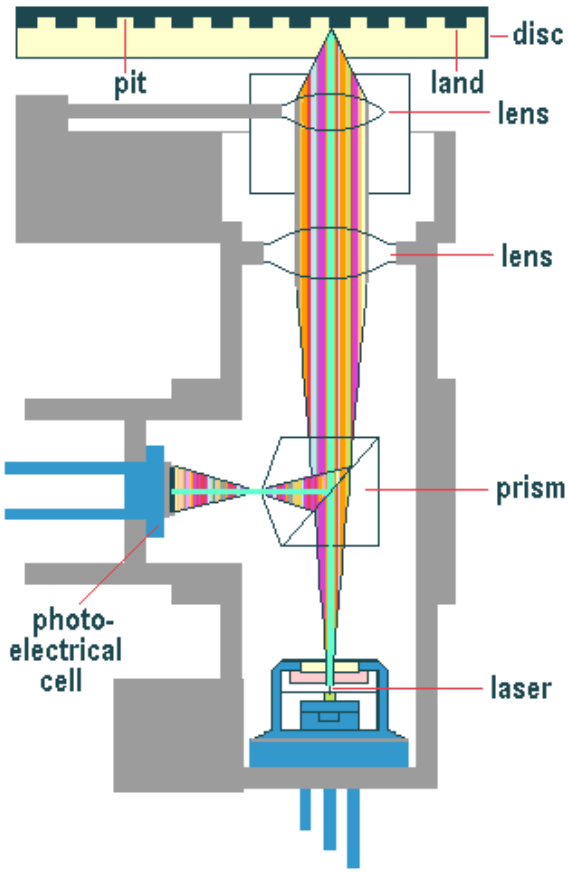

Figure **1-2**. Principle of Reading optical disk
http://www.pctechguide.com/32CD-ROM_Operation.htm

The principle of the reading process is shown in Figure **1-2**. A laser beam from the laser head will cross the prism and lens and hit the pits and bumps on the disk. The laser beam is then reflected back to the prism, and the prism will send the laser to the photoelectrical cell, which will recognize the signals and change the optical signal to an electronic signal. The processor can then decode the data reading from the disc.

Currently the latest optical disc is a blue-ray disc, which can store 25GB (single layer) of data in a 12cm diameter disc. The size of the track pitch of a blue-ray disc is around 320 nm. Figure **1-3** shows the size differences of pits and bumps between CD and DVD data layers.

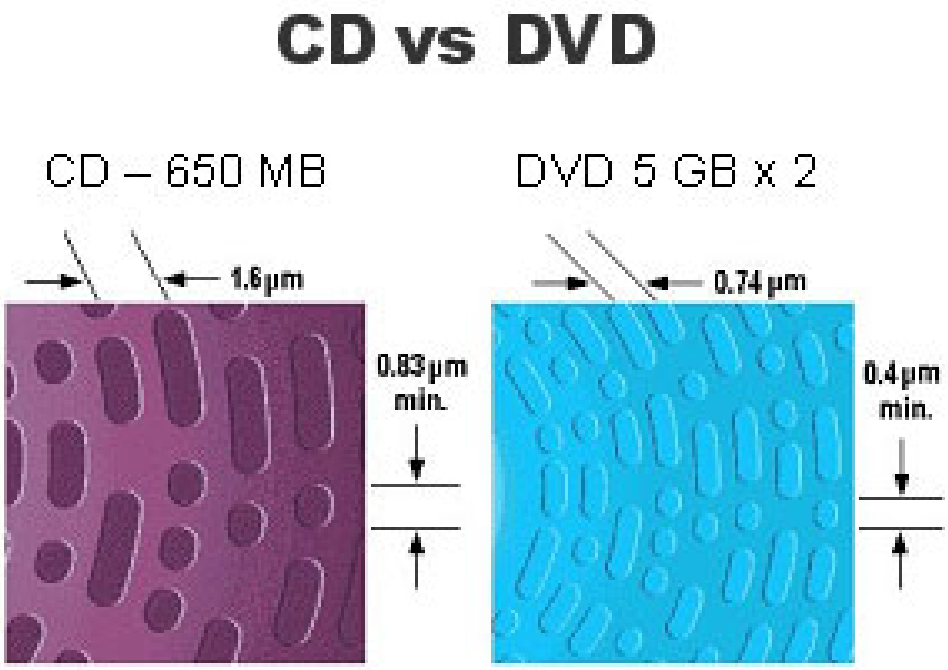

Figure **1-3**. Pits and bumps on the data layer
From http://www.williams-adv.com/tools/dvd-technology-review.php

1.2 The Bottleneck of current information storage system

The way to increase capacity of the hard-drive is to increase the data density of the plate and minimize the area of each record region. In addition, if we keep using the same magnetic particles and only reduce the size of the record region, the signal to noise ratio (SNR) will decrease because of the staggered packing of particles. In order to maintain the SNR and to increase the data density, we must decrease the magnetic particle size. However it is currently very difficult to make magnetic alloy particles of uniform size with diameter lower than 7 nm diameters.

A similar development occurred with respect to the optical disc area. As we described before, the latest optical disc is a 25 GB blue-ray disc and the size of the pits is around 320 nm. To increase the data volume to more than 100 GB, the laser beam becomes the bottleneck. Because of the limited diffraction, even if manufacturers could make the pits and bumps small enough; we still cannot concentrate the laser beam on the small area. To solve this problem, people have developed near-field optical microscopy technologies and thus, have manufactured the newest type optical disc with more than 100 GB per volume. However, the size of the pits and bumps becomes another bottleneck when we are talking about making optical discs with more than 100 GB volume.

Limited hard-drive storage space is becoming one of the most annoying bottlenecks in IT industry. In order to increase the density of information storage, high tech companies are trying their best to make really small magnetic particles from iron, iron oxide, or other magnetic materials. The key of increasing storage capacity is molecular information storage technology. Single molecular magnet may solve this problem and

increase storage capacity a lot. During the last 20 years, many single-molecule magnets have been discovered. As George Christou said, “We could get 30,000 billion of single-molecule magnets into one square centimeter, and thus a storage density of 30,000 billion bits (or 30 terabits) is feasible. This is 10,000 times greater than the storage ability of current hard-drive.” [1]

1.3 Molecular Information Storage: Single Molecule Magnet (SMM)

With the increasing development of technology, there have been devices synthesized on the nano or molecular level. [3]-[8]

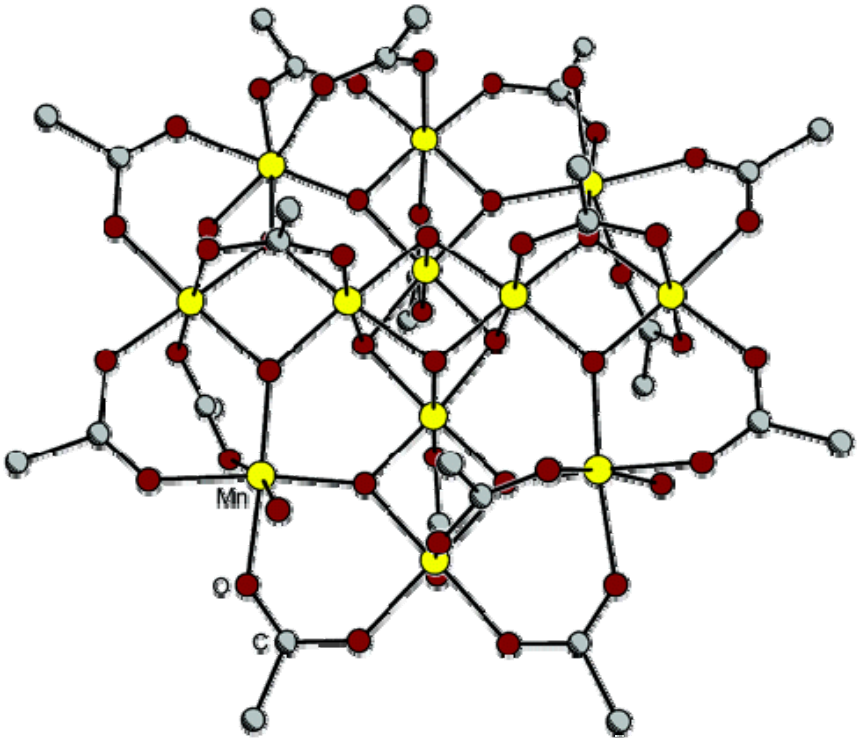

Figure.**1-4**. Molecular structure of the first single molecule magnets: Mn_{12} cluster. This Figure was abstracted from reference [9].

In order to find small magnetic particles and use them to store information, more and more scientists are conducting research in their labs, hoping to make these single molecular magnets. The unit of data density is GB per square inch. A single molecular magnet with 1 nm diameter can easily get 200,000 GB per square inch area density, which is essentially impossible to achieve, simply through the use of alloy magnet particles that we currently using. The $Mn_{12}O_{12}(CH_3COO)_{16}(H_2O)_4$ complex was the first single-molecule magnet to be synthesized as early as 1980 [9] and was reported as single molecule magnet in 1991 [10]. David Hendrickson first coined the term of "single-molecule magnet" in 1996 [11]. Since then, many chemists are trying to make more SMM [12]. Unfortunately, until now, the earlier version works best. In other words, $Mn_{12}O_{12}(CH_3COO)_{16}(H_2O)_4$ is still the most effective single molecule magnet, because of its magnitude of the spin-reversal barrier being around $50cm^{-1}$. [11]

The structure of the first SMM of the $Mn_{12}O_{12}(CH_3COO)_{16}(H_2O)_4$ is shown in Figure **1-4**. Yellow circles indicate Manganese atoms, the red circles indicate oxygen atoms and the grey circle indicate carbon atoms. The molecule is disc-shaped with 1 nm diameter and 0.5 nm thicknesses. In the center of the disc, there is a $Mn^{IV}{}_4O_4$ cubane unit surrounded by a ring of eight oxo- and acetato- linked Mn^{III} centers.

Due to the ferromagnetic coupling between the paramagnetic metal centers, SMMs have a large ground state spin value. Another important property of SMMs is that they have a negative value for the anisotropy of the zero field splitting.[13] To describe the magnetic properties of this magnetic material, scientists often imploy the μ_{eff} vs T plot. Because the molecule structures of SMMs are very complicated, and theoretical model are not simple to build, scientists use energy level diagrams instead. Figure 1-4 shows a

plot of the potential energy of an S = 10 molecule exhibiting easy-axis type anisotropy (negative D value) as its magnetization (magnetic moment) vector changes from spin "up" (M_s = -10) to spin "down" (M_s = +10) via intermediate orientations. [14] From Figure **1-5** we also can see that the Mn_{12} cluster has the large magnetic spin reversal potential energy barrier. Actually, the Mn_{12} cluster has the highest energy barrier value of -50 cm^{-1}.

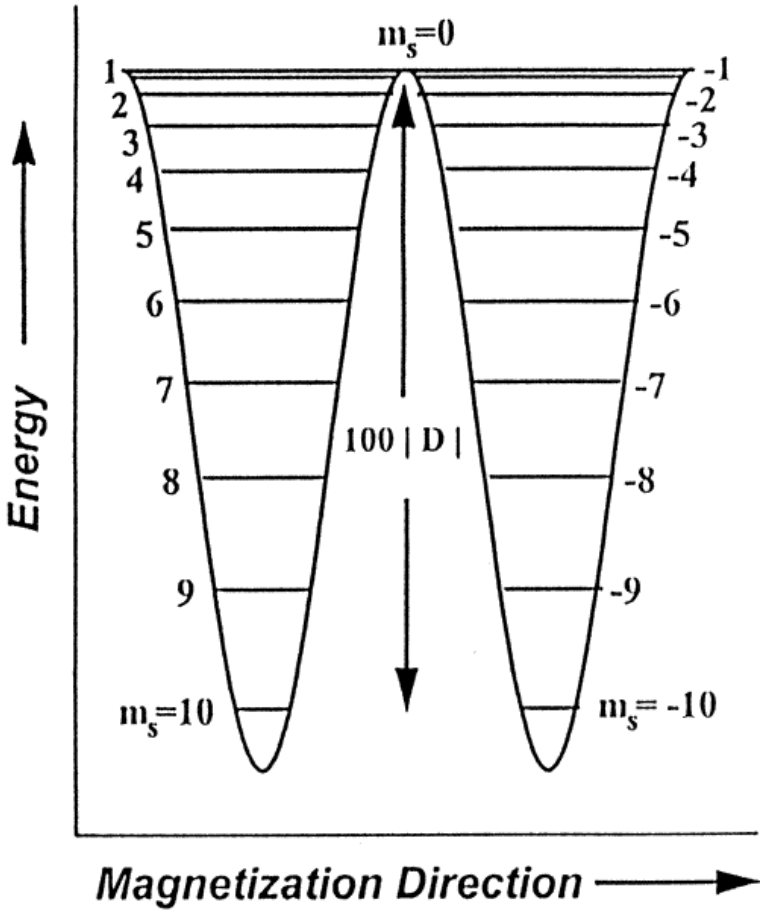

Figure **1-5**. Double-well potential energy plot for an S = 10 molecule with axial symmetry and easy-axis type anisotropy. The energy separation between the $M_s = \pm 10$ and $M_s = 0$ orientations of the magnetization is given by $S^2|D|$. This Figure was abstracted from reference [14].

In comparison to with alloy particles, there are several advantages of SMMs. The sizes of magnet molecules are the same, whereas it is impossible to make nano-size alloy particles that are all in exactly same size. Second, most of the single-molecule magnets are able to dissolve in organic solvents, which is very important in making a monolayer film and subsequently coating on the disk surface with the film. However, we still need to wait for a couple of years for the utilization of single-molecule magnets to be realized, because currently there is only limited number of SMMs with ferromagnetic properties above room temperature.

For a SMM molecule, when the temperature is high, the magnetic moment will change very quickly between the two states, which is common paramagnetic behavior. If the temperature is low enough, magnetic moment will be frozen at certain direction. This low temperature is called the blocking temperature. [15] Currently the blocking temperature of SMMs is less than 10K, which makes it impossible to be used as a real data storage device. This low blocking temperature (T_B) is the disadvantage that keeps SMMs away from industry.

1.4 Polyoxometalates and their potential application in information storage devices

Polyoxometalates (abbreviated POMs) are clusters with frameworks built from the transition metals found in groups V or VI with oxide ions linkages. Polyoxometalates have great potential as catalysts and in medicinal applications. [16] Because plenary polyoxometalates can lose one or more metal centers under different pHs, they are ideal

building blocks for the fabrication of coordination polymers. This is why supramolecular materials are another important application area of polyoxometalates. Many polyoxometalate coordination polymers that have been reported are developed by hydrothermal syntheses techniques. However, it is important to note that a few polyoxometalate polymers have been made at room temperature and low pressure conditions.[17], [18]

Because of the metal oxide surfaces and diversity in geometric topology, metal substituted derivatives of polyoxometalate could prove to be interesting in possible applications such as luminescence and through their magnetic properties. [17] In this project, we concentrate on the reaction between mono vacant Keggin polyoxometalates and lanthanide ions.

The Keggin structure is one of the most famous structural forms of polyoxometalates. α–Keggin anions have a general formula of $[XM_{12}O_{40}]^{n-}$, where X is a p-block atom and M is a transition metal atom such as W or Mo addenda atom. After the removal of one addenda atom, the α–Keggin anion becomes a monovacant Keggin structure $[XM_{11}O_{39}]^{n-}$. Monovacant tungstosilicate α-Keggin $[SiW_{11}O_{39}]^{8-}$ and its metal substituted derivatives are the first monovacant Keggin lanthanide derivatives that have been studied. [17] M.T. Pope reported two crystal structures of α-Keggin $[SiW_{11}O_{39}]^{8-}$ lanthanide substituted compounds as polymer chain structure. [19] Other dimensional structures of α-Keggin $[SiW_{11}O_{39}]^{8-}$ lanthanide derivatives have also been studied. [20], [21] Magnetic properties of α-Keggin $[SiW_{11}O_{39}]^{8-}$ lanthanide derivatives have been studied in 2006. [22] Recently α-Keggin $[GeW_{11}O_{39}]^{8-}$ lanthanide derivatives were reported as possessing similar

structural and magnetic properties as the α-Keggin $[SiW_{11}O_{39}]^{8-}$ lanthanide derivatives. [23]

Weinstock et al. reported the analogue of $[SiW_{11}O_{39}]^{8-}$ Keggin, α- $[AlW_{12}O_{40}]^{5-}$, and monovacant Keggin α- $[AlW_{11}O_{39}]^{9-}$. They also reported their metal derivatives α- $[Al(AlOH_2)W_{11}O_{39}]^{6-}$, α- $[AlCo^{III}W_{11}O_{39}]^{6-}$, α- $[AlMn^{II}W_{11}O_{39}]^{7-}$, α- $[AlMn^{III}W_{11}O_{39}]^{6-}$ and α- $[AlV^{V}W_{11}O_{40}]^{6-}$. In the crystal structure of α- $[AlW_{12}O_{40}]^{5-}$ derivatives, each addendum-atom site was assigned 1/12 transition metal character and 11/12 W character. [24]

To serve as binary memory unit, the material of choice has to be able to quickly transfer between two or more states. As a well-known reservoir of electrons, POM's possess redox state that are normally stable and reversible, we envision that, due to their reversible redox properties, POMs can potentially be used in molecular information storage application, which we refer to as redox disk drives.

1.5 The self-assembly method of creating molecules evenly aligned on a plane: Coordination Polymer

It is very difficult to regularly align nanoparticles on a plane. In a traditional hard disk drive plate, hundreds of nanoparticles represent a binary digit so that there is no need to perfectly align nanoparticles absolutely evenly and make all nanoparticles 100% identical. Because single molecule of POMs are 1 nm in diameter, we do not need to worry about POM's size and shape deviation at all. However, we have to make POMs perfectly evenly spread out on the plane if we want to use a single POM molecule to represent a binary digit. If we can not figure out a way of spreading them out evenly,

reading/writing data from POM redox drive will be impossible because the reading/writing head will never locate its positioning action. Here, we are giving a typical example: the hexafluorophosphate salt of the reduced amorphous cluster $[Mn_{12}O_{12}(bet)_{16}(EtOH)_4]^{14+}$ (bet = betaine = $^{+}N(CH_3)_3$-CH_2-COO-) monolayer is shown in Figure **1-6**. The cluster molecules in the amorphous monolayer are distributed in a very random orientation so that it is impossible to use in a data storage application.[25]

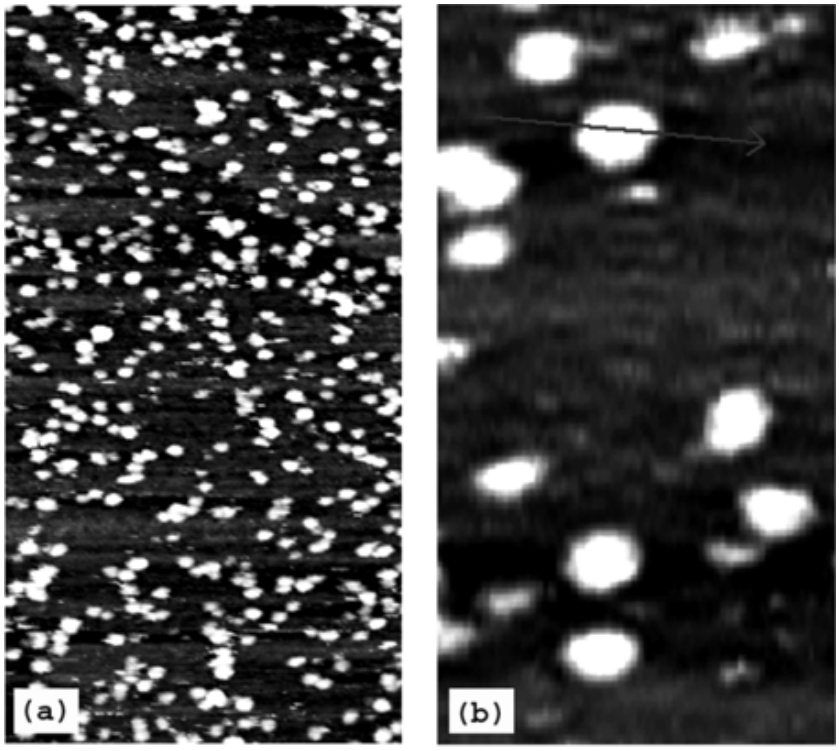

Figure **1-6** Constant-current (30 pA and 2 V) STM images of $[Mn_{12}]^{14+}$ isolated molecules grafted onto a MES-functionalized Au(111) surface: 110 × 190 nm^2 (a); 23 × 42 nm^2 (b). This Figure was abstracted from reference [25].

In this research, we are introducing coordination polymer structures, which can help POMs form even alignment on a plane without any error. Coordination polymers are

inorganic supramolecular compounds containing networks of coordinated metal ions and ligands.[26]-[33] With repeating units of coordination complexes, coordination polymers are perfect self-assembly molecule storage models. Shown in Figure **1-7**, coordination polymers can be classified as one, two, or three dimensional according to the number of direction that repeating units extend to. A one dimensional coordination polymer extends in a straight line. A two-dimensional coordination polymer extends on a plane. A three-dimensional polymer has networks that extend in three dimensions. By carefully adjusting the ligand size, we can control the size of pores in the coordination polymer so as to intercalate guest into the porous coordination polymers.

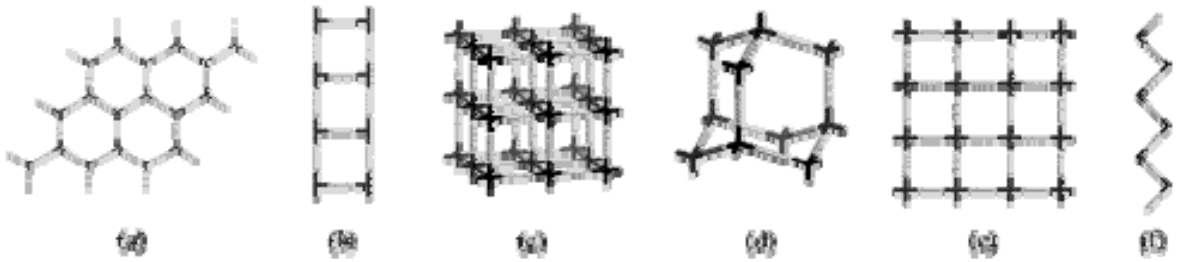

Figure **1-7**. Simple Network Architectures Structurally Characterized for Metal−Organic Polymers: (a) 2D Honeycomb, (b) 1D Ladder, (c) 3D Octahedral, (d) 3D Hexagonal Diamondoid, (e) 2D Square Grid, and (f) 1D Zigzag Chain. This Figure was abstracted from reference [34].

Resently, Kong et al. reported a series of polyoxometalates-based 2D coordination polymers recently. [35] This is the only article about such honeycomb-lava like 2D structure. One example is $\{[Cu(pz)_{1.5}]_4(SiW_{12}O_{40})\cdot 2H_2O\}_n$, a porous 2D coordination polymer with polyoxometalate $SiW_{12}O_{40}^{4-}$ in the void. The structure of $\{[Cu(pz)_{1.5}]_4(SiW_{12}O_{40})\cdot 2H_2O\}_n$ is shown on Figure **1-8**. Each unit of the 2D polymer

consists of four copper (I) cations, six pyrazine ligands, one $SiW_{12}O_{40}^{4-}$ anion, and two water molecules. There is one square void and two octagonal voids in each unit, which gives rise to it being called $4^1 8^2$ networks. The $SiW_{12}O_{40}^{4-}$ anion guest is located in the octagonal voids.

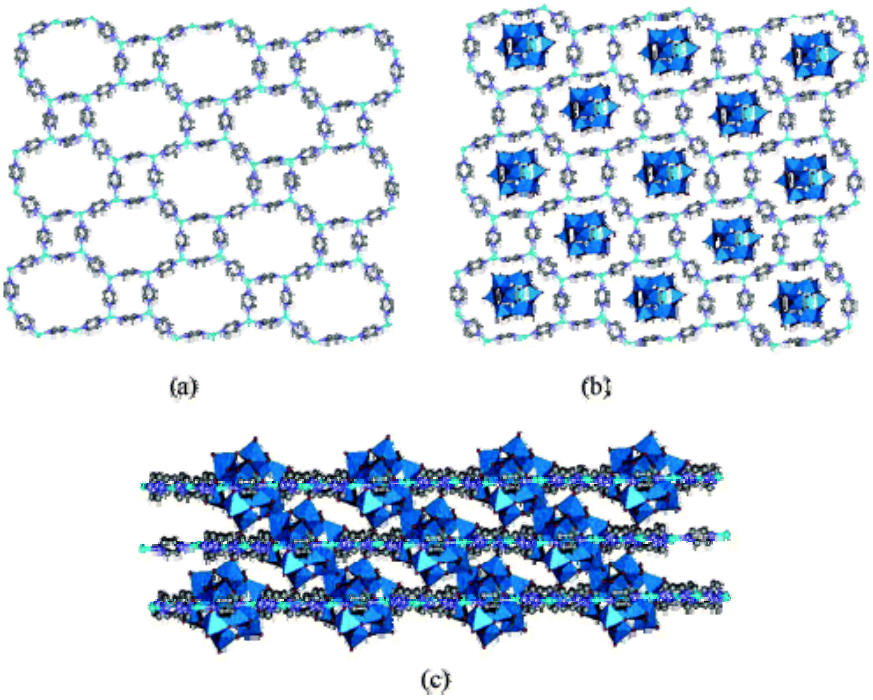

Figure **1-8** (a) Structure of the $4^1 8^2$ network of $[Cu(pz)_{1.5}]_n^{n+}$, (b) arrangement of the $SiW_{12}O_{40}^{4-}$ anion in the $4^1 8^2$ network, and (c) 3D structure of the cluster-based coordination polymer (Cu, cyan; O, red; W, blue; Si, gray; C, gray; N, Cambridge blue). This Figure was abstracted from reference [35].

There is another way of using coordination polymers to control POM alignment evenly on a plane. Instead of making a coordination polymer and introducing a guest into the pore on the coordination polymer, POMs can be used as a ligand connected by metal cations to form a one, two or three dimensional network. Our group published a

novel 2D POM polymer structure with Al^{3+} cation connectors, shown in Figure **1-9**. In this structure, all POM units are regularly aligning on the plane so that met the requirement of the information storage device very well. [36]

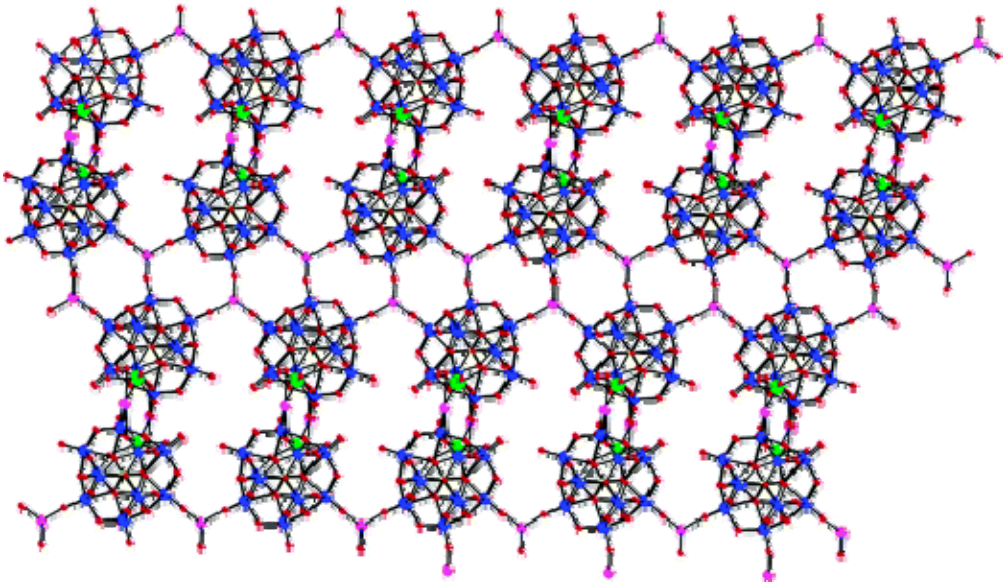

Figure **1-9** Packing diagram of $\{Eu(H_2O)_3(\alpha\text{-}2\text{-}P_2W_{17}O_{61})\}_2$, viewed along the *c* axis. Uncoordinated H_2O molecules have been removed for clarity. Legend: W, blue; O, red; Eu, green; P, yellow; Al, pink. This Figure was abstracted from reference [36].

1.6 Polyoxometalate (POM) Redox Chemistry on the nano scale

Traditionally POM redox chemistry has been studied in the solution phase. Kurth et al. studied how to reduce solid-state layer-by-layer POM in the past a few years. [37],[38]

Figure **1-10** showed how electrochemical reduction effect an ITO coated quartz sample. Before electrochemical reduction was done, a transparent film was obtained.

After ECR, 700nm absorption was seen. Based on this experiment, the film transparency can be controlled.

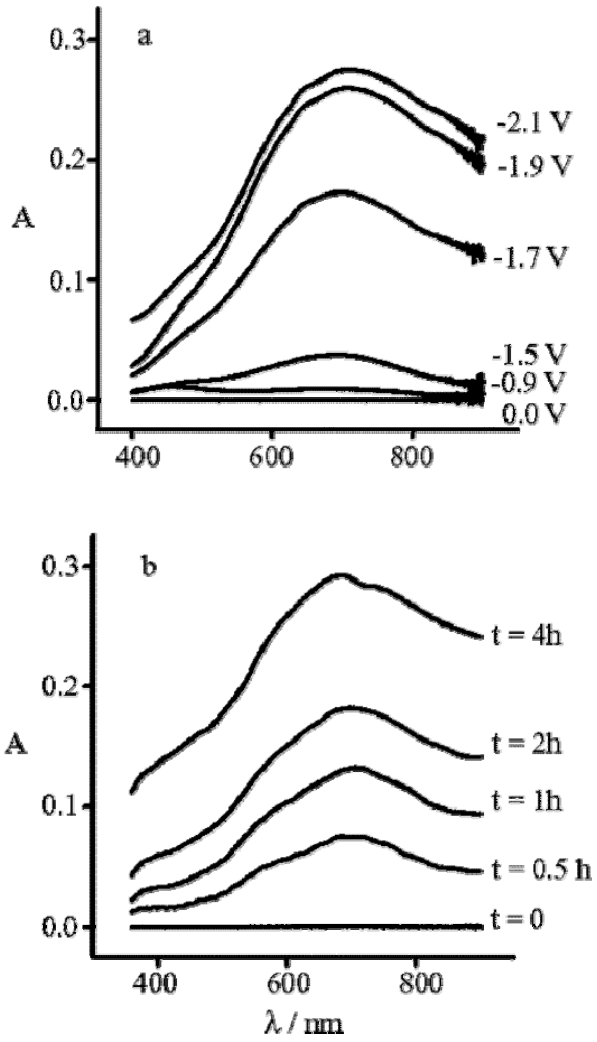

Figure **1-10** (a) UV−vis spectra of a PSS(P4VP/P-POM)$_{40}$ multilayer on an indium tin oxide (ITO)-coated quartz substrate before and after reduction. The transparency of the window is readily controlled by the applied potential. The six spectra are recorded at 0.0, −0.9, −1.5, −1.7, −1.9, and −2.1 V, giving rise to 0, 2, 15, 60, 94, and 100% coloration. (b) Time-dependent photochromic coloration of the multilayer. A low-intensity UV lamp was used to measure the spectra changes. After 4 h of irradiation, no further change in coloration is observed. This Figure was abstracted from reference [37].

1.7 Speciation Studies of polyoxometalates

We focus on studying on aluminum tungstate α-Keggin POM for two reasons: First, they have wonderful redox properties: Different redox states are stable and reversible. The POM can be reduced by multiple electrons and maintain structural integrity. In addition, these POMs are very nice building block for making self-assembly supermolecular coordination polymers.

In the study of the mono-vacant compound α-$K_9AlW_{11}O_{39}$, we successfully determined its single crystal structure, which is the first time that this had been done. The vacancy is delocalized so that it looks as though there are 12 tungstate atoms with 0.91 occupancy, but actually there are only 11 tungstate atoms. Water solvent units and POM units pack together and form a body centered cubic system. We studied α-$K_9AlW_{11}O_{39}$ POM's redox property on nano scale by using Atomic Force Microscopy (AFM) and Electronic Force Microscopy (EFM) imaging techniques.

In the study of lanthanide aluminum tungstate POM, we use a lanthanide as a building block to connect and regulate POMs on a two dimensional flat plane. We have synthesized eight new lanthanide Tungstoaluminate compounds, $H_6KY(\alpha\text{-}AlW_{11}O_{39})Cl(H_2O)_{20}$, **2,** $K_3Ln^{III}_2(\alpha\text{-}AlW_{11}O_{39})(H_2O)_{20}$ (Ln^{III} = La^{III} **3**, Ce^{III} **4**, Sm^{III} **5**, Gd^{III} **6**, Dy^{III} **7**, Lu^{III} **9**) and **8**, $H_{2.5}Dy^{III}_{2.5}(\alpha\text{-}AlW_{11}O_{39})Cl_{0.5}(H_2O)_{28.5}$**,** which have all been synthesized and characterized by IR spectroscopy, NMR spectroscopy and single-crystal X-ray diffraction. Because of the lanthanide contraction, the single-crystal structure of **3**, **4** and **5** show that each α-$AlW_{11}O_{39}$ is connected by Lanthanide (III) cations and, thus, formed a 2D network. The single-crystal structure of **6** and **7** showed that each $AlW_{11}O_{39}$ unit is connected by Lanthanide (III) cations and formed a 1D chain structure in two

different ways. We also studied Lanthanide Aluminum Tungstate POM's nanoscale layer-by-layer morphology by using Scanning Electron Microscopy (SEM) and Tunneling Electron Microscopy (TEM). After comparing microscopic d-spacing data to calculated d-spacing results, calculated from single crystal data, we confirmed that this data perfectly matched.

By studying rhenium derivatives of [α- $AlW_{11}O_{39}$] POM and α_1-$P_2W_{17}O_{61}$, we attempted to understand how the solution conditions, structural differences, and nano structures of the POM affect the speciation and stabilities of their rhenium complexes. The rhenium complex of the $[\alpha_1\text{-}P_2W_{17}O_{61}]^{10-}$ isomers are prepared and characterized by multinuclear NMR, single crystal structure, and preliminary electrochemical studies are reported. We also compared Rhenium $[\alpha_1\text{-}P_2W_{17}O_{61}]^{10-}$ complexes to rhenium $[\alpha_2\text{-}P_2W_{17}O_{61}]^{10-}$ complexes by comparing electrochemical properties. We prepared a rhenium complex of mono-vacant Keggin POM $[\alpha\text{-}AlW_{11}O_{39}]^{9-}$ and characterized it by multinuclear NMR, light scattering and transmission electron microscopy.

1.8 References

[1] R. Kurzweil**,** *Exponential Growth of Computing for 110 Years*, From http://www.kurzweilai.net/exponential-growth-of-computing

[2] Indiana University (**2000**, March 27). Several New Single-Molecule Magnets Discovered. *ScienceDaily*. Retrieved March 16, 2011, from http://www.sciencedaily.com/releases/2000/03/000327084104.htm

[3] B. Xu, X. Xiao, X. Yang, L. Zang, and N. Tao; *J. Am. Chem. Soc.*, **2005**, 127 (8), 2386–2387

[4] L. Brousseau, III, *J. Am. Chem. Soc.*, **2006**, 128 (35), pp 11346–11347

[5] P. Solomon and N. Lang, *ACS Nano*, **2008**, 2 (3), pp 435–440

[6] H. Li, X. Yan, G. Luo, R. Qin, Q. Liu, L. Yu, C. Xu, J. Zheng, J. Zhou, J. Lu, Z. Gao, S. Nagase, and W. Mei, *J. Phys. Chem. C*, **2010**, 114 (37), 15816–15822

[7] S. Klokishner, S. Ostrovsky, O. Reu and A. Palii, P. Tregenna-Piggott, T. Brock-Nannestad and J. Bendix, H. Mutka, *J. Phys. Chem. C*, **2009**, *113* (20), 8573–8582

[8] K. Stokbro, *J. Phys. Chem. C*, **2010**, 114 (48), 20461–20465

[9] T. Lis, *Acta Crystallogr.* **1980**, B36, 2042

[10] A. Caneschi, D. Gatteschi, R. Sessoli, A. Barra, L. Brunel, M. Guillot, *J. Am. Chem. Soc.*, **1991**, 113(15), 5873-5874.

[11] S. Aubin,.; M. Wemple; D. Adams,; H. Tsai; G. Christou; D. Hendrickson, *J. Am. Chem. Soc.*,**1996**, 118(33), 7746-7754.

[12] L., Beltran; J. Long, *Acc. Chem. Res.*, **2005**, 38(4); 325-334.

[13] S. Aubin, D. Hendrickson, S. Spagna, H. Eppley, R. Sager, H. Eppley, G.

Christou, *Chem. Commun.*, **1998**, (7),803-804

[14] M. Soler, P. Artus, K. Folting, J. Huffman, D. Hendrickson, G. Christou, *Inorg. Chem.*, **2001**, 40(**19**), 4902-4912.

[15] R. Sessoli, H. Tsai, A. Schake, S. Wang, J. Vincent, K. Folting, D. Gatteschi, G. Christou, D. Hendrickson, *J. Am. Chem. Soc.* **1993**, *115*, 1804

[16] M. Pope, A. Muller, *Polyoxometalates: From Platonic solid to Anti-Retroviral Activity*; Kluwer Academic Publishers: Dordrecht, The Nederlands, **1994**.

[17] M. Sadakane, M. Dickman, M. Pope, Angew. Chem. Int. Ed. **2000**, 39, No.16 2914

[18] P. Mialane, L. Lisnard, A. Mallard, J. Marrot, E. Antic-Fidancev, P. Aschehoug, D. Vivien, and F. Sécheresse, Inorg Chem. **2003**, 42, 2102-2108

[19] T. Yamase, M. Pope, *Polyoxometalate Chemistry for Nano-Composite Design*; Kluwer: Academic Publishers: Dordrecht, The Netherlands, **2002**

[20] R. Peacock and T. Weakley, *J. Chem. Soc. A***, 1971**, 1836 - 1839

[21] J. Wang, J. Zhao, X. Duan, and J. Niu, *Crystal Growth & Design*, **2006**, vol.6, No. 2, 507-513

[22] F. Li, L. Xu, Y. Wei, G. Gao, L. Fan, Z. Li, *Inorg Chim Acta,* 359, 3795

[23] J. Wang, X. Duan, X. Du, and J. Niu, *Crystal Growth & Design*, **2006**, vol6, No. 2, 2266-2270

[24] J. Cowan, A. Bailey, R. Heintz, B. Do, K. Hardcastle, C. Hill, and I. Weinstock, *Inorg. Chem.,* **40** (26), 6666 -6675, 2001

[25] E. Coronado, A. Forment-Aliaga, F. Romero, V. Corradini, R. Biagi, V. Renzi, A. Gambardella, U. Pennino, *Inorg. Chem.*; (Communication); **2005**; 44(22); 7693-7695.

[26] R. Robson; B. Abrahams, S. Batten, R. Gable, B. Hoskins, J. Liu, *ACS Symp. Ser.* **1992**, *499*, 256−273.

[27] B. Abrahams, B, Hoskins, R. Robson, *J. Am. Chem. Soc.* **1991**, *113*, 3606−3607.

[28] M. Fujita, Y. Kwon, S. Washizu, K. Ogura, *Am. Chem. Soc.* **1994**, *116*, 1151−1152.

[29] B. Abrahams, B. Hoskins, J. Liu, R. Robson, *J. Am. Chem. Soc.* **1991**, *113*, 3045−3051.

[30] S. Batten, B. Hoskins, R. Robson, *Chem. Commun.* **1991**, 445−447.

[31] R. Gable, B. Hoskins, R. Robson, *Chem. Commun.* **1990**, 762−763.

[32] B. Hoskins, R. Robson, *J. Am. Chem. Soc.* **1990**, *112*, 1546−1554.

[33] B. Abrahams, B. Hoskins, R. Robson, *Chem. Commun.* **1990**, 60−61.

[34] B. Moulton and M. Zaworotko, *Chem. Rev.*, **2001**, 101 (**6**), 1629–1658

[35] X. Kong, Y. Ren, P. Zheng, Y. Long, L. Long, R. Huang, L. Zheng, *Inorg. Chem.*; **2006**; 45(26); 10702-10711.

[36] C. Zhang, R. Howell, K. Scotland, F. Perez, L. Todaro, and L. Francesconi, *Inorg. Chem.*, **2004**, 43 (24), pp 7691–7701

[37] S. Liu, H. Möhwald, D. Volkmer, and D. Kurth, *Langmuir*, **2006**, 22 (5), 1949–1951

[38] S. Liu and Z. Tang, *Nanotoday* Volume 5, Issue 4, August **2010**, 267-281

Chapter 2 Tungstoaluminates Keggin: The Syntheses, Single Crystal Structure and Redox in EFM

2.1 Introduction

The Keggin structure is one of the most famous structural forms of polyoxometalate (POM). α–Keggin anions have a general formula of $[XM_{12}O_{40}]^{n-}$, where the heteroatom, X, is a p-block atom such as Si, P, Al or Ge. The addenda atom, M, is a transition metal atom such as a W or Mo atom. Berzelius reported the first Keggin anion, phosphomolybdate $[PMo_{12}O_{40}]^{3-}$ in 1826. [1]Blomstrand attempted to understand the Keggin structure as a chain or ring configuration in 1892. Alfred Werner first proposed that the SiO_4 unit is located in the central region of silicotungstic acid. [2] Linus Pauling announced that α-Keggin structure has a $[XO_4]^{n-8}$ center unit surrounded by twelve MO_6 octahedral units. [3] In 1934, using an X-ray diffraction experiment, J.F. Keggin solved the structure of α-Keggin anions, which was the widely accepted, and can work on both hydrated and dehydrated Keggin structures.[4] Keggin structures possesses five isomers marked as α-, β-,γ-, δ- and ε-. These isomers rotate the three adjacent MO_6 units to different orientations and lower the overall symmetry in different ways. [5] The Al_{13} anion $(Al_{13}O_4(OH)_{24}(H_2O)_{12})^{7+}$ and Ge_{13} anion $(Ge_{13}O_4(OH)_{24}(H_2O)_{12})^{7+}$ are the only two examples that have the same heteroatom and addenda atoms. [6]-[7]

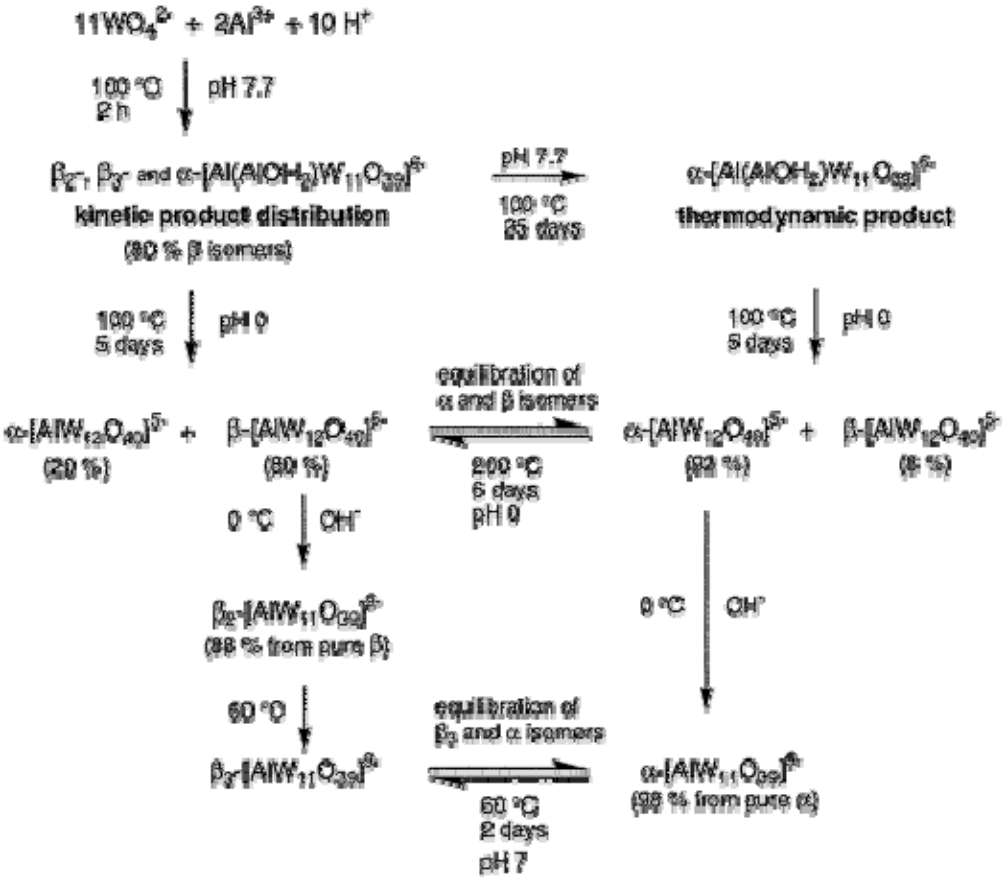

Figure **2-1** After heating of β- or α-$[AlW_{12}O_{40}]^{5-}$ at 200 °C for 10 days at pH 0, an equilibrated mixture ($K_{\beta\rightarrow\alpha}$ = 9.1) is obtained. After heating of β_2- or α-$[AlW_{11}O_{39}]^{9-}$ at 60 °C for 2 days at pH 7, an equilibrated mixture of β_3- and α-$[AlW_{11}O_{39}]^{9-}$ is obtained ($K_{\beta3\rightarrow\alpha}$ = 0.67). β_3-$[AlW_{11}O_{39}]^{9-}$ (no percentage yield indicated) was not isolated as a kinetically stable product but rather was identified by ^{183}W NMR after equilibration at 60 °C. This Figure was abstracted from reference [8].

After removing one MO_4^- unit, the α–Keggin anion becomes a monovacant Keggin structure $[XM_{11}O_{39}]^{n-}$, which is also known as a lacunary Keggin structure because it has a missing fragment. Weinstock et al. reported the syntheses and properties of Keggin tungstoaluminates, $[\alpha\text{-}AlW_{12}O_{40}]^{5-}$ and monovacant Keggin $[\alpha\text{-}AlW_{11}O_{39}]^{9-}$. [8] These aluminum centered Keggin anions are more stable than other Keggin POMs in water because a more negative charge correlates to a better base stability. [9][10] The new, higher yield syntheses method of making Keggin tungstoaluminates is shown in Figure **2-1**, [8]

Keggin POMs can be easily reduced and kept stable in a certain pH range. [11] For example, $\alpha\text{-}SiW_{12}O_{40}^{4-}$ has three stable charge states shown in its electrochemical data.[12] Tungstoaluminates Keggin POM has great stability in a wide pH range in comparison to to its Si and P analogs. [13] Shown in Figure **2-2** [13], the stable pH ranges of the first and second one-electron reduction potentials of $\alpha\text{-}AlW_{12}O_{40}^{6-}$ is 1.8 to 7.5, which is significantly larger than that of $\alpha\text{-}SiW_{12}O_{40}^{4-}$ and $\alpha\text{-}PW_{12}O_{40}^{3-}$ anions. Kurth et. al studied the redox properties of POM material in a thin layer phase. [14]

In this chapter we report the syntheses, single crystal structure, ^{27}Al NMR, and the redox properties on the nanoscale and in the solid state phase.

Table **2-1** First and Second One-Electron Reduction Potentials of α-$XW_{12}O_{40}^{n-}$. This Figure was abstracted from reference [12].

X	$-n/-(n+1)$	pH range	mV
Al	-5/-6	1.8-7.5	-130
Al	-6/-7	2.05	-330
Al	-6/-7	3.0	-350
Al	-6/-7	7.2	-360
Si	-4/-5	1.0-4.5	55
Si	-5/-6	1.0-4.5	-205
P	-3/-4	1.0-2.0	255
P	-4/-5	1.0	-15

2.2 Experimental Section

2.2.1 General.

Reagent grade chemicals were commercially available and used without further purification. Deionized water was used from a Millipore Reverse Osmosis Direct-Q System. IR spectra were recorded on a Perkin-Elmer 1625 FT-IR at room temperature from KBr pellets. Pure water, obtained using a Millipore Direct Q5 system (conductivity =18 μΩ), was used throughout. α-Nonapotassium undecatungstoaluminate (α-$K_9AlW_{11}O_{39}\cdot 12H_2O$) was prepared according to a published method and identified by infrared spectroscopy. [8]

2.2.2 Synthesis of compounds.

2.2.2.1 Syntheses of α-$K_9AlW_{11}O_{39}$, 1.

The syntheses of α-$K_9AlW_{11}O_{39}\cdot 12H_2O$ was prepared according to a published method and identified by infrared spectroscopy. [11]

0.3 g α-$K_9AlW_{11}O_{39}\cdot 12H_2O$ was leaved in a 25 ml vial. 20 ml 60˚C hot water was added to the vial to dissolve the POM and get clear solution. Leave the vial in 5˚C refrigerator for 3 days. Transparent cubic crystals appear at the bottom of the vial.

2.2.2.2 Syntheses of organic soluble $(TBA)_n H_{9-n} [\alpha\text{-}AlW_{11}O_{39}^{9-}]$, 2.

2 was synthesized by emploring a metathesis method and crystallized from CH_3CN. 0.07g (0.02mmol) α-$K_9AlW_{11}O_{39}$ was dissolved in 2ml water. 0.063g (0.2mmol) of Solid TBA·Br (tetrabutylammonium tribromide) was added to the solution, and a pH between 4 and 5 was maintained through the addition of 1M HCl. After this solution was stirred and centrifuged, a blue precipitate was observed. This blue solid was dissolved in CD_3CN and analyzed via ^{31}P NMR.

2.2.3 Analytical techniques

2.2.3.1 Collection of NMR Data

^{27}Al NMR spectra were recorded on a Varian Inova 500 MHz spectrometer with 5 mm tubes. ^{27}Al has resonance frequencies of 130.24 MHz. ^{183}W NMR spectra were recorded on a JEOL GX-400 spectrometer with 10 mm tubes. ^{183}W has resonance frequencies of 16.7 MHz. Chemical shifts are given with respect to 1 M $AlCl_3$ for ^{27}Al and 1 M Na_2WO_4 for ^{183}W. Typical acquisition parameters for ^{183}W spectra includes a 10000 Hz spectral width, 1.6 second acquisition time, 1second pulse delay, and a 50 μs pulse width. Anywhere from 1000 to 60000 scans were acquired. Typical acquisition parameters for ^{27}Al spectra includes a 500 ppm spectral width, a 0.31456 second acquisition time, a 1 second pulse delay, and a 5μs pulse width. Anywhere from 1000 to 3000 scans were acquired. For both the ^{27}Al and ^{183}W, the more negative chemical shifts donates the more upfield resonance.

Table 2-2 Selected crystallographic data for compound 1

	1
Empirical Formula	$K_xH_y(\alpha\text{-}AlW_{11}O_{39})(H_2O)_{20}$
MW	3205.23
Crystal System	Cubic
Space Group	F432
a / Å	21.254(3)
b / Å	21.254(3)
c / Å	21.254(3)
α / º	90
β / º	90
γ / º	90
V / $Å^3$	9601(2)
Z	4
Crystal Size / mm	0.16×0.16×0.04
R indices [I >2 σ (I)]	R1 = 0.0754
	wR2 = 0.2348
Final R (all data)	R1 = 0.0571
	wR2 = 0.2070

2.2.3.2 Single-Crystal X-ray structure Determination

Crystals of **1** were collected under a thin layer of mineral oil using a polarizing microscope. Selected crystals were mounted on a glass fiber and quickly placed in a cold stream of nitrogen on a Bruker SMART CCD diffractometer, equipped with a sealed tube Mo anode (Kə radiation, λ= 0.71073 Å), and a graphite monochromator or, a Nonius Kappa CCD diffractometer. Data collection, indexing, and initial cell refinements were collected at around 100 K using SHELXTL software to solve and refine the restructures. [15] The heaviest atoms were located by direct methods, and the remaining atoms were found in subsequent Fourier difference syntheses. All refinements were fullsquares on F^2. Crystal data and structure refinement parameters for **1** are listed in table **2-2**.

2.2.3.3 AFM/EFM Experiement

The experiment was performed on a Nanoscope III (Vecco, Inc.) AFM (Atomic Force Microscope. The DPE probe tip purchased from MicroMasch Inc. (tip radius is 40 nm) was utilized for voltage application and image scanning. The entire detection circuit was set-up as Figure **2-5**. The POM liquid was evenly spread out on the Au substrate disc to form a uniform layer with a speed-controlled rotor, and the sample was completely dried in the oven for two days at a temperature of < 100 ˚C. The Au disc was glued on the magnetic AFM dish by using a silver pen (all purchased from Ted Pella Co.). It is important to note that the entire sample holder was conductive. Next, we applied a negative 10 V on certain regions of the POM layer in order to reduce the POM. The reduced POM was tested using fluorescence microscopy, and EFM (Electrostatic force microscope) detection was obtained using the AFM under Interleave mode by lifting the tip 50 nm.

2.3 Result and discussion

2.3.1 Syntheses

The detailed syntheses procedure of $K_9[\alpha\text{-}AlW_{11}O_{39}]$ and $TBA_nH_{9-n}[\alpha\text{-}AlW_{11}O_{39}]$ are shown below. Crystals were grown from slowly evaporating an aqueous solution of $\alpha\text{-}K_9AlW_{11}O_{39}\cdot 12H_2O$.

Synthesis of $[\alpha\text{-}AlW_{12}O_{40}]^{5-}$:

Step 1: $11[WO_4]^{2-} + 2Al^{3+} + 10H^+ \rightarrow [Al(AlOH_2)W_{11}O_{39}]^{6-} + 5H_2O$

Step 2: $12[Al(AlOH_2)W_{11}O_{39}]^{6-} + 56H^+ \rightarrow 11[AlW_{12}O_{40}]^{5-} + 13Al^{3+} + 28H_2O$

From $[\alpha\text{-}AlW_{12}O_{40}]^{5-}$ to $[\alpha\text{-}AlW_{11}O_{39}]^{9-}$:

$$H_5[AlW_{12}O_{40}] + 7.5K_2CO_3 + 0.5H_2O \rightarrow \alpha\text{-}K_9[AlW_{11}O_{39}] + KHWO_4 + 5KHCO_3 + 2.5CO_2(g)$$

The organic soluble $TBA_nH_{9-n}[\alpha\text{-}AlW_{11}O_{39}]$ was prepared by :

$$nTBABr + K_9[\alpha\text{-}AlW_{11}O_{39}] + (9-n)H^+ \rightarrow TBA_nH_{9-n}[\alpha\text{-}AlW_{11}O_{39}] + 6Br^- + 9K^+$$

2.3.2 Crystal Structure

There are twelve tungstate atoms with 0.91 occupancy in each structural unit, which can be understood through the idea that the vacancy is delocalized so that it cannot be distinguished from tungstate atoms on POM. $AlW_{12}O_{40}^{5-}$ and $AlW_{11}O_{39}^{9-}$, we suggest that the crystal isolated is the $\alpha\text{-}K_9AlW_{11}O_{39}$ species because the crystalline product has significantly lower solubility than $\alpha\text{-}K_5AlW_{12}O_{40}$. Another important issue is that we use same product for reaction with lanthanides, and we obtain $LnAlW_{11}O_{39}$ POM species (in Chapter 3). There are twelve water solvent molecules that stay together as a unit in the

crystal. Solvent units and POM units pack together and form a body centered cubic system. The structure is shown in Figure **2-2**.

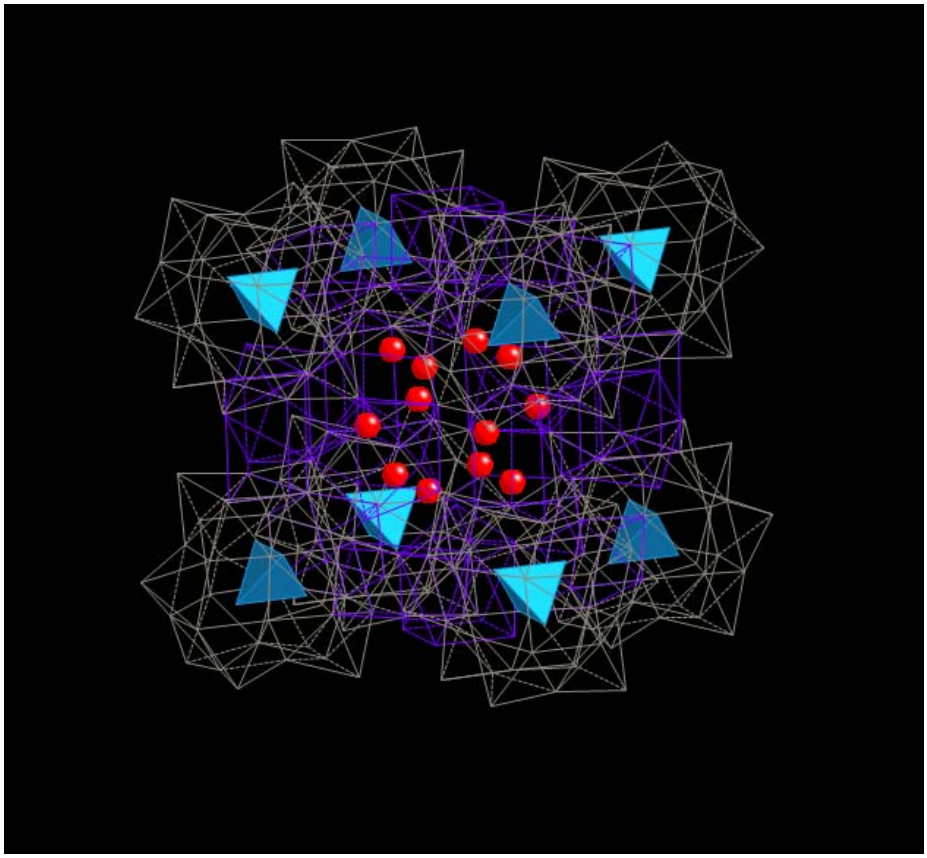

Figure **2-2** Body centered cubic system of α-$K_9AlW_{11}O_{39}\cdot 12H_2O$. W-O framework is shown in grey tetrahedron. Blue tetrahedrons are Al-O_4 units. Red colored balls are H_2O.

2.3.3 ^{27}Al NMR Spectra

As a quadrupolar nucleus, ^{27}Al has 5/2 spin. In a highly symmetric environment, the ^{27}Al signal width is very narrow. [16] When the symmetry is low, the signal width increases so that we will observe broad peaks. Here a broad peak suggests that the POM unit is asymmetric due to the vacancy. Shown in Figure **2-3**, a α-$K_9AlW_{11}O_{39}$ NMR spectra sample was made with D_2O solvent in 5 mm tubes. The ^{27}Al NMR shows a broad peak at 66.4 ppm with a width of about 11.5 ppm at half height, and a sharp peak at 72.2 ppm (about 16% from integration), which can be attributed to trace amount of α-$K_5AlW_{12}O_{40}$. This $K_5AlW_{12}O_{40}$ is likely due to the equiblium established in water with the $AlW_{11}O_{39}^{9-}$ species that is governed by pH. The preparation of $AlW_{11}O_{39}^{9-}$ involves increasing the pH of an aqueous $AlW_{12}O_{40}^{5-}$ solution to 8.5 .. Because the solubility of $AlW_{11}O_{39}^{9-}$ is much less than $AlW_{12}O_{40}^{5-}$, the $AlW_{11}O_{39}^{9-}$ potassium salt precipitates out as a white solid. Organic soluble α-$TBA_nH_{9-n}AlW_{11}O_{39}$ NMR spectra sample was made with CD_3CN solvent in 5 mm tubes. We obtained the ^{27}Al NMR spectra of TBAnH9-n[α-$AlW_{11}O_{39}$] from CD_3CN solvent. The ^{27}Al NMR shows a broad peak at 55.1 ppm with width of about 20 ppm at half height, and a sharp peak at 71.9 ppm (about 14% from integration), which is very similar to the ^{27}Al NMR spectra of α-$K_9AlW_{11}O_{39}$.

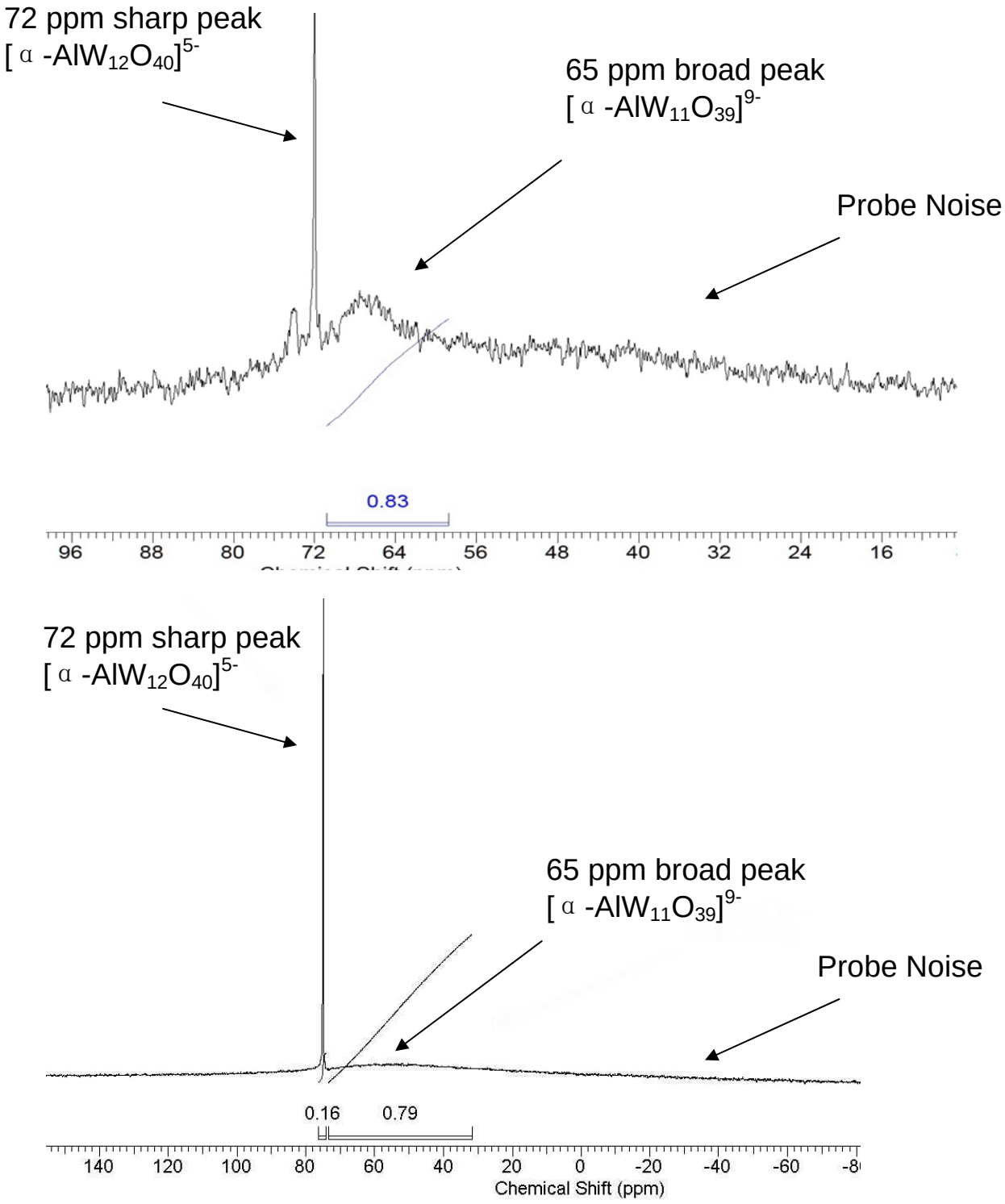

Figure **2-3** ^{27}Al NMR of α-$K_9AlW_{11}O_{39}$ (upper) and $TBA_nH_{9-n}[\alpha\text{-}AlW_{11}O_{39}]$ (lower).

2.3.4 AFM/EFM Microscopy

The POM sample was prepared by adding one small drop of α-$K_9AlW_{11}O_{39}$ aqueous solution (4 mmol·L^{-1}) on to a gold plate that was attached to a magnetic AFM dish by emulsified-Ag-conductive glue. The solution was evenly dispersed on the gold plate via spinning the entire sample plate on a spinner for 5 min, and was dried in a 60˚C oven overnight. The emulsified-Ag-conductive glue was manufactured by Circuitworks Co. and purchased from Spi Co. The conduction AFM tips were purchased from μMasch Co. and its tip radius is less than 40 nm and its force constant is 46 N/m.

The POM layer was reduced by conduction AFM tips by application of a potential under -12 V and the EFM (electrical force microscopy) was performed under interleave mode of Veeco Nanoscope III instrument. The potential test voltage was + 2V, the conduction tip was lifted up for 25 nm from the engaging the surface of POM to do the electical force test.

Since TEM and SEM results (in Chapter **4**) suggest the possibility that POMs may be used as a potential information storage device, we should know whether the solid POM could be reduced or oxidized into different states that are similar to the ones shown in CV curves under various applied voltages, in order to test the feasibility on the technical level. The oxidization or reduction voltage values acquired from CV experiments (Figure **2-2**) could be directly referred to the future design of storage devices, since the different states relating to those voltages could represent different storage statuses, and could, thus, be read / written by a probe and subsequently decoded. There is a gap between the CV experiment and future storage in that CV is performed in liquid solutions, while the storage process necessarily occurs in the solid state.

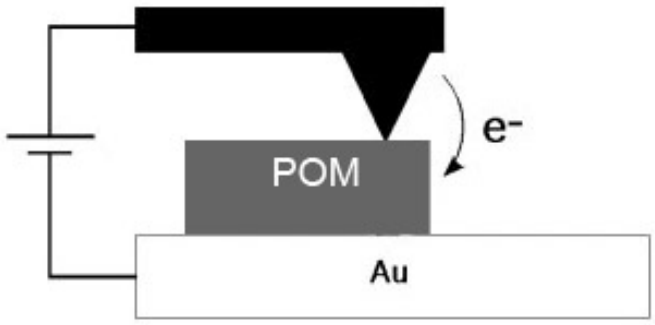

Figure **2-4** Applied potential voltage was given via conductive tip on AFM instrument.

We need to design an experiment performed in the solid state that should have a conductive substrate to spread POM as an even layer and a conductive tip that is able to apply different potential voltages on the layer. In addition, the oxidized or reduced parts on the POM layer should be capable of being detected by either the spectral method or by a potential probe. Atomic force microscopy (AFM) could satisfy this requirement because all scanning and detecting using this instrument is done so on the nanoscale. Figure **2-4** showed how to apply voltage to POM sample via conductive tip on AFM instrument. The scanned region can be accurately manipulated by a piezo-electric based stage and by an electrostatic force microscope (EFM), which can apply voltages directly on the sample. By doing this, the distribution of potentials in interleave mode can be detected [17][18]. All scanning and probing are driven by a cantilever with a sharp and hard tip at its end. If we use a special tip coated with metal, we can utilize EFM on dried POM compounds.

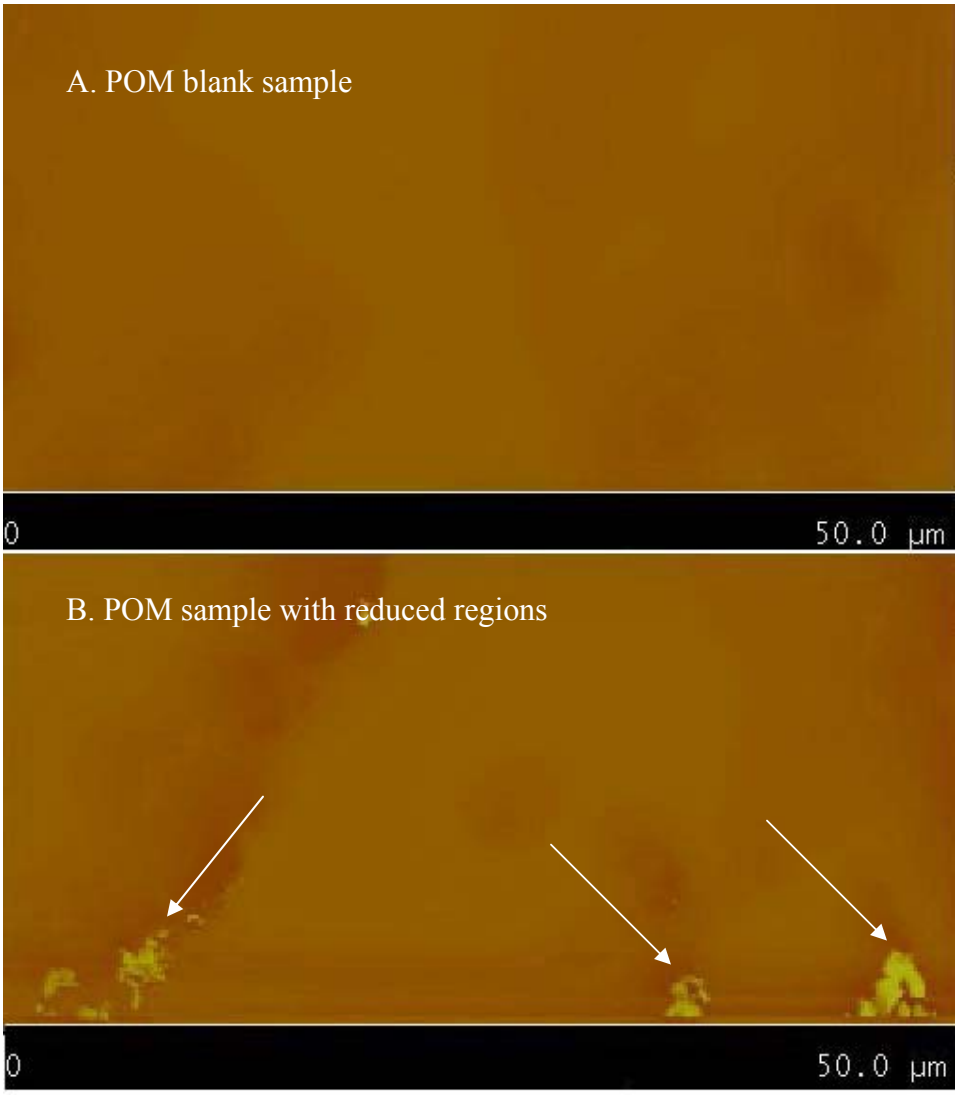

Figure **2-5** Potential Diagram of POM surface monitored by EFM microscopy (EFM detection voltage: +2 V). A. Blank sample: POM coated on the surface of gold plate without reduction. B. Reduced sample: POM coated on the surface of gold plate reduced under – 12 V DC voltage: Bright patterns show different potential distribution.

The image shown in Figure **2-5**A is POM coated on the surface of gold plate without reduction. The image shown in Figure **2-7**B, we observed the surface potential diagram has two regions in bright color (the left and right regions, shown in Fig 2-5 B) in which the POM surface has been reduced by the AFM conduct tip under -12 V DC voltage. The EFM scanning test was done under +2 V, under this small oxidation voltage the POM surface after reduction shows different scene with the place without reduction that showed smooth and uniform potential diagram shown in Fig 2-5A, which indicate the charge distribution of POM surface and proved the redox states of POM could be detected by EFM. The POM in solid state after reduced is stable and detectable, which support the hypothesis that POM material can be used as data store material.

2.4 References

[1] N. Greenwood; A. Earnshaw., **1997**. *Chemistry of the Elements*, 2nd Edition, Oxford:Butterworth-Heinemann. ISBN 0-7506-3365-4

[2] A. Searle, **1913**, *the Silicates in Chemistry and Commerce*

[3] G. Kauffman, *Coordination Chemistry A Century of Progress*, **1994**, Volume 565

[4] J. Bailar, Jr. *The Chemistry of the Coordination Compounds,* Reinhold Publishing Corporation, **1956**, 472-482

[5] L. Baker, J. Figgis, *J.Am. Chem. Soc*, **1970**, 92(12), 3794-3797

[6] N. Greenwood; A. Earnshaw, **1997**, *Chemistry of the Elements* (2nd ed.), Oxford: Butterworth-Heinemann, ISBN 0080379419

[7] S. Bradley, R. Kydd and R. Yamdagni *J. Chem. Soc., Dalton Trans.*, **1990**, 413 – 417

[8] J. Cowan, A. Bailey, R. Heintz, B. Do, K Hardcastle, C. Hill, and I. Weinstock, *Inorg. Chem.*, **2001**, 40 (26), 6666–6675

[9] D. Smith and M. Pope, Inorg. Chem. 12, 331 (1973).

[10] I. Weinstock, R. Atalla, R. Reiner, M. Moen, K. Hammel, C. Hill, and M. Harrup, *J. Mol. Catal. A, Chemical*, **116**, 59 (1997).

[11] M. Sadakane and E. Steckhan, *Chem. Rev.*, **1998**, 98 (1), pp 219–238

[12] B. Keita, L. Nadjo, *J. Electroanal. Chem*. **1987**, *217*, 287

[13] Y. Geletii, C. Hill, A. Bailey, K. Hardcastle, R. Atalla, and I. Weinstock, *Inorg. Chem.*, 2005, 44 (24), pp 8955–8966

[14] S. Liu, D. Kurth, H. Mohwald, D. Volkmer, *Adv. Mater.* **2002**, 14, 225.

[15] SHELXTL,Brucker AXS, Inc., Bruker Advanced X-ray Solutions, **1999**

[16] J. Mason, *Multinuclear NMR*, 1987

[17] N. Nuraje, K.Su, A. Haboosheh, J. Samson, *et al.*, *Adv. Mater.* 2006, *18*, 807.

[18] N. Nuraje, S. Mohammed, L. Yang, Matsui, H., *Angew. Chem. Int. Ed.* 2009, *121*, 1.

Chapter 3. Coordination Polymers of Lanthanide Tungstoaluminates: Synthesis, Characterization

3.1 Introduction

Lanthanide polyoxometalate research is an important area in coordination chemistry and lanthanide chemistry. The majority of previous work is related to luminescence properties of lanthanide complexes. [1][2][3] Other areas of study include supramolecular functional assemblies and magnetic properties [4][5][6]. Because the atomic radii of lanthanides get smaller from left to right, different lanthanides show interesting trends which affect their coordination complexes and supramolecular assemblies . [7] This property is very interesting and useful in molecular design. [8]

The Keggin structure is one of the most famous structural forms of POMs. α–Keggin anions have a general formula of $[XM_{12}O_{40}]^{n-}$, where X is a p-block atom, M is a transition metal atom such as W or Mo. After removal of one MO^{4-} unit, the α–Keggin anion becomes a monovacant Keggin structure $[XM_{11}O_{39}]^{n-}$. Weinstock et al. reported the tungstoaluminate Keggin, $[\alpha\text{-}AlW_{12}O_{40}]^{5-}$ and monovacant Keggin $[\alpha\text{-}AlW_{11}O_{39}]^{9-}$. They also reported several metal derivatives $[\alpha\text{-}Al(AlOH_2)W_{11}O_{39}]^{6-}$, $[\alpha\text{-}AlCo^{III}W_{11}O_{39}]^{6-}$, $[\alpha\text{-}AlMn^{II}W_{11}O_{39}]^{7-}$, $[\alpha\text{-}AlMn^{III}W_{11}O_{39}]^{6-}$ and $[\alpha\text{-}AlV^{V}W_{11}O_{40}]^{6-}$ which are all synthesized under mild conditions. Shown in Figure **3-1**, in the solution of the crystal structure, atoms occupying the vacancy site were assigned 1/12 transition metal character and 11/12 W charater. Both electrochemical data and single crystal structures of $[\alpha\text{-}AlCo^{III}W_{11}O_{39}]^{6-}$, $[\alpha\text{-}AlMn^{II}W_{11}O_{39}]^{7-}$ are shown in Figure **3-1**. [9] These properties are very similar to the starting material's electrochemical properties.

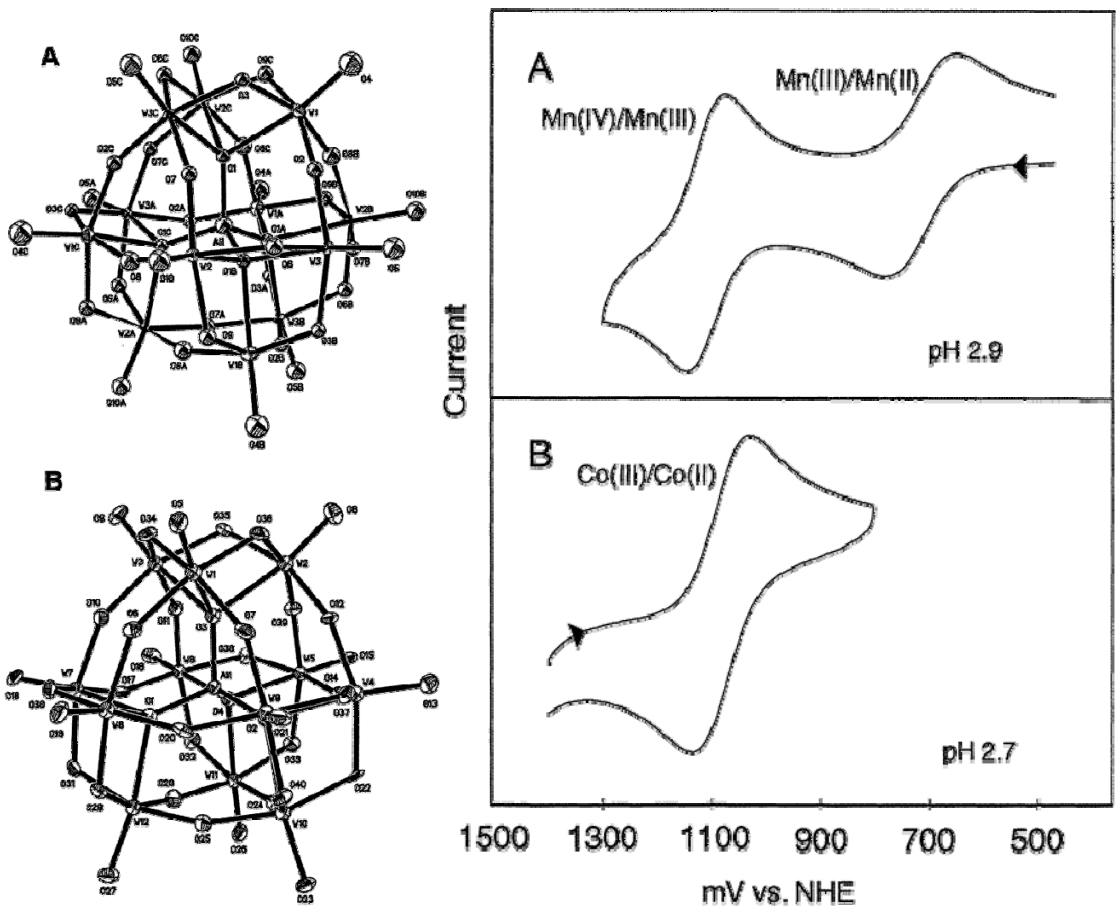

Figure **3-1** Cyclic voltammograms and single crystal structures of $[\alpha\text{-AlCo}^{III}W_{11}O_{39}]^{6-}$, $[\alpha\text{-AlMn}^{II}W_{11}O_{39}]^{7-}$. Data abstracted from reference [9].

There are several groups interested in incorporating lanthanides into monovacant Keggin structures. Lacunary tungstosilicate $[\alpha\text{-SiW}_{11}O_{39}]^{8-}$ and its metal substituted derivatives were the first monovacant Keggin lanthanide derivatives studied by Pierre Mialane et al. These silicon Keggin POMs have three different one dimensional structures built up of $[\alpha\text{-SiW}_{11}O_{39}]^{8-}$ anions connected by lanthanide cations: linear chain, zigzag chains, and dimeric chains. [10] M.T. Pope reported two crystal structures of α-Keggin $[SiW_{11}O_{39}]^{8-}$ lanthanide substituted compounds as having same zigzag polymer chain structure. [11] Other one or multiple dimensional structures of α-Keggin

$[SiW_{11}O_{39}]^{8-}$ lanthanide derivative also have been studied. [12]. Magnetic properties of α-Keggin $[SiW_{11}O_{39}]^{8-}$ lanthanide derivatives were studied in 2006. [13] Recently α-Keggin $[GeW_{11}O_{39}]^{8-}$ lanthanide derivatives were reported to possess similar structural and magnetic properties as the α-Keggin $[SiW_{11}O_{39}]^{8-}$ lanthanide derivatives. [14].

We have synthesized 7 different lanthanide α-Keggin tungstate aluminum POM and identified their solid-state structure and solution chemistry properties. Parameters such as stoichiometry and countercations impact the product structure. Several of these products have novel two dimensional layer-by-layer crystal packing structures which have potential supramolecular applications.

3.2 Experimental Section

3.2.1 General.

Commercially available reagent grade chemicals were used without further purification. Deionized water was used from a Millipore Reverse Osmosis Direct-Q System. Elemental analyses were carried out on a SEPCTROFLAME M120E Inductive Coupled Plasma Atomic Emission Spectrometer (ICP-AES). IR spectra were recorded on a Perkin-Elmer 1625 FT-IR at room temperature from KBr pellets. α-Nonapotassium undecatungstoaluminate (α-$K_9AlW_{11}O_{39}\cdot 12H_2O$) was prepared according to a published method and identified by infrared spectroscopy. [15]

3.2.2 Synthesis of compounds.

3.2.2.1 Syntheses of $H_6KY(\alpha\text{-}AlW_{11}O_{39})Cl(H_2O)_{20}$, (2).

α-K_9 $[AlW_{11}O_{39}]\cdot 12H_2O$ (150 mg, 0.04 mmol) was stirred as a slurry in 2 ml of deionized water. 2ml of a $YCl_3\cdot 6H_2O$ (24 mg, 0.08 mmol) solution was added with

vigorous stirring. The cloudy solution was stirred for 30 min to 1 hour until the precipitate partly dissolved. The precipitate was removed after centrifuging for 10 min.

The clear solution was tested by ^{183}W NMR (D_2O, ppm): 2 (2), -6 (2), -17 (1), -39 (2), -81 (2), -84 (2). ^{27}Al NMR (D_2O, ppm): 68 ($\Delta\nu_{1/2}$ = 278 Hz). The ^{27}Al NMR signal is broad, and we give measured linewidth ($\Delta\nu_{1/2}$) here.

Add 1ml saturated KCl (1M) and leave the clear solution in a refrigerator at 5ºC for seven weeks. Solid products are transparent crystals and an amorphous white powder. We estimate that the crystal yield is 135 mg, 75%.

IR (KBr plate): 935 (sh), 873 (s), 803 (m), 695 (m), 609 (s), 535 (w), 495 (w), 470 (w) cm^{-1}. Anal. Calcd (Found) for $H_6KY(\alpha\text{-}AlW_{11}O_{39})Cl(H_2O)_{20}$: Al, 0.85 (0.55);W, 63.27 (61.85); Y, 2.79 (1.96).

3.2.2.2 Syntheses of K_3 $[La^{III}_2(\alpha\text{-}AlW_{11}O_{39})(H_2O)_{20}]$, (3).

3 was prepared according to the procedure described above but using $LaCl_3{\cdot}7H_2O$ (30 mg, 0.08 mmol) as the lanthanide reactant.

The transparent solution was tested by ^{27}Al NMR (D_2O, ppm): 68 ($\Delta\nu_{1/2}$ = 461 Hz).

Yield: 44mg (24%). IR (KBr plate): 934 (sh), 876 (m), 814 (s), 701(m), 446 (w), 429 (w) cm^{-1}. Anal. Calcd (Found) for K_3 $[La^{III}_2(\alpha\text{-}AlW_{11}O_{39})(H_2O)_{20}]$: Al, 0.79 (0.73);W, 58.95 (49.71); La, 8.11 (5.58).

3.2.2.3 Syntheses of K_3 $[Ce^{III}_2(\alpha\text{-}AlW_{11}O_{39})(H_2O)_{20}]$, (4).

α -K_9 $[AlW_{11}O_{39}]{\cdot}12H_2O$ (300 mg, 0.08 mmol) was stirred as a slurry in 4 ml of deionized water. 4 ml $Ce(NO_3)_3{\cdot}6H_2O$ (70 mg, 0.16 mmol) solution was added with vigorous stirring. The cloudy solution was stirred for 30 min to 1 hour until the precipitate partly dissolved. Any solid was removed after centrifuging for 10 min. The

orange colored reaction solution was tested by ^{183}W NMR (D_2O, ppm (integration)): 124 (2), -3 (2), -8 (1), -38 (2), -88 (2)

The reaction solution was divided into two equal portions, portion A and portion B. After adding 1ml saturated KCl to portion A, it was left in a refrigerator for 7 days at 5ºC. An amorphous orange powder was collected for further study from A. Yield: 72 mg, 40%. IR (KBr plate): 932 (sh), 871 (s), 817 (m), 681 (s), 531 (m), 499 (w), 488 (w) cm^{-1}. Anal. Calcd (Found) for K_3 [Ce^{III}_2(α-$AlW_{11}O_{39}$)(H_2O)$_{20}$]: Al, 0.78 (0.69);W, 58.90 (55.66); Ce, 8.18 (7.60). A solution of portion B was left at room temperature for two weeks producing red crystals suitable for X-ray crystallography. Estimated yield of crystals: 17 mg, 9.4%.

3.2.2.4 Syntheses of K_3 [Sm^{III}_2(α- $AlW_{11}O_{39}$)(H_2O)$_{20}$], (5).

α -K_9 [$AlW_{11}O_{39}$] 12H_2O (300 mg, 0.08 mmol) was stirred as a slurry in 4 ml of deionized water. 4 ml $SmCl_3 \cdot 6H_2O$ (58 mg, 0.16 mmol) solution was added with vigorous stirring resulting in a cloudy solution which was kept stirring for 30 min to 1 hour until the precipitate partly dissolved. The precipitate was removed after centrifuging for 10 min.

The reaction solution was divided into two equal portions, labeled A and B. After adding 1ml saturated KCl to portion A, it was left in a refrigerator at 5ºC for 7 days. This produced an amorphous white powder. Both the reaction solution and powder were colorless. Precipitate yield: 60.8 mg, 33.8%. IR (KBr pellet): 935 (m), 876 (m), 792 (s), 692 (m), 601 (w), 563 (w), 501 (w), 471 (w), cm^{-1}. Anal. Calcd (Found) for K_3 [Sm^{III}_2(α-$AlW_{11}O_{39}$)(H_2O)$_{20}$]: Al, 0.78 (0.56);W, 58.55 (55.10); Sm, 8.72 (8.46).

Portion B was left at room temperature for five weeks, producing transparent crystals suitable for X-ray crystallography. Estimated yield: 15.6 mg, 8.7%

3.2.2.5 Syntheses of K_3 [Gd^{III}_2(α-$AlW_{11}O_{39}$)$(H_2O)_{20}$], (6).

6 was prepared according to the procedure described for **4** but using $GdCl_3 \cdot 6H_2O$ (59 mg, 0.16 mmol) as the lanthanide reactant.

Precipitate yield: 94 mg, 52.2%.. IR: 932(m), 866.685(m), 794.746(s), 675.643(s), 470.64(w), 440.581(w). Anal. Calcd (Found) for K_3 [Gd^{III}_2(α-$AlW_{11}O_{39}$)$(H_2O)_{20}$]: Al, 0.78 (0.63);W, 58.32 (53.29); Gd, 9.09 (9.45). Single crystal estimated yield: 17 mg, 9.2%.

3.2.2.6 Syntheses of K_3 [Dy^{III}_2(α-$AlW_{11}O_{39}$)$(H_2O)_{20}$], (7).

7 was prepared according to the procedure described for **5** but using $DyCl_3 \cdot 6H_2O$ (60 mg, 0.16 mmol) as the lanthanide reactant.

Yield: 52mg (22.6%). ^{27}Al NMR (D_2O, 298K): 67.50 ppm ($\Delta\nu_{1/2}$ = 299 Hz). IR: 937.34(m),875.62(m), 804.26(s), 692.39(m), 538.1(w), 497.6(w). Anal. Calcd (Found) for K_3 [Dy^{III}_2(α-$AlW_{11}O_{39}$)$(H_2O)_{20}$]: Al, 0.78 (0.54);W, 58.14 (61.93); Dy, 9.36 (8.35). Single crystal estimated yield: 16 mg, 6.9%.

3.2.2.7 Syntheses of $H_{2.5}Dy^{III}_{2.5}$(α-$AlW_{11}O_{39}$)$Cl_{0.5}$ $(H_2O)_{28.5}$ (8)

α −K_9 [$AlW_{11}O_{39}$] $12H_2O$ (290 mg, 0.085 mmol) was stirred as a slurry in 10 ml of deionized water. 2ml $Dy(NO)_3 \cdot 6H_2O$ (98 mg, 0.26 mmol) solution was added with vigorous stirring at 70^o C. The cloudy solution was stirred for 50 minutes. The white precipitate was removed by centrifuging for 10 min and the clear solution was kept at room temperature for eight weeks. From the clear solution, a transparent crystallized product was collected for further study. Yield: 199mg (51%).

IR (KBr pellet): 877 (w)，804(s)， 720 (s), 695 (s), 635 (s), 614.393 (s), 578 (s) , 539 (w), 499 (s), 471 (s). Anal. Calcd (Found) for $H_{2.5}Dy^{III}_{2.5}(\alpha\text{-}AlW_{11}O_{39})Cl_{0.5}$ $28.5H_2O$: Al, 0.75 (0.53);W, 56.37 (62.76); Dy, 11.34 (8.46).

3.2.2.8 Syntheses of K_3 $[Lu^{III}_2(\alpha\text{-}AlW_{11}O_{39})(H_2O)_{20}]$, (9).

α -K_9 $[AlW_{11}O_{39}]\cdot 12H_2O$ (150 mg, 0.04 mmol) was stirred as a slurry in 2 ml of deionized water. 2ml $Lu(NO_3)_3\cdot xH_2O$ (29 mg, 0.08 mmol) solution was added with vigorous stirring. The pH was adjusted to 5.5 with 5 drops of 1M LiOAc. The cloudy solution was stirred for another 20 min. White precipitate was removed by centrifuging for 10 min. 1ml saturated KCl (1M) was added to the clear solution and the solution was stored in the refrigerator at 5ºC for three weeks. Transparent crystallized product was collected for further study. Yield: 100mg (56%). ^{27}Al NMR (D_2O, 298K): 67.50 ppm ($\Delta\nu_{1/2}$ = 299 Hz). IR (KBr plate): 939(s), 877(m), 800(s), 671(s), 545(m), 504(w), 493(w), 481(w), 467(w), 453(w). Anal. Calcd (Found) for K_3 $[Lu^{III}_2(\alpha\text{-}AlW_{11}O_{39})(H_2O)_{20}]$: Al, 0.77 (0.83);W, 57.77 (59.58); Lu, 10.00 (9.53).

3.2.3 Analytical techniques

3.2.3.1 Collection of NMR Data

^{27}Al NMR spectra were recorded on a Varian Inova 500 MHz spectrometer with 5 mm tubes. The resonance frequency is 130.24 MHz for ^{27}Al. ^{183}W NMR spectra were recorded on a JEOL GX-400 spectrometer with 10 mm tubes. The resonance frequency is 16.7 MHz for ^{183}W. Chemical shifts are given with respect to 1M $AlCl_3$ for ^{27}Al and 1M Na_2WO_4 for ^{183}W. Typical acquisition parameters for ^{183}W spectra included the following spectral width 10000Hz, acquisition time 1.6 s, pulse delay 1 s, pulse width 50 μs. From 1000 to 60000 scans were acquired. Typical acquisition parameters for ^{27}Al spectra

included the following spectral width 500 ppm, acquisition time 0.31456 s, pulse delay 1 s, pulse width 5μs. From 1000 to 3000 scans were acquired. For both ^{27}Al and ^{183}W chemical shifts, the convention used is the more negative chemical shifts denote more upfield resonance.

3.2.3.2 Single-Crystal X-ray structure Determination

Crystals of **2, 3, 4, 5, 6, 7, 8** and **9** were collected under a thin layer of mineral oil using a polarizing microscope. Selected crystals were mounted on a glass fiber and quickly placed in a cold nitrogen stream on a Bruker SMART CCD diffractometer equipped with a sealed tube Mo anode (Kα radiation, λ= 0.71073 Å) and graphite monochromator or Nonius Kappa CCD diffractometer. Data collection, indexing, and initial cell refinements were collected at around 100 K using SHELXTL software. The SHELX package of software was used to solve and refine the restructures. [16] The heaviest atoms were located by direct methods, and the remaining atoms were found in subsequent Fourier difference syntheses. All refinements were full squares on F^2. Crystal data and structure refinement parameters for **2 - 9** are listed in Table **3-1**, **3-2**, **3-3** and **3-4**.

Table 3-1 Selected crystallographic data for compounds 2 and 3

	2	**3**
Empirical Formula	$H_6KY(\alpha\text{-}AlW_{11}O_{39})Cl\ (H_2O)_{20}$	$K_3\ [La^{III}_2(\alpha\text{-}AlW_{11}O_{39})(H_2O)_{20}]$
MW	3032.95	3428.61
Crystal System	Monoclinic	Orthorhombic
Space Group	C2/c	Pna2(1)
a / Å	37.604(8)	27.041(5)
b / Å	12.340(3)	16.351(3)
c / Å	22.336(5)	11.626(2)
α / º	90	90
β / º	100.28(3)	90
ɣ / º	90	90
V / $Å^3$	10198(4)	5140.4(18)
Z	8	4
Crystal Size / mm	0.40×0.30×0.10	0.20×0.14×0.06
R indices [I >2 σ (I)]	R1 = 0.072	R1 = 0.0340
	wR2 = 0.1855	wR2 = 0.0742
Final R (all data)	R1 = 0.075	R1 = 0.0360
	wR2 = 0.1874	wR2 = 0.0752

Table 3-2 Selected crystallographic data for compounds 4 and 5

	4	**5**
Empirical Formula	K_3 [Ce^{III}_2(α-$AlW_{11}O_{39}$)(H_2O)$_{20}$]	K_3 [Sm^{III}_2(α-$AlW_{11}O_{39}$)(H_2O)$_{20}$]
MW	3431.03	3451.52
Crystal System	Orthorhombic	Orthorhombic
Space Group	Pna2(1)	Pna2(1)
a / Å	27.011(5)	26.765(5)
b / Å	16.349(3)	16.271(3)
c / Å	11.602(2)	11.512(2)
α / º	90	90
β / º	90	90
γ / º	90	90
V / $Å^3$	5123.5(18)	5013.4(17)
Z	4	4
Crystal Size / mm	0.38×0.20×0.06	0.20×0.17×0.03
R indices [I >2 σ (I)]	R1 = 0.0478	R1 = 0.0273
	wR2 = 0.1331	wR2 = 0.0620
Final R (all data)	R1 = 0.0486	R1 = 0.0286
	wR2 = 0.1324	wR2 = 0.0626

Table 3-3 Selected crystallographic data for compounds 6 and 7

	6	**7**
Empirical Formula	K_3 [Gd^{III}_2(α-$AlW_{11}O_{39}$)(H_2O)$_{20}$]	K_3 [Dy^{III}_2(α-$AlW_{11}O_{39}$)(H_2O)$_{20}$]
MW	3465.30	3475.80
Crystal System	Orthorhombic	Monoclinic
Space Group	Pna2(1)	P2/c
a / Å	26.755(5)	11.823(2)
b / Å	16.286(3)	11.496(2)
c / Å	11.526(2)	36.034(7)
α / º	90	90.00
β / º	90	98.03(3)
γ / º	90	90.00
V / $Å^3$	5022.2(18)	4849.7(17)
Z	4	4
Crystal Size / mm	0.18×0.06×0.03	0.18×0.18×0.08
R indices [I >2 σ (I)]	R1 = 0.0509	R1 = 0.0360
	wR2 = 0.1263	wR2 = 0.0992
Final R (all data)	R1 = 0.0556	R1 = 0.0408
	wR2 = 0.1300	wR2 = 0.0970

Table 3-4 Selected crystallographic data for compounds 8 and 9

	(**8**)	(**9**)
Empirical Formula	$H_{2.5}Dy^{III}_{2.5}(\alpha\text{-}AlW_{11}O_{39})Cl_{0.5}\ (H_2O)_{28.5}$	$K_3\ [Lu^{III}_2(\alpha\text{-}AlW_{11}O_{39})(H_2O)_{20}]$
MW	3553.30	6173.93
Crystal System	Triclinic	Monoclinic
Space Group	P1	P2(1)/n
a / Å	12.531(3)	11.400(2)
b / Å	15.302(3)	12.552(3)
c / Å	15.561(3)	33.985(7)
α / º	85.86(3)	90
β / º	74.85(3)	91.66(3)
γ / º	87.44(3)	90
V / $Å^3$	2871.6(10)	4861.0(17)
Z	2	4
Crystal Size / mm	0.30×0.30×0.16	0.07×0.04×0.02
R indices [I >2 σ (I)]	R1 = 0.0574	R1 = 0.0431
	wR2 = 0.1294	wR2 = 0.0977
Final R (all data)	R1 = 0.0614	R1 = 0.0561
	wR2 = 0.1374	wR2 = 0.1032

3.3 Results and discussion

3.3.1 Synthesis

The formation of compounds **2** to **9** were affected by pH, counter ions and periodic properties of lanthanides. The pH was maintained between 5 and 7 because the starting material, α-$K_9AlW_{11}O_{39}$ will become α-$K_5AlW_{12}O_{40}$ Keggin when pH is lower than 5. We tried adding KCl to reaction solutions to get the products to crystallize quickly, but this produces an amorphous precipitate. We hypothesize that in these crystal structures K^+ is a counter ion that binds to the surface of POMs and initiates formation of coordination polymers. [15] Excess K^+ accelerates the polymer reaction so that no crystal can be formed. Periodic properties of lanthanides are another important issue. The stoichiometry of our products are Ln : AlW_{11} = 2 : 1. However, the lanthanide complexes on the left of the gadolinium gap form two dimensional complexes, and lanthanides on the right of the gadolinium gap form one dimensional complexes. As a transition metal, yttrium cation reacts with α-$K_9AlW_{11}O_{39}$ to form a 1:1 dimer, even though the reaction stoichiometry is 2:1.

3,3.2 NMR Spectroscopy

All measurements were made in D_2O. After adding lanthanide ions to the starting material slurry, we measured the ^{27}Al NMR of the reaction mixture. The spectral results are presented in Table **3-5** and Figure **3-2**. The low signal to noise ratio can be attributed to low concentration of samples in water. As a quadrupolar nucleus, ^{27}Al has 5/2 spin. In a high symmetric environment, ^{27}Al signal width is very narrow. [17]

Table 3-5. Multinuclear NMR Data

Compound	^{27}Al NMR Chemical Shift (δ, ppm)	Half-width (δ, Hz)
$[\alpha\text{-YAlW}_{11}O_{39}]^{6-}$	68 ppm	278 Hz
$[\alpha\text{-CeAlW}_{11}O_{39}]^{6-}$	66 ppm	274 Hz
$[\alpha\text{-LuAlW}_{11}O_{39}]^{6-}$	67.50 ppm	299 Hz
Compound	^{183}W NMR data [δ, ppm (integration)]	
$[\alpha\text{-YAlW}_{11}O_{39}]^{6-}$	2 (2), -6 (2), -17 (1), -39 (2), -81 (2), -84 (2)	
$[\alpha\text{-CeAlW}_{11}O_{39}]^{6-}$	124 (2), -3 (2), -8 (1), -38 (2), -88 (2)	

When Al environment symmetry is low, the signal width increases so that we observe broad peaks. Here broad peaks suggest that the POM unit is asymmetric because a lanthanide atom occupies the vacancy. Some lanthanide POM samples do not have NMR signal because of low solubility or paramagnetism. [18] The base line is not flat because the NMR probe was made by aluminum, and there is an Al signal from the probe.

Figure 3-2 ^{27}Al NMR Spectra of lanthanide tungstoaluminates.

a. $[\alpha\text{-}YAlW_{11}O_{39}]^{6-}$

b. $[\alpha\text{-}CeAlW_{11}O_{39}]^{6-}$

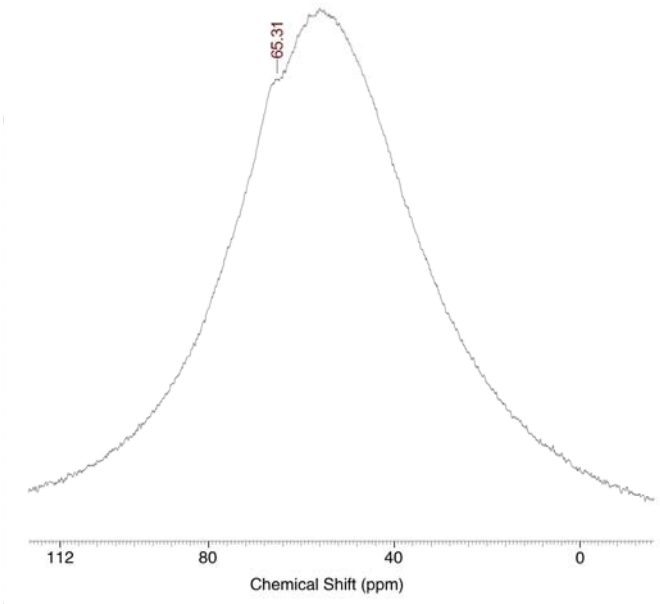

c. $[\alpha\text{-}LuAlW_{11}O_{39}]^{6-}$

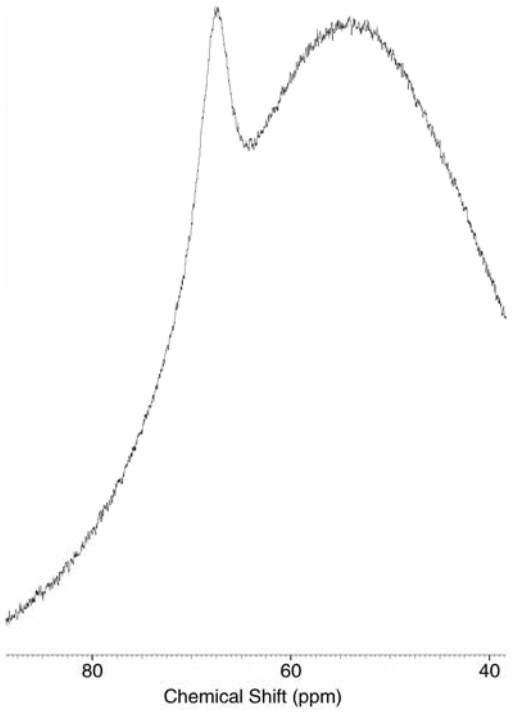

Figure **3-3**. ^{183}W NMR Spectra of lanthanide tungstoaluminates

A: $[\alpha\text{-}YAlW_{11}O_{39}]^{6-}$

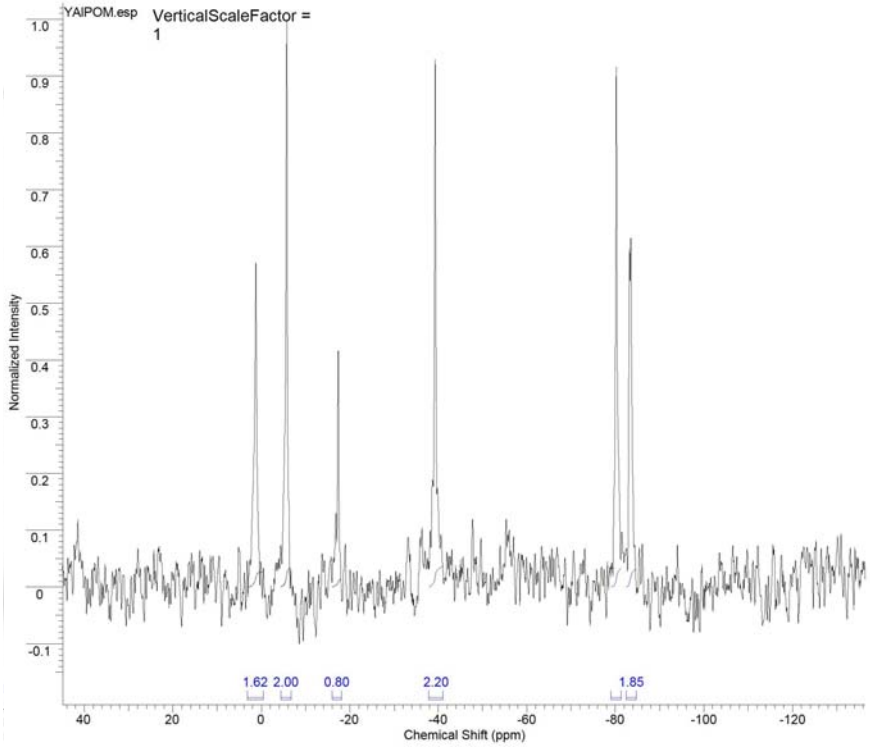

B: $[\alpha\text{-}CeAlW_{11}O_{39}]^{6-}$

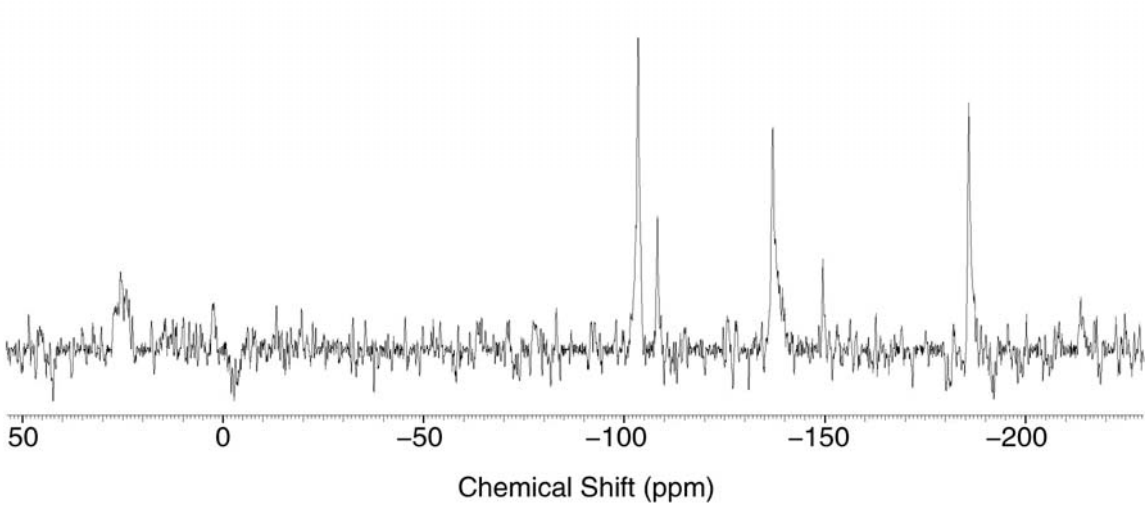

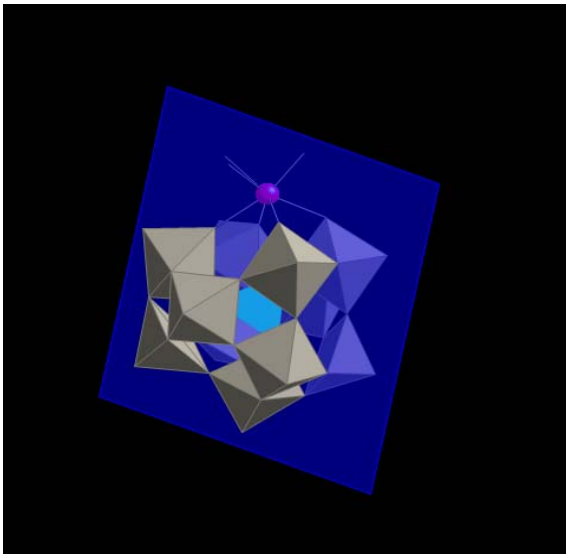

Fig **3-4** Cs symmetry of Lanthanide POM **5**

Only compounds **2** and **4** are soluble enough in D_2O to get reasonable ^{183}W NMR , and the results are shown in Figure **3-3**. The $LnAlW_{11}O_{39}$ unit has Cs symmetry. From the single crystal structure in Figure **3-4**, we can find that here are five pairs of identical tungstate atoms located at each side of the symmetric plane and one tungsten atom is on the plane. The ^{183}W NMR of **1** shows good agreement with Cs symmetry, which is very similar to other monovacant Keggins and their derivatives such as $[\alpha\text{-}SiW_{11}O_{39}]^{8-}$ and $[\alpha\text{-}PW_{11}O_{39}]^{7-}$.[19][20] The ^{183}W NMR of **3** also shows that it has Cs symmetry. Because Ce^{3+} is paramagnetic, few peaks are observed. Presumably some peaks are shifted and / or broadened due to the paramagnetic Ce^{3+}.

3.3.3 Crystal Structures.

There are two important subunits that can be found in the crystal structures: the $[\alpha\text{-}MAlW_{11}O_{39}]^{9-}$ (M = Y (III) or Lanthanide (III) ion) anion units and cations binding to

the surface of the POM. The $[\alpha\text{-MAlW}_{11}O_{39}]^{9-}$ anion has an internal AlO_4 tetrahedron, surrounded by eleven $W^{VI}O_3$ fragments constituting the polyoxometalate surface.

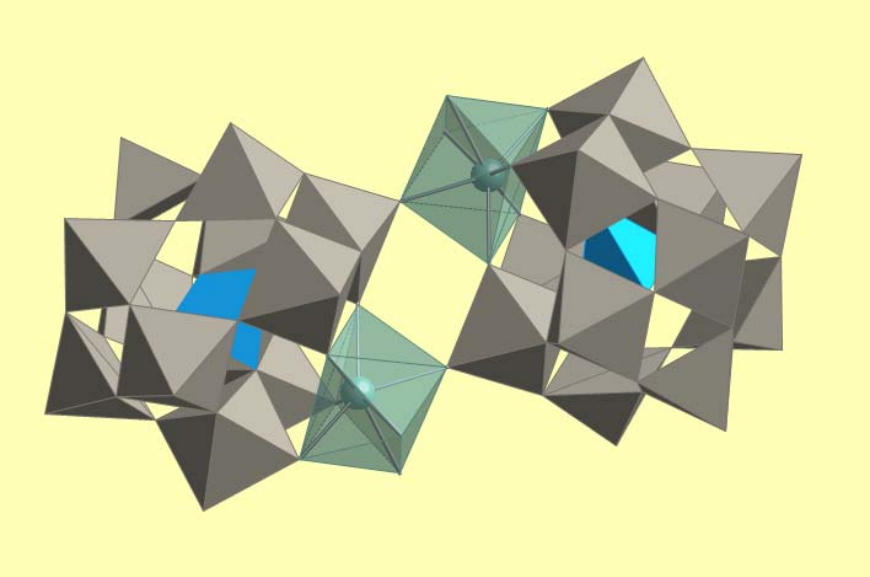

Figure 3-5 Compound **2** ($H_6KY(\alpha\text{-AlW}_{11}O_{39})Cl\ (H_2O)_{20}$) 1:1 Dimer Structure . Blue: Al; Grey: W; Green: Y

Shown on Figure **3-5**, compound **2** is a dimer structure with $Y^{3+}/[\alpha\text{-AlW}_{11}O_{39}]^{9-}$ in a 1:1 ratio. Coordinated by four unsaturated oxygen atoms of $[\alpha\text{-AlW}_{11}O_{39}]^{9-}$ anions, a 7-coordinate Yttrium cation is located in the vacancy position of lacunary anion. There are three terminal oxygen atoms coordinated to the Yttrium center. The Yttrium atom bonds to the other POM anion in the dimer via the terminal oxygen atom along the x-axis. The distance between Yttrium and O616, one of the oxygen atom of tetrahedral AlO_4 unit, is only 2.68 Å. The distance between the Yttrium and Al center is only 3.96 Å, which is currently the smallest vacancy to center distance in this type of lanthanide Aluminum Keggin mono derivative. The ORTEP representation of one $Y(III)AlW_{11}O_{39}$ unit of compound **2** is shown in Figure **3-6**.

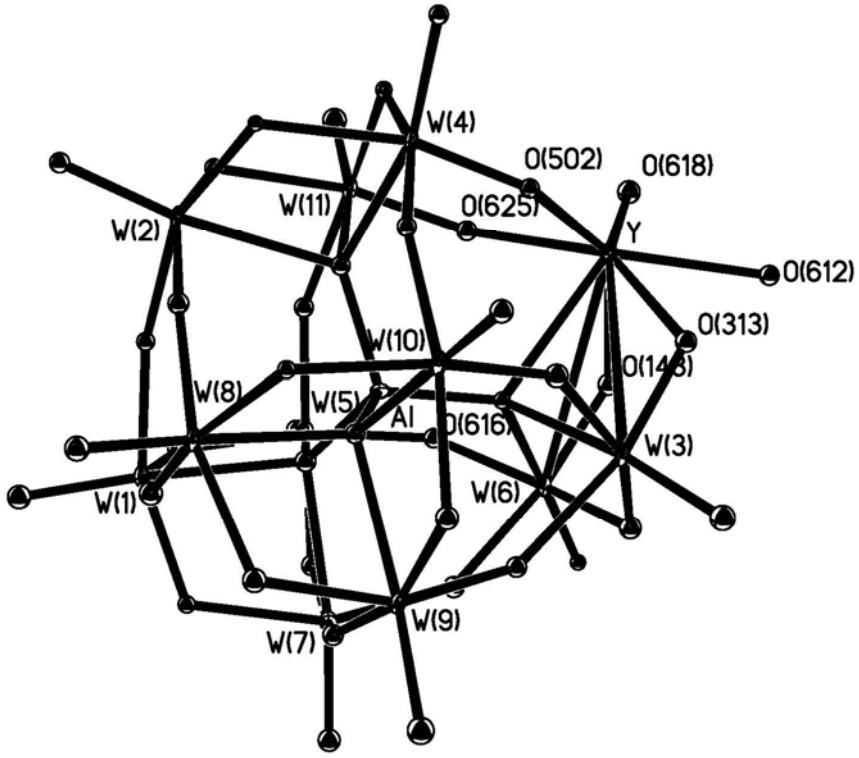

Figure **3-6** ORTEP representation of Compound **2**.

Compound **3**, **4**, **5** and **6** have very similar structure to each other. The structure of compound **5**, K_3 $[Sm^{III}_2(\alpha\text{-}AlW_{11}O_{39})(H_2O)_{20}]$, is shown in Figure **3-7**. The ORTEP representation of Compound **5** is shown in Figure **3-8**. Compound **5** is representative of one structure type which we will call A. In this type of structure, $Ln^{3+}/[\alpha\text{-}AlW_{11}O_{39}]^{9-}$ ratio is 2:1. There are two lanthanide cations per POM unit. One eight-coordinate lanthanide cation is bound to 4 exposed lacunary oxygen atoms. This lanthanide center is in a distorted square antiprismatic geometry. The other lanthanide cation is bound to the surface of the POM anion via a terminal oxygen of a WO_3 unit close to the lacunary site.

In compounds **3** to **6**, the surface-bound, nine coordinate lanthanide acts as a bridging unit to another $[\alpha\text{-}LnAlW_{11}O_{39}]^{6-}$ unit.

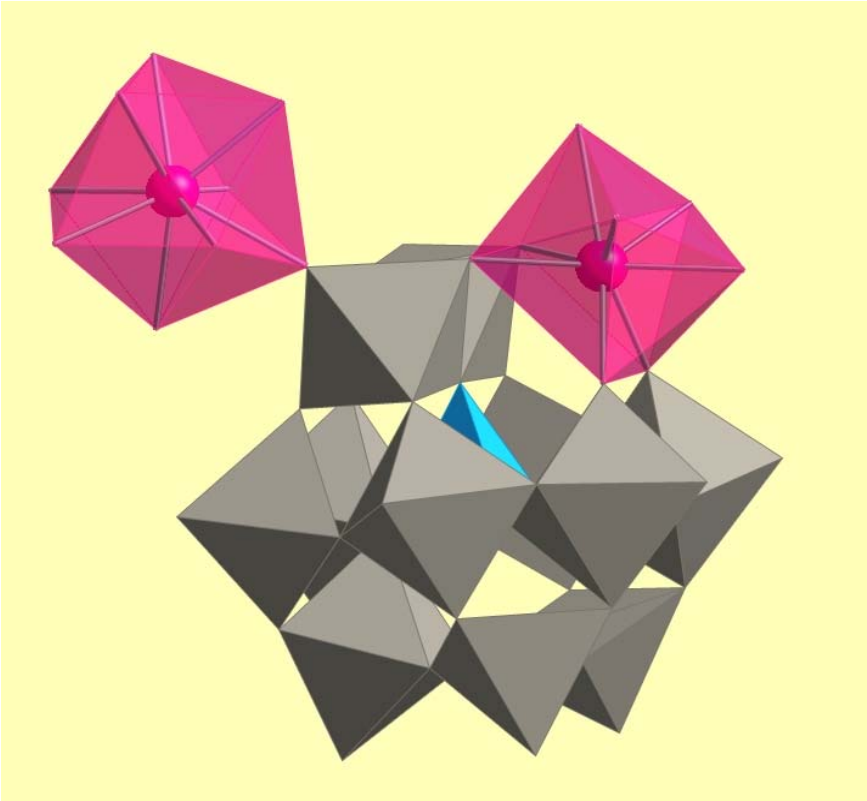

Figure 3-7 Structure of Compound **5**. Blue: Al; Grey: W; Red: Sm. This A type structure is shared by compounds **3**, **4**, **5** and **6**.

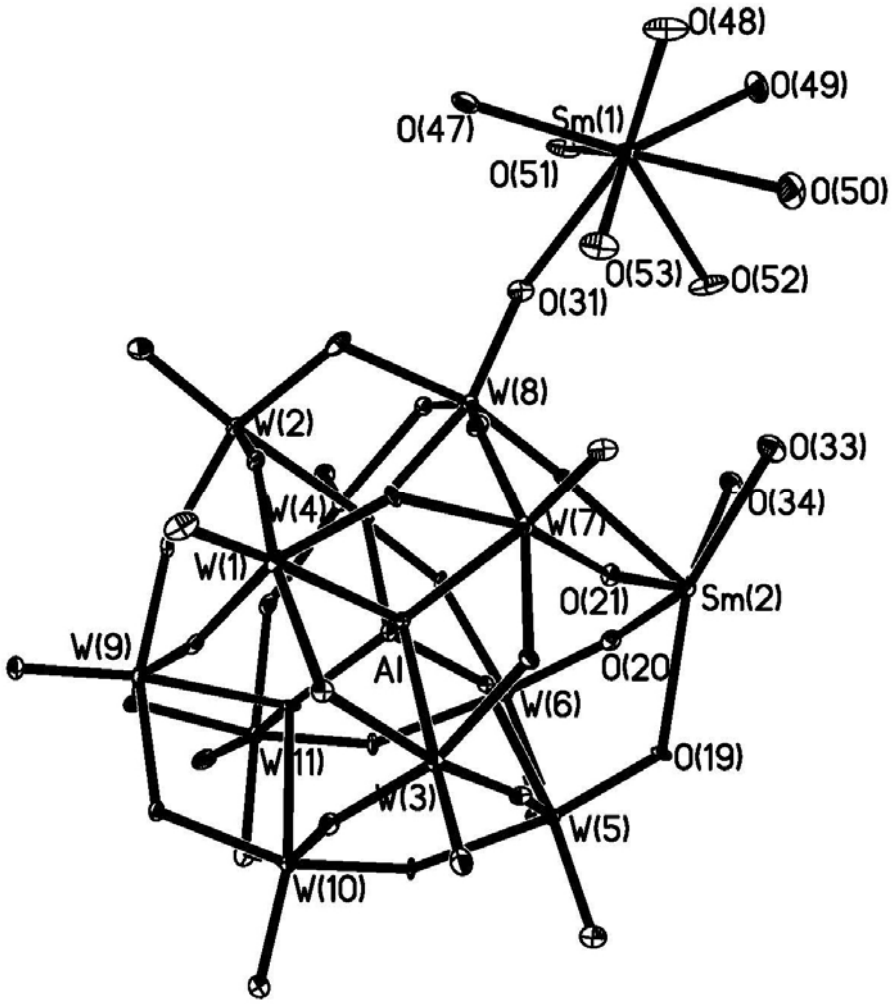

Figure **3-8** ORTEP representation of Compound **5**.

Figure **3-9** and **3-10** are packing diagrams for compound **5**. The packing diggrams for **3**, **4**, **5**, and **6** are identical. The structure units pack into a layer-by-layer structure. Each of the two dimensional layers are parallel to the xy plane and perpendicular to the z axis.

a.

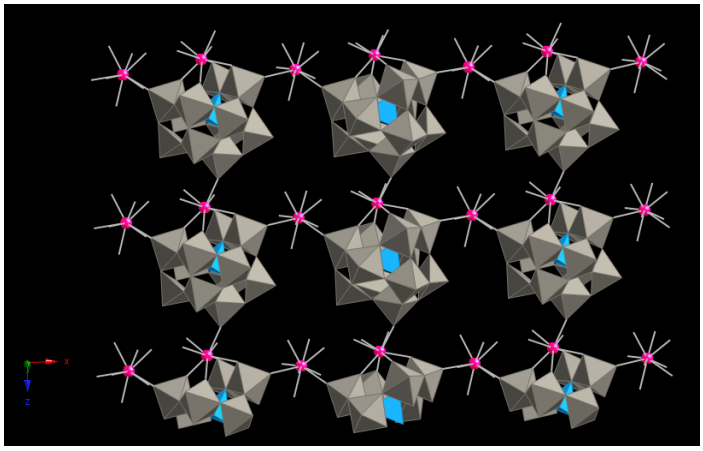

b.

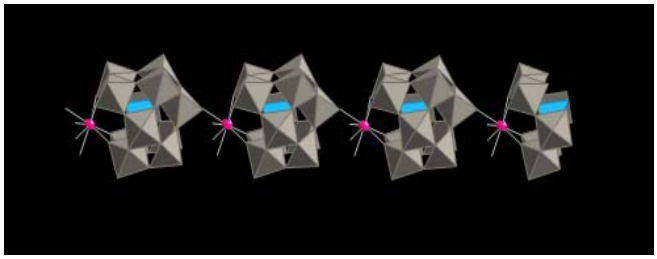

c.

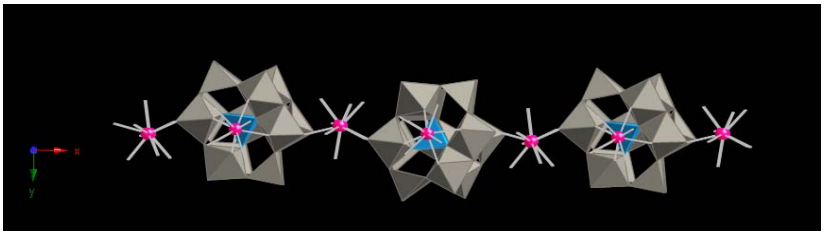

Figure 3-9 Two-dimensional layer in compound **5**, K_3 [Sm^{III}_2(α-$AlW_{11}O_{39}$)$(H_2O)_{20}$], single crystal. Blue: Al; Grey: W; Red: Sm. This is type A crystal structure is found for compounds **3**, **4**, **5,** and **6**. **3-8**a: view in x-z plane. **3-8**b: view in y-z plane. **3-8**a: view in x-y plane.

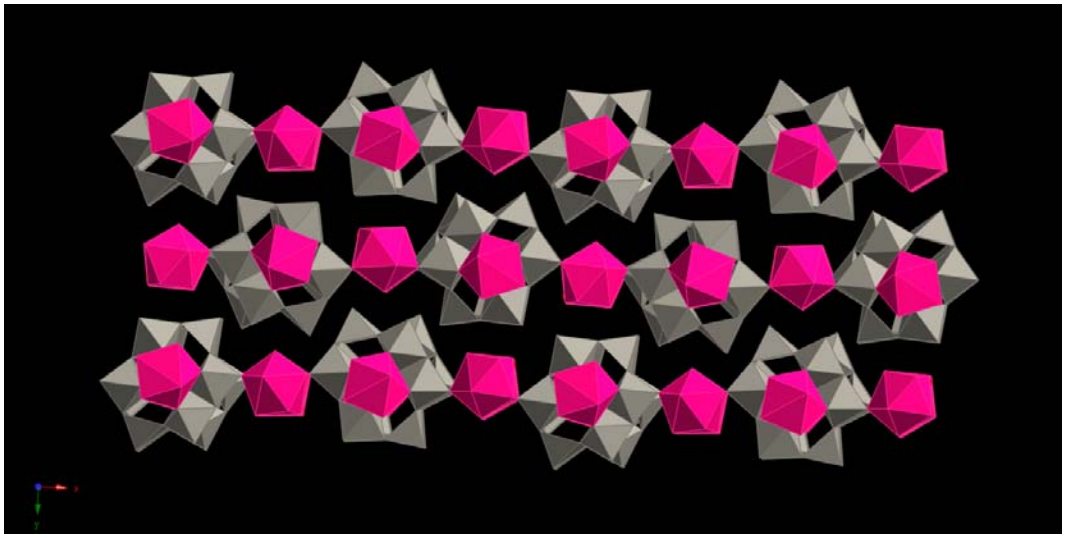

Figure 3-10 layer-by-layer structure in compound 5 single crystal. Blue: Al; Grey: W; Red: Sm. This view is down the z axis, and look at the x-y plane.

The eight-coordinate Ln^{3+} in the vacancy of the polyoxometalate is bound to the base of another [α-$AlW_{11}O_{39}$] unit in a head-to-toe fashion, forming an infinite linear arrangement along the z axis. These linear chains are interconnected by surface-bound Ln^{3+} ions. Each Lanthanide is 9-coordinate and connects each discrete [α-$LnAlW_{11}O_{39}$]$^{6-}$ unit from the shoulder position, forming the two dimensional layer. Each [α-$LnAlW_{11}O_{39}$]$^{6-}$ one dimensional chain is alternately flipped 180º around the z axis. In other words, the two dimensional layer was formed by zigzag chains if we look from z-axis direction. The layer-by-layer structure actually is very similar to an interdigitated supramolecular laminate structure, a cartoon of this structure shown in Figure **3-10**. [21]

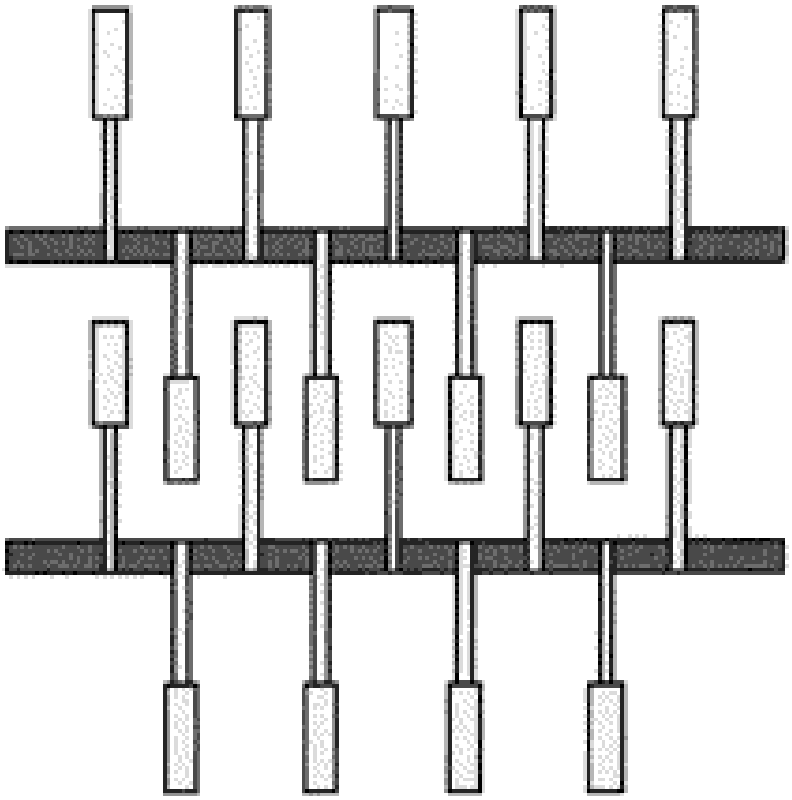

Figure 3-11 A example of interdigitation mode. This figure was abstracted from reference [21].

Compounds **7** and **9,** K_3 $[Lu^{III}_2(\alpha\text{-}AlW_{11}O_{39})(H_2O)_{20}]$, share similar unit structures. The structure and ORTEP representation of Compound **7** (a B-type structure) is shown in Figure **3-12** and **3-13**. Similar to compound **3** to **6**, the type B structure has an eight-coordinate lanthanide atom in vacancy. This vacancy lanthanide is also in a distorted square antiprismatic geometry. The second lanthanide ion is also bound to a terminal oxygen of a WO_3 unit but is located further away from the lacunary site than for the A structure and does not act as a bridging unit between the $[\alpha\text{-}LnAlW_{11}O_{39}]^{6-}$ POMs. This terminal lanthanide, unlike the 9-coordinate bridging lanthanide in the compound **3** to **6**, is eight coordinate in a distorted square anti prismatic geometry.

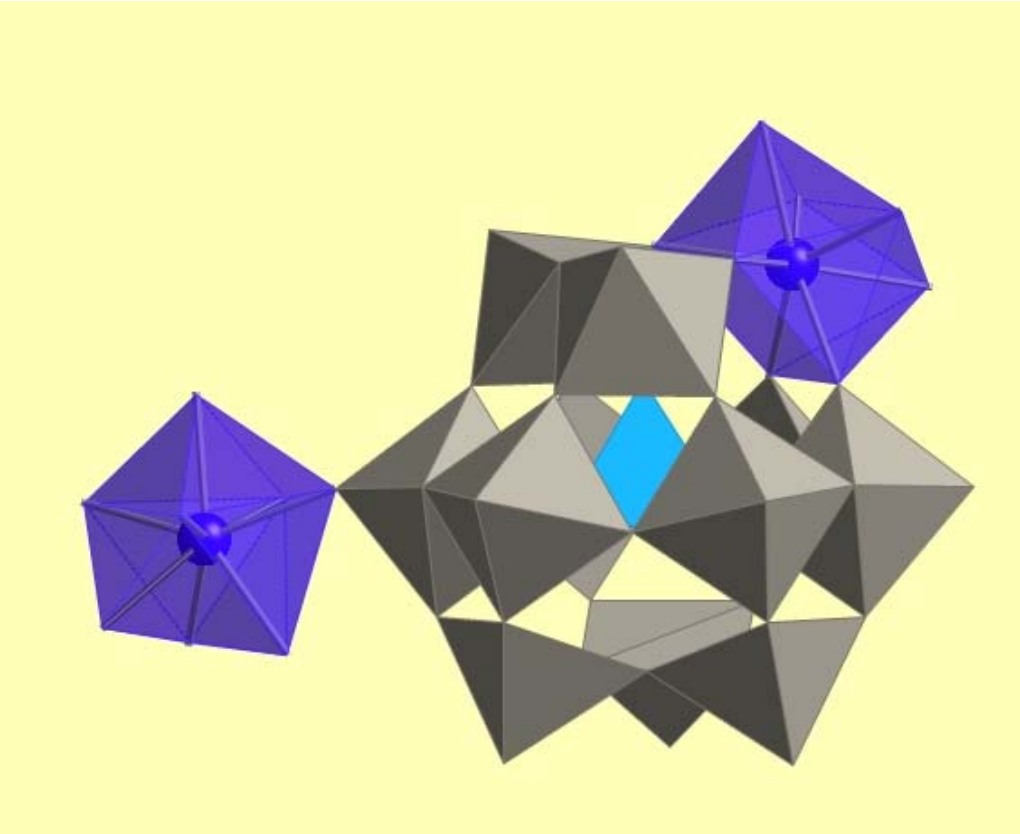

Figure **3-12** Structure of Compound **7**. Blue: Al; Grey: W; Red: Dy. This is designed as B-type structure that is common to compound **7** and **9**.

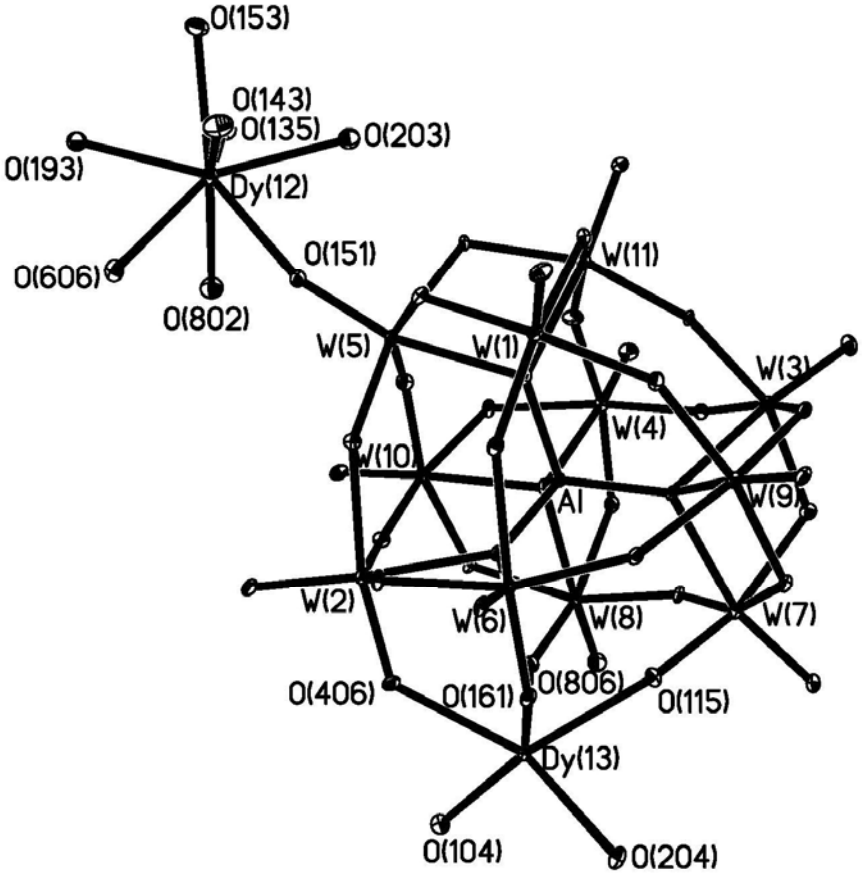

Figure **3-13** ORTEP representation of Compound **7**, K_3 [Dy^{III}_2(α-$AlW_{11}O_{39}$)$(H_2O)_{20}$]. This structure type is denoted as Type B. Compounds **7** and **9** share this structure.

Because the lanthanide occupying the vacancy coordinates to an adjacent POM through the face WO_3 unit that is next to the vacancy, compound **7** and **9**'s packing structure is a one dimensional zigzag chain (Shown in Figure **3-14,** Figure **3-15**, and Figure **3-16**). On each chain, all POM subunits are on the same plane parallel to the x

axis. If we view a chain from the x axis, the chain looks like a dimer, so we call the plane a dimer plane.

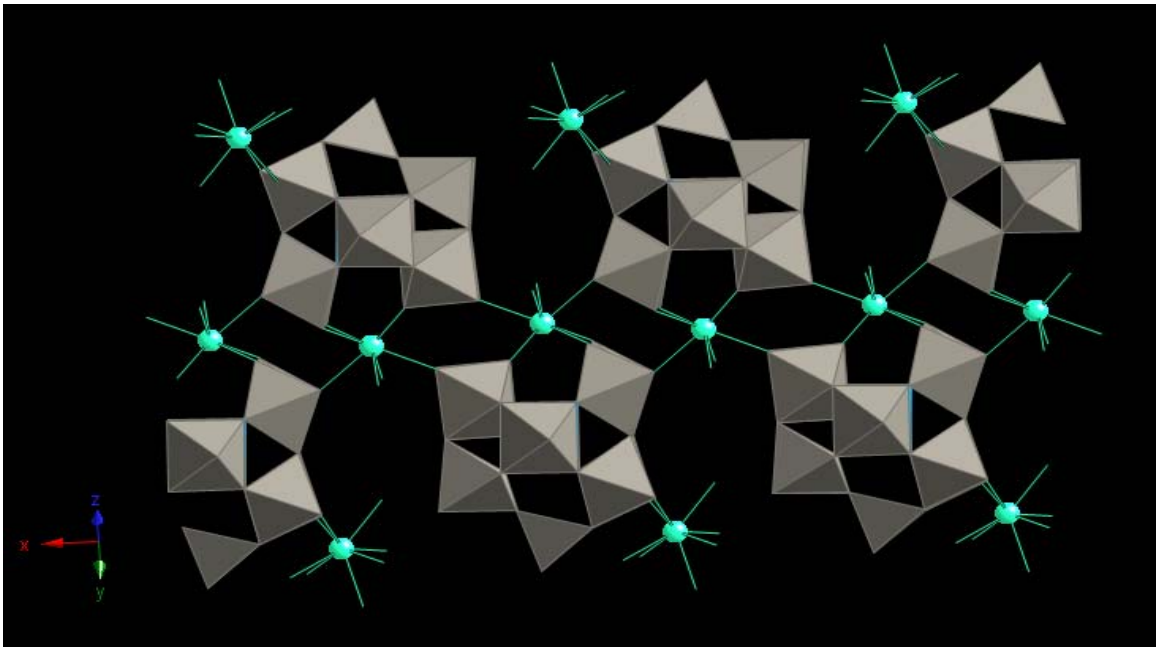

Figure **3-14** One dimension packing structure of compound **9**, K_3 [Lu^{III}_2(α-$AlW_{11}O_{39}$)$(H_2O)_{20}$] showing the Lu(III) and the Al POM. Grey: W; Green: Lu.

Compound **7** and **9**'s chains are in different alignments because potassium cations bind to the surface of the POM in different positions. For compound **6**, all one-dimensional chains are parallel to the y axis, and all dimer planes are parallel to each other. For compound **7**, all one-dimensional chains are parallel to the x axis. Viewed from the x axis, there are two different dimer plans that are oriented 143.2 degrees from each other.

Although using same starting materials, the structure of compound **8** is different from compound **7**. **8** has the formula $H_{2.5}Dy^{III}_{2.5}$(α-$AlW_{11}O_{39}$)$Cl_{0.5}$ $(H_2O)_{28.5}$,

there is 0.5 more Dy^{3+} cation on the surface of each POM unit. Compared to **7**, these Dy^{3+} cations connect POMs and form the one dimensional structure shown in Figure **3-17**.

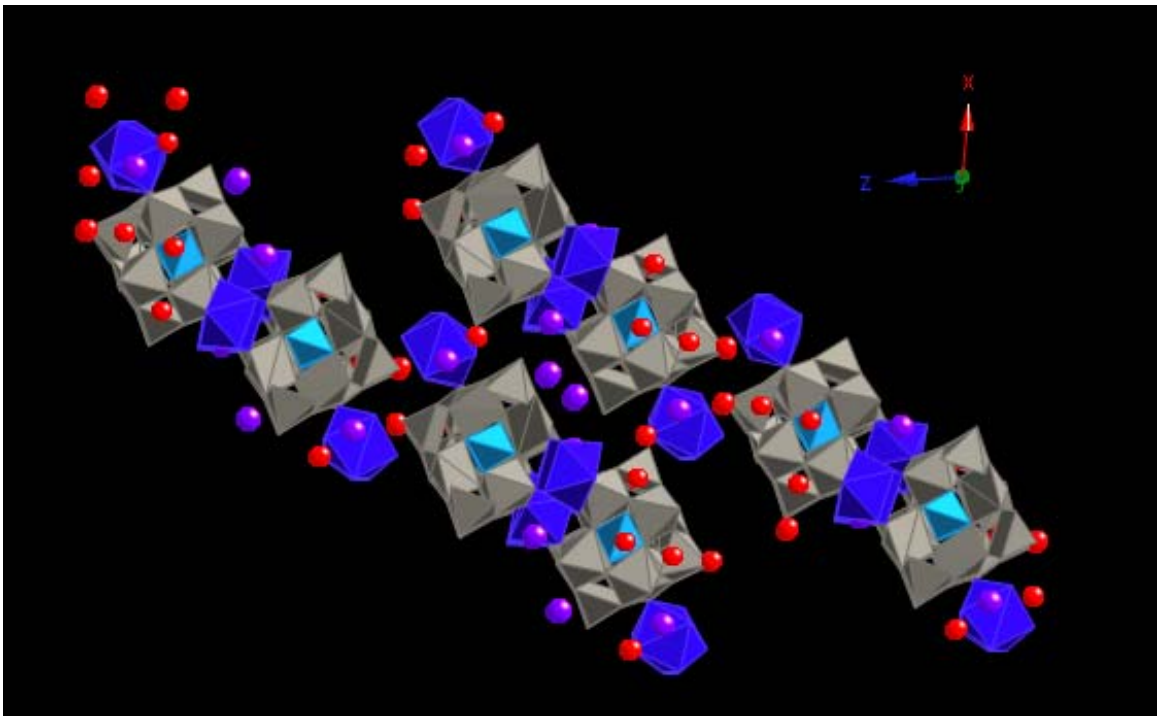

Figure **3-15** 1-D chains distribution in compound **7,** K_3 $[Dy^{III}_2(\alpha\text{-}AlW_{11}O_{39})(H_2O)_{20}]$, single crystal. This picture shows the water molecules as red sphere, and potassium atoms as purple sphere. Deep Blue: Dy; Blue: Al; Grey: W; Red: O; Purple: K.

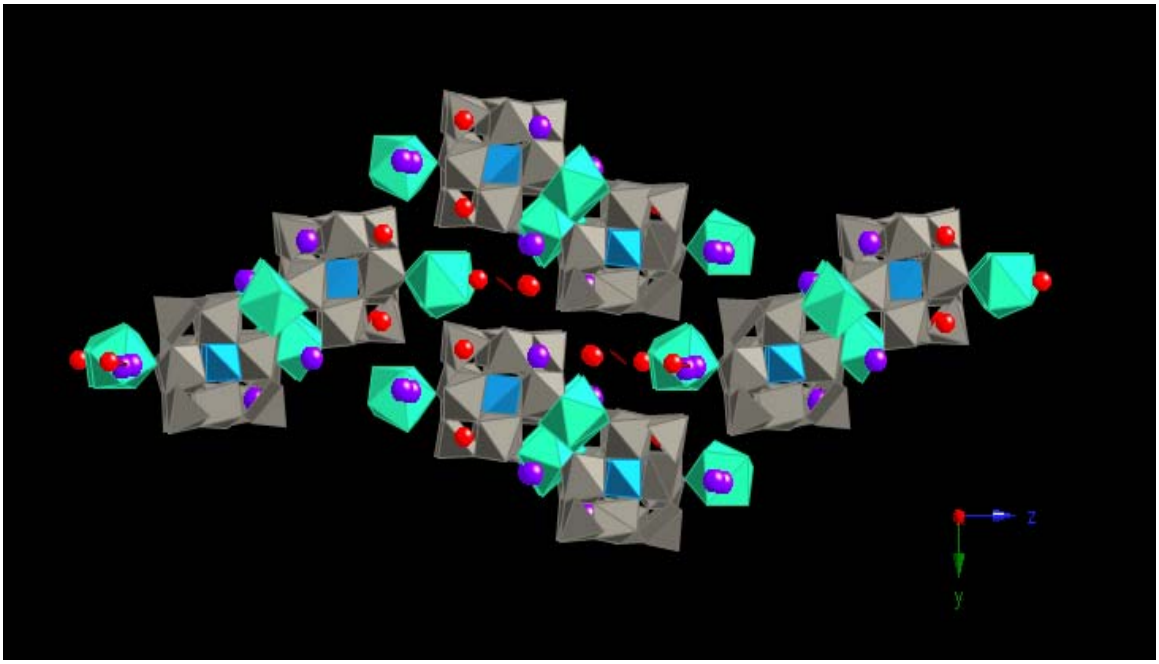

Figure **3-16** 1-D chains distribution in compound **9,** K_3 [Lu^{III}_2(α-$AlW_{11}O_{39}$)$(H_2O)_{20}$] viewed down y-z plane. This picture shows the water molecules as red sphere, and potassium atoms as purple sphere. Green: Lu; Blue: Al; Grey: W; Red: O; K:purple.

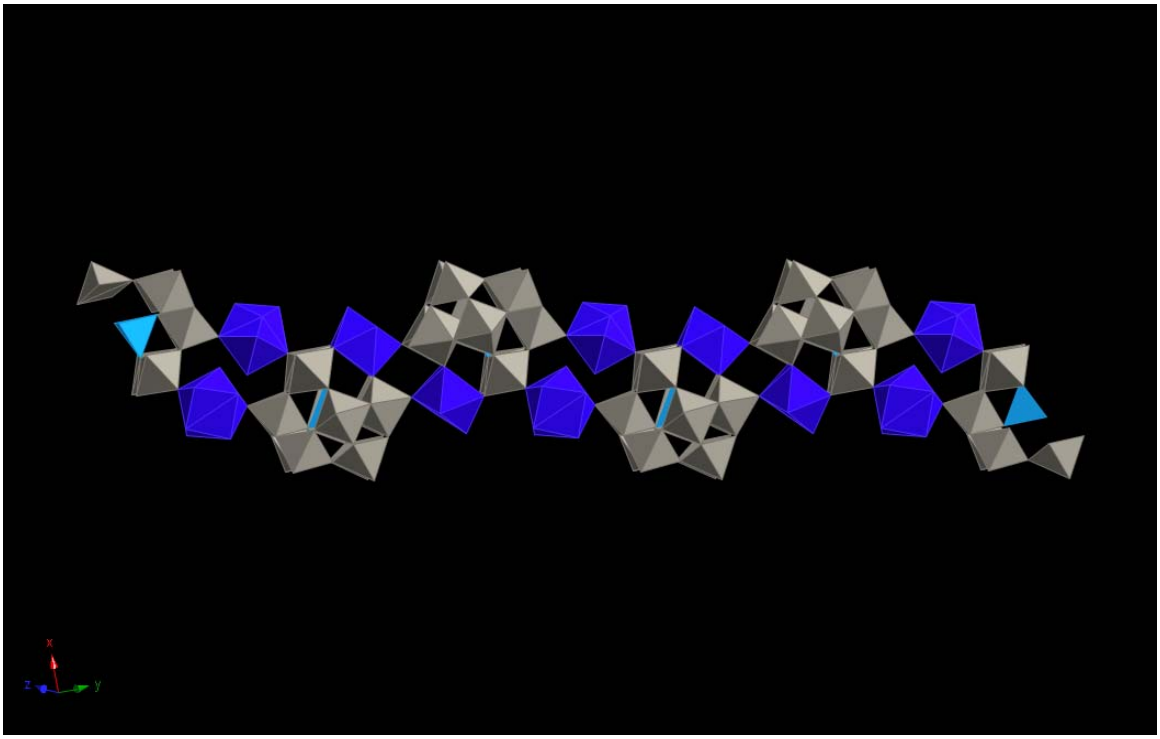

Figure **3-17** One dimension packing structure of compound **8**, $H_{2.5}Dy^{III}_{2.5}(\alpha\text{-}AlW_{11}O_{39})Cl_{0.5}\ (H_2O)_{28.5}$, Deep Blue: Dy; Blue: Al; Grey: W; Red: O

These compounds are dimers, two-dimensional layers or one-dimensional chain structures. Since POM units are relatively large, there is lots of empty space between different POM units. There are likely water molecules and K^+ counter ions in that space. There are three potassium cations and many water molecules binding to each POM unit in compound **3**, **4**, **5** and **6** structures. We call this little space between POMs as solvent channels. There are six potassium atoms binding to each POM unit and connecting to adjacent POMs in compound **6**. 3 × 4 Å holes with water molecules inside were found in the POM molecule (Figure **3-18**). The average interlayer separations are approximately 2.7 Å. Between different layers there are channels with a 17.2 × 11.2 Å cross sectional

area that contain water molecules. Shown in Figure **3-19**, water solvent holes were found in **8** in the x axis direction with a 13.3 ×5.8 Å cross sectional area and in the y axis direction with a 4 ×2.5 Å cross sectional area. Compound **9** shown in Figure **3-20**, water solvent holes were found in the x axis direction with a 5.5 ×6 Å cross sectional area and in the y-axial direction with a 5.3 ×2.8 Å cross sectional area.

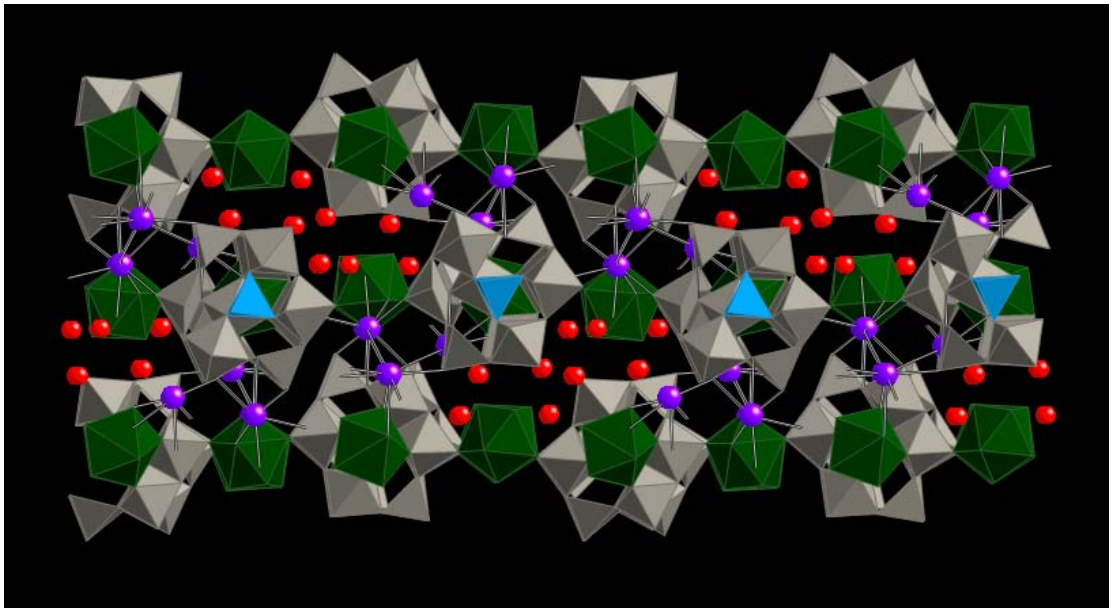

Figure **3-18** Solvent Channels between 2D layers in compound **6.** Green: Gd; Grey: W; Purple: K; Red: Water

The ionic radius of the heteroatom influences how lanthanide ions are incorporated into the POM framework. The ionic radius of Al^{3+} (53.5 pm) is similar to that of Ge^{4+}(53 pm), and is significantly larger than Si^{4+} (40 pm) and the lanthanide cation can be incorporated into the polyoxometalate framework to the same degree as analogous [α-$GeW_{11}O_{39}]^{8-}$ complexes and much deeper than in [α-$SiW_{11}O_{39}]^{8-}$ examples. [10][14] For instance, in **4**, ($K_3[Sm^{III}_2(\alpha\text{-}AlW_{11}O_{39})(H_2O)_{20}]$), the Al···Sm distance is 4.311 Å, which is

significantly shorter than Si···Sm (4.537 Å). [14]

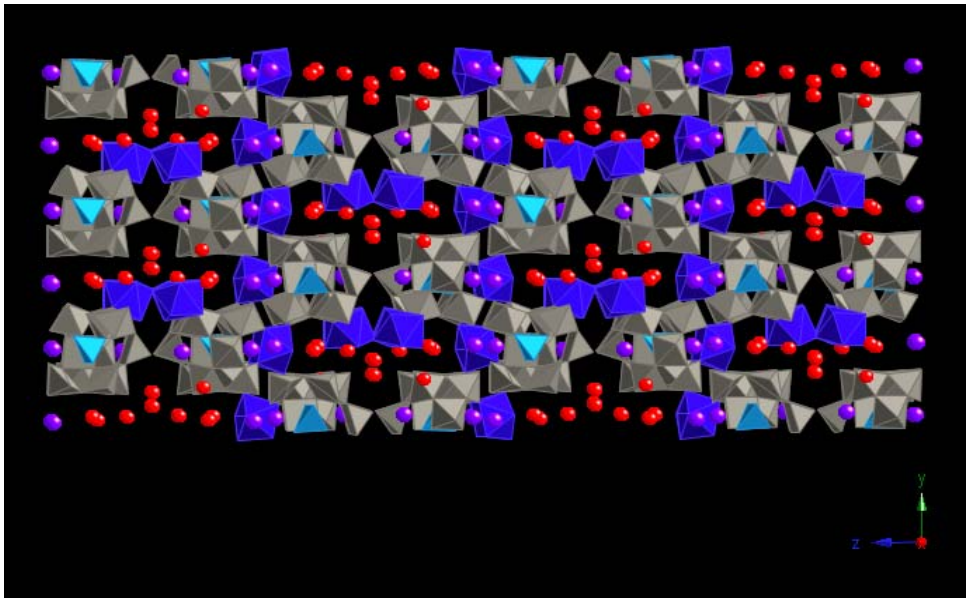

Figure **3-19** Solvent Channels found in compound **7**. Deep blue: Dy; Blue: Al; Grey: W; Purple: K; Red: Water

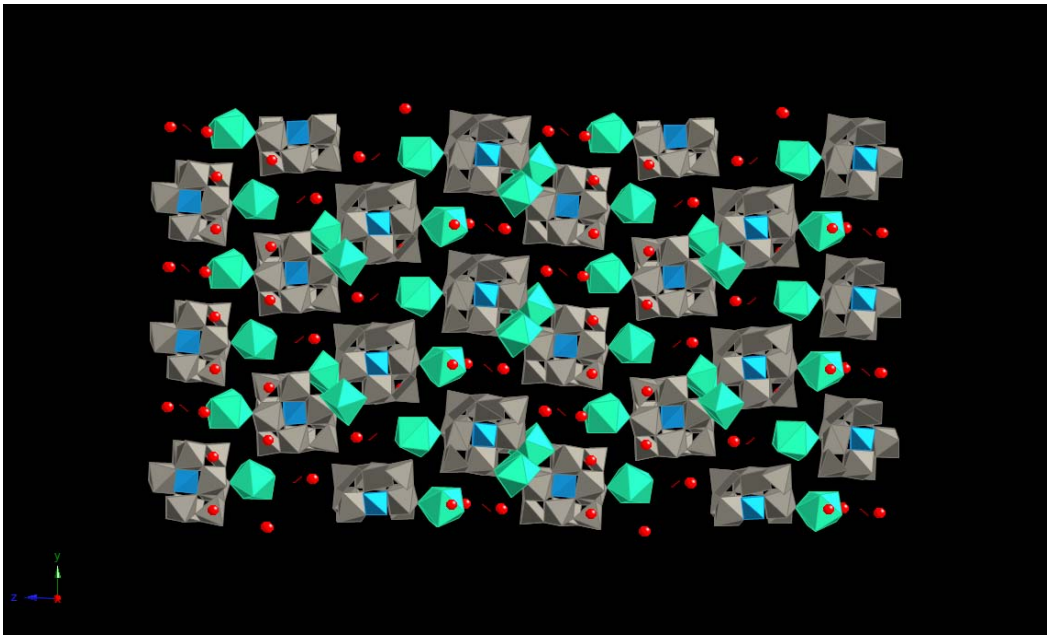

Figure **3-20** Solvent Channels found in compound **9**. Green Lu; Blue: Al; Grey: W; Purple: K; Red: Water

Table **3-6** is a list of lanthanide-oxygen bond lengths and lanthanide-aluminum distances. In the vacancy, lanthanide-oxygen bond lengths decrease across the lanthanides series. Bridging lanthanide-oxygen bond lengths decrease from the left side of lanthanide period to the right. Type B compounds possess a longer bridging lanthanide-oxygen bond length than type A. The Ln…Al distances also decrease from left to the right, however, Dy (**6**) is significantly larger than Gd (**5**).

Table 3-6 Selected bond length and atom distance.

	Vacancy Metal-Oxygen Bond Length (Å)	Bridging Metal-Oxygen Bond Length (Å)	Vacancy Metal to Aluminum Center Distance (Å)
Y (**2**)	2.33(6) Max 2.24(5) Min 2.28(8) Average	n/a	3.96(3)
La (**3**)	2.46(2) Max 2.39(0) Min 2.43(8) Average	2.50(4) (v) 2.51(2) (e) 2.58(0) (e)	4.37(1)
Ce (**4**)	2.46(0) Max 2.40(2) Min 2.43(2) Average	2.47(7) (v) 2.51(7) (e) 2.57(7) (e)	4.36(7)
Sm (**5**)	2.38(8) Max 2.34(2) Min 2.37(1) Average	2.40(6) (v) 2.46(6) (e) 2.55(9) (e)	4.31(2)
Gd (**6**)	2.35(8) Max 2.32(4) Min 2.34(2) Average	2.37(4) (v) 2.47(2) (e) 2.57(8) (e)	4.30(6)
Dy (**7**)	2.35(4) Max 2.29(6) Min 2.33(5) Average	2.42(6) (v) 2.41(2) (e)	4.34(8)
Lu (**9**)	2.29(5) Max 2.26(6) Min 2.28(2) Average	2.41(1) (v) 2.29(7) (e)	4.29(4)

v = metal in vacancy position

e = metal bonding to surface terminal oxygen

From previous literature, normally Keggin lanthanide complexes like to form one dimensional packing structure. Shown in Figure **3-21**, there are three different kinds of 1D packing structures: linear, zigzag, and dimeric chains. One dimensional compound **7** and **9** are actually 1D zigzag chain structure which is very similar to $[Eu(\alpha\text{-}SiW_{11}O_{39})(H_2O)_2]^{5-}$ zigzag chain. [10] Compound **8** actually is a dimeric structure which is very similar to) $[Nd_2(\alpha\text{-}SiW_{11}O_{39})(H_2O)_{11}]^{2-}$, [10] but one of the Dy^{3+} on the POM surface of **8** has 50% occupancy.

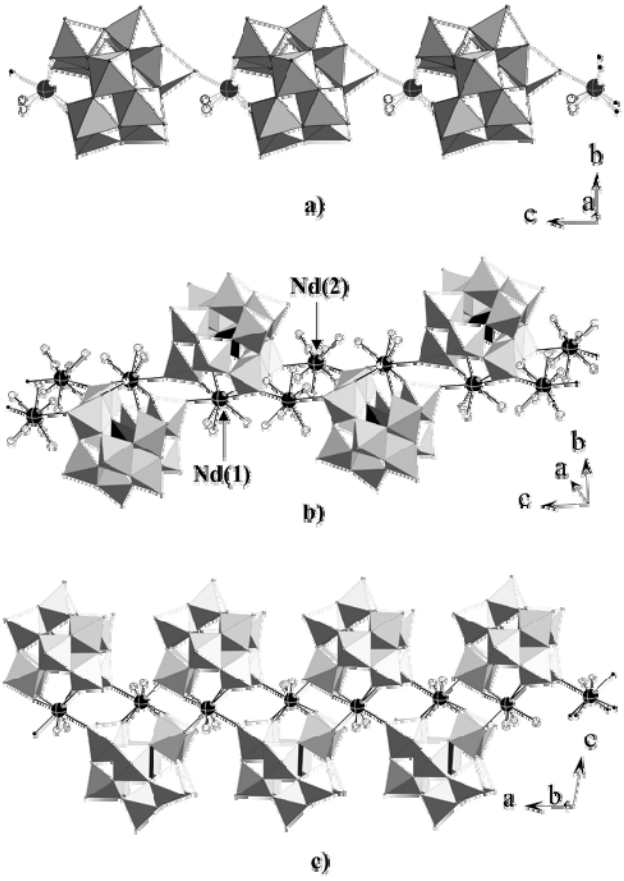

Figure **3-21** Polyhedral representation of $\alpha\text{-}SiW_{11}O_{39}$ coordination 1D polymers which is a) $[Yb(\alpha\text{-}SiW_{11}O_{39})(H_2O)_2]^{5-}$ linear chain b) $[Nd_2(\alpha\text{-}SiW_{11}O_{39})(H_2O)_{11}]^{2-}$ dimeric chain and c) $[Eu(\alpha\text{-}SiW_{11}O_{39})(H_2O)_2]^{5-}$ zigzag chain. Abstracted from reference [10].

When 1D chains are connected by more lanthanide building blocks, 2D polymers formed. Observing from x axis direction, compound **3**, **4**, **5**, and **6** are linear chain structures (Figure **3-8**), which are different from the other previously reported 2D structures in Figure **3-22**, where the 1D chains are zigzag structure (Figure **3-21**b). [10]

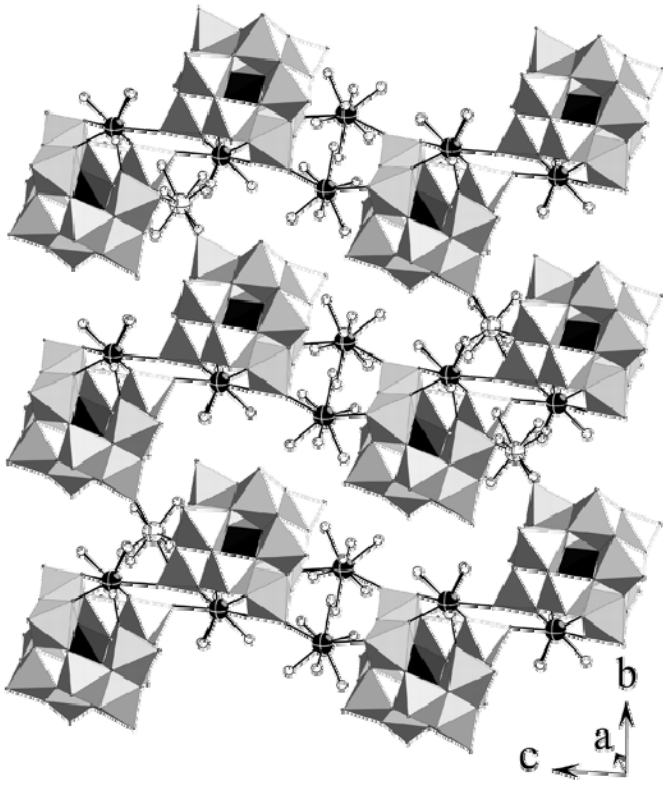

Figure **3-22** 2D arrangement of $[Nd_2(\alpha\text{-}SiW_{11}O_{39})(H_2O)_{11}]^{2-}$. This picture was abstracted from reference [10]

3.4 Conclusion

In this chapter, eight new lanthanide tungstoaluminate compounds, $H_6KY(\alpha\text{-}AlW_{11}O_{39})Cl(H_2O)_{20}$, **2,** $K_3Ln^{III}_2(\alpha\text{-}AlW_{11}O_{39})(H_2O)_{20}$ (Ln^{III} = La^{III} **3**, Ce^{III} **4**, Sm^{III} **5**, Gd^{III} **6**, Dy^{III} **7**, Lu^{III} **9**) and $H_{2.5}Dy^{III}_{2.5}(\alpha\text{-}AlW_{11}O_{39})Cl_{0.5}$ $(H_2O)_{28.5}$**, 8** have been

synthesized and characterized by IR spectroscopy, NMR spectroscopy, and single-crystal X-ray diffraction. ^{27}Al NMR of **2, 4** and **9** showed that the Al $(O)_4$ unit in the center is a distorted tetrahedral structure. ^{183}W NMR of **2** and **4** showed that these lanthanide Keggin anions have Cs symmetry in aqueous solution. **2** is a dimer structure. The single-crystal structures of **3**, **4**, **5**, and **6** showed that each α-$AlW_{11}O_{39}$ was connected by lanthanide (III) cations and formed a 2D network. The single-crystal structure of **7** and **9** showed that each $AlW_{11}O_{39}$ unit was connected by Lanthanide (III) cations and formed a 1D chain structure in two different ways.

3.5 Reference

[1] D. Parker, R. Dickins, H. Puschmann, C. Crossland, and J. Howard, *Chem. Rev.*, **2002**, 102 (6), 1977–2010

[2] J. Kido and Y. Okamoto, *Chem. Rev.*, **2002**, 102 (6), 2357–2368

[3] T. Yamase, and H. Naruke, *Coordination Chemistry Reviews*, Vol. 111, **1991**, 83-90

[4] J. Bünzli and C. Piguet, *Chem. Rev.*, **2002**, 102 (6), 1897–1928

[5] U. Kortz, A. Müller, J. Slageren, J. Schnack, N. Dalal and M. Dressel, *Coordination Chemistry Reviews*, Vol. 253, Issues 19-20, **2009**, 2315-2327

[6] T. Akutagawa, D. Endo, S. Noro, L. Cronin and T. Nakamura, *Coordination Chemistry Reviews*, Vol 251, Issues 21-24, **2007**, 2547-2561

[7] N. Kaltsoyannis, P. Scott, *The f-Elements*; Oxford University, **1999**.

[8] M. Drew, *Coord. Chem. Rev.* **1977**, *24*, 179.

[9] J. Cowan, A. Bailey, R. Heintz, B. Do, K. Hardcastle, C. Hill, and I. Weinstock, *Inorg. Chem.,* **2001**, 40 (26), 6666 -6675.

[10] P. Mialane, L. Lisnard, A. Mallard, J. Marrot, E. Antic-Fidancev, P. Aschehoug, D. Vivien, and F. Sécheresse, *Inorg Chem.* **2003**, 42, 2102-2108

[11] M. Sadakane, M. Dickman, M. Pope, *Angrew. Chem. Int. Ed*. **2000**, 39, No.16 2914

[12] J. Wang, J. Zhao, X. Duan, and J. Niu, *Crystal Growth & Design*, **2006**, Vol. 6, No. 2, 507-513

[13] F. Li, L. Xu, Y. Wei, G.Gao, L. Fan, Z. Li, *Inorg. Chim Acta.,* 359, 3795

[14] J, Wang, X, Duan, X, Du, and J, Niu, *Crystal Growth & Design*, **2006**, Vol. 6, No. 2, 2266-2270

[15] J. Cowan; C. Hill; R. Reiner and I. Weinstock., *Inorg. Synth*, Vol. 33

[16] *SHELXTL*, Brucker AXS, Inc., Bruker Advanced X-ray Solutions, **1999**

[17] J. Mason, *Multinuclear NMR*, **1987**

[18] M. Zimmermann , N. Frøystein, A. Fischbach, P. Sirsch, H. Dietrich, K. Törnroos, E. Herdtweck, R. Anwander, *Chem. Eur. J.* **2007**, 13, 8784-8800

[19] C. Zhang, R. Howell, K. Scotland, F. Perez, L. Todaro, L. Francesconi, *Inorg Chem.* **2004**. 43, 7691-7701

[20] T. Yamase, M. Pope, *Polyoxometalate Chemistry for Nano-Composite Design*; Kluwer: Academic Publishers: Dordrecht, The Netherlands, **2002**.

[21] B. Moulton and M. Zaworotko *Chem. Rev.*, **2001**, 101 (6),1629–1658.

Chapter 4. Potential Material for Molecular Information Storage Device: Nanoscale properties of Coordination Polymers of Lanthanide Tungstoaluminates

4.1 Introduction

As we find ourselves in the 21st century, we notice that the IT industry is suffering because Moore's law is reaching its ultimate limit. Hard drive manufacturers are no exception to this statement that is all the more becoming a reality. Invented by IBM in 1956, the hard drive has become an important information storage device in our modern lives. The structure of the hard drive is shown in Figure 4-1. Information is stored on the disk plate which can be read and written by a read/write head. The movement of the motor and actuator can easily locate where on the disk plate, the information is stored. The higher the spin speed of the motor is, the faster the read/write speed is.

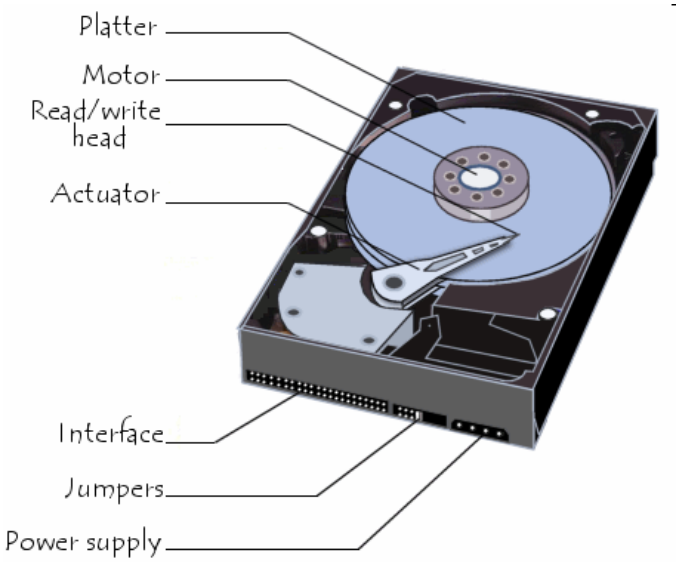

Figure 4-1 Hard drive structure

Figure 4-2 shows a closer look of the disk platter's surface. [1] The disk platter is divided into small sub-micrometer-sized magnetic regions. These magnetic regions are composed of hundreds of ferromagnetic iron oxide or cobalt alloy nanoparticles. The sizes of these nanoparticles are between 8 and 9 nm. In each of these regions, the polarity of magnetic particles is in the same direction. Because there are two different kinds of directions that magnets can point in, this property can be used to represent a single binary unit of information. Currently, the smallest diameter of these magnetic regions is about 300 nm.

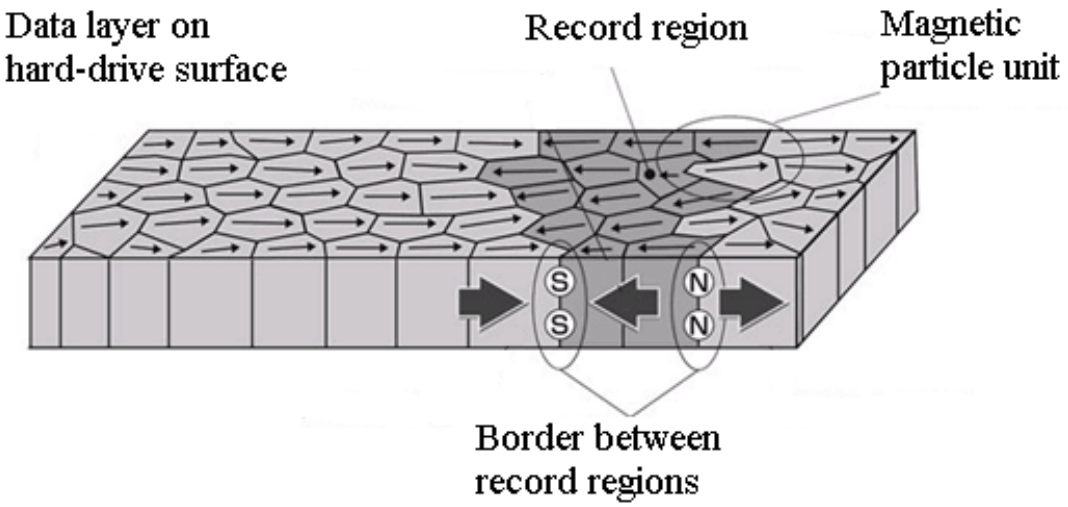

Figure 4-2 Microscopic structure of hard-drive plate surface. Abstracted from reference [1].

The unit that one associates with hard drive information storage capacity is the Gigabyte (Gb) or Terabyte (Tb). Currently, the biggest single platter information storage

volume is about 667 Gb, made by Samsung. [2] The data storage density unit is Gb per inch (Gbpsi). Because the size of the hard drive remains constant, the storage density must be increased. In order to increase the storage density, the data storage magnetic region must be made smaller. However, because of the uneven distribution of the nanoparticles sizes, we cannot simply use a lesser amount of particles in the region, due to the impact this will have on worsening the signal to noise ratio. [3] In other words, we have to use smaller magnetic nanoparticles to coat the surface of the disk platter in order to increase the storage volume.

There is a fatal issue that arises when one shrinks the sizes of the magnetic nanoparticles, known as the super-paramagnetic effect. [4] Because of this effect magnetization can randomly flip directions under the influence of temperature, in small enough nanoparticles. The smaller the magnetic nanoparticles are, the lower the flip temperature is. In other words, if the size of the magnetic particles is small enough, magnetization can randomly flip under room temperature. Many methods in the past ten years have been implored in order to prevent this super-paramagnetic effect from taking place. The most successful method is known as horizontal recording, which increases the thickness of magnet layer to fight against the super- paramagnetic effect. However, the maximum data density that current hard drive structures can reach is about 600 Gbpsi. If we want to keep increasing the hard drive volume when we reach 600 Gbpsi in the next few years, we will have to change the basic structure of the traditional hard drive. As far as we know, new generation hard drive ideas all have some serious cost-effectiveness issues and technical problems. [5]

We suggest a possible method which provides us with the possibility of increasing storage density to 500 to 600 Tbpsi, which is about 10,000 times more than current technology. Instead of utilizing magnetic material, our method uses polyoxometalate (POM) coordination polymers to store data.

Table **4-1.** First and Second One-Electron Reduction Potentials of α-Keggin POMs. Data taken from reference [7].

X	$-n/-(n+1)$	pH range	mV
Al	-5/-6	1.8-7.5	-130
Al	-6/-7	2.05	-330
Al	-6/-7	3.0	-350
Al	-6/-7	7.2	-360
Si	-4/-5	1.0-4.5	55
Si	-5/-6	1.0-4.5	-205
P	-3/-4	1.0-2.0	255
P	-4/-5	1.0	-15

In our method, we use POM (polyoxometalate) as a potential material to replace magnetic nanoparticles due to its interesting reduction and oxidation properties. POM is a well-known reservoir of electrons; it can easily gain or lose electrons without changing its structure. [6] In addition, POM's redox state is normally stable and reversible. [7] In Table **4-1**, Weinstock et.al studied α- Keggin Tungstoaluminate POMs and compared its

first and second one-electron reduction potentials to other α- Keggin POMs. From these results, we can see that Keggin POMs are stable within a certain pH range and how their different redox states can be transferred by applying a voltage. The well-known area of electrochemical research, cyclic voltammetry, also gives a beautiful graph, which can easily confirm that POM's different states can be both stable and reversible. In this cyclic voltammetrical graph of the α-$SiW_{12}O_{40}^{3-}$ complex in acidic solution (Figure 4-3), three reductions are reversible and well defined. These waves can be assigned to several redox state transactions. [8]-[10] Dirk Kurth et. al studied the redox chemistry of POM in thin layer-by-layer structure. [11], [12] His research confirmed that POMs have similar redox properties in thin solid state phase.

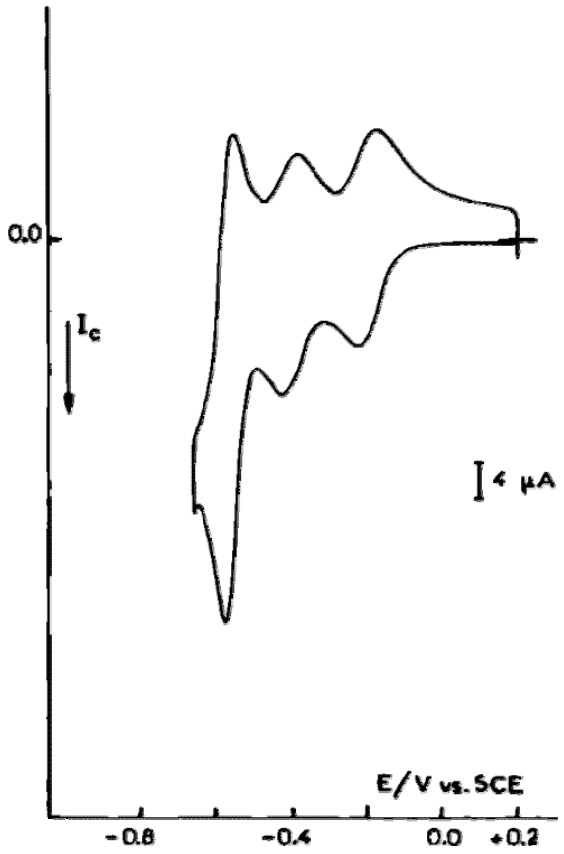

Figure **4-3** Cyclic voltammogram of $SiW_{12}O_{40}^{4-}$ (1 mM) in 1 M $HClO_4$ aqueous solution. Data taken from reference [6].

From our previous work in Chapter **2**, we studied the redox properties of α-Keggin Tungstoaluminate POM in the nanoscale solid state phase. Our results also confirmed that POM's redox properties are maintained in the nanoscale solid phase.

There are several advantages in applying and using POM for data storage utilities. Because most POMs are uniform in size, size distribution and bad signal to noise ratio become trivial concerns. We need to find a way to reduce or oxidize POM molecules and regularly arrange single POM molecules in a 2D plane. There is an additional requirement where the electron transfer process to a single POM molecule must not affect any of the other nearby POM molecules. If we can solve these problems, we will be able to use single POM molecules to store data after we find a small enough read/write head. Another advantage lays in the 1 nm size of POM molecules, which is much smaller when comparing it to a 300 nm diameter magnetic recording area.

Although there are several examples about cluster monolayer structures, it is not easy to control the regular arrangement of the molecule on a surface. [13]-[16] Another important issue is that, in most methods, the limitation of evenly distributing nanoparticles resides in using 50-100 nm sized nanoparticles. Because this size is much larger than a single molecule, these methods cannot make a theoretical single molecular information storage device, which use a single molecule (1 nm in diameter or smaller) to represent a binary digit.

In order to investigate the structure of our POM compounds and verify the morphology of the layer-by-layer structure on the molecular level shown in chapter 3, we tested POM single crystals by Transmission Electron Microscopy (TEM) and Scanning Electron Microscopy (SEM), and compared these results to the X-ray single crystal data.

SEM give accessment of layer-by-layer structure at relative low resolution. HRTEM give assessment of layer structure at higher resolution, and we can estimate the scale/size of the layers from HRTEM data. EDX give elemental composition. X-ray crystalgraphy increase the resolution to molecular level.

4.2 Experimental Section

4.2.1 Experiment

Because the TEM and SEM specimen holders could carry a very small amount of crystals, we firstly ground the chunky single crystals into the smallest possible pieces. The small pieces were redispersed in hexane as the organic solvent of choice. We then either dropped 3μl of the sample solution onto the carbon film of a TEM copper grid, or the specimen plate of the SEM, and waited until the solvent evaporated.[17] Since POM is an insulator and in order to the see the morphology, we covered the entire sample with a thin film of carbon. The HRTEM specimen image and diffraction pattern were tested with the Jeol 2100 at 200 kV (CUNY Hunter), while the SEM specimen was tested in the Zeiss Supra 55 VP in (CCNY). Both HRTEM and SEM has them has a Gatan CCD, and the software name is Gatan DigitMicrograph. We also used the energy dispersive X-ray spectra (EDX) to acquire the elemental analysis through the EDAX accessory in the Jeol 2100 instrument.

4.3 Result and Discussion

We tested the $Lu_2AlW_{11}O_{39}$ (compound **9** in chapter 3) crystals prepared as described above. The TEM image of a piece of $LuAlW_{11}O_{39}$ POM single crystals and its diffraction pattern is shown in Figure 4-7a and b, and in high resolution in Figure **4-4** c, d, and e. We

observed six different types of lattice fringe values which could represent various crystalline phases and domains.

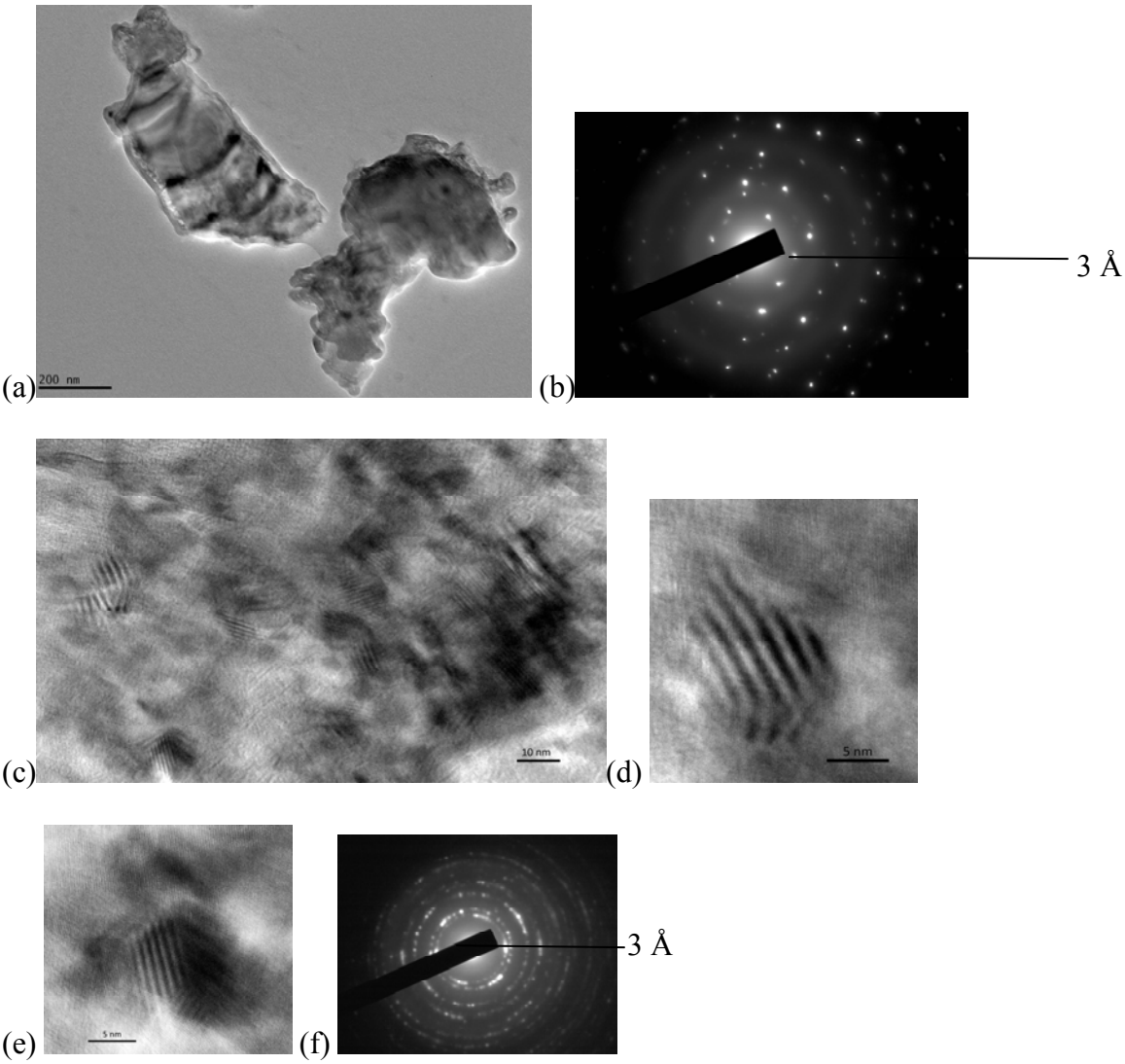

Figure **4-4** (a) The entire $LuAlW_{11}O_{39}$ POM single crystal and (b) its diffraction pattern and 3 Å lattice value calculated from CCD software, (c) HRTEM of (a) that had six types of lattice fringes, (d) lattice fringe showing a value of 12 Å, (e) lattice fringe shown value of 10 Å, (f) diffraction pattern taken from area (c). 3 Å lattice value calculated from CCD software.

Lattice fringe pictures are often obtaind by using high-resolution transmission electron microscopy (HRTEM) to observe crystaline material. Lattice fringe pictures are important because we can calculate lattice fringe size from pictures and compare it to XRD data of the crystaline material. After measuring the lattice fringe directly with the TEM imaging software (GATAN Digit), we acquired a series of values: 17Å, 12 Å, 10 Å, 7 Å, 4 Å and 3 Å. The 12 Å lattice fringe is exhibited in Figure **4-4**d and the 10 Å in Figure 4-7e. Due to the limitation of diffraction on the large lattice fringe, we could only observe the diffraction patterns shown in Figure **4-4**b and the selected area electron diffraction (SAED) pattern shown in Figure **4-4** of no more than 3 Å. In order to verify our hypothesis that those observed lattice fringes in the high resolution TEM (HRTEM) image in Figure **4-4**c represent various crystalline phases, we used the goniometer-tilting function to monitor the images of tilted crystal under a tilting angle of +30 degree and -30 degree, which are shown in Figure **4-5**a and **4-5**b separately. We observed the previous lattice fringes disappear and a new fringe pattern emerge in the same place as before. SEM give accessment of layer-by-layer structure at relative low resolution. HRTEM gives an assessment of layer structure at higher resolution than SEM, and we can estimate the scale/size of the layers from HRTEM data. EDX give elemental composition. X-ray crystallography provides molecular level resolution. This occurrence proved our hypothesis that the crystalline growths depend on certain angles and directions, and that those domains represent certain crystal phases, 17Å and 12 Å, which correspond to the POM crystal structure of compound **9** shown in Figure **3-14** in chapter **3**. Once samples were tested using SEM, we observed the layer-by-layer morphology shown in Figure **4-7**. In addition, the peaks of W and Lu were clearly observed in the EDX spectrum taken on

the sample shown in Figure **4-8**. These elemental composition results proved the existence of those elements, which was consistent with the NMR result in Figure **3-2**c. [18]

(a) 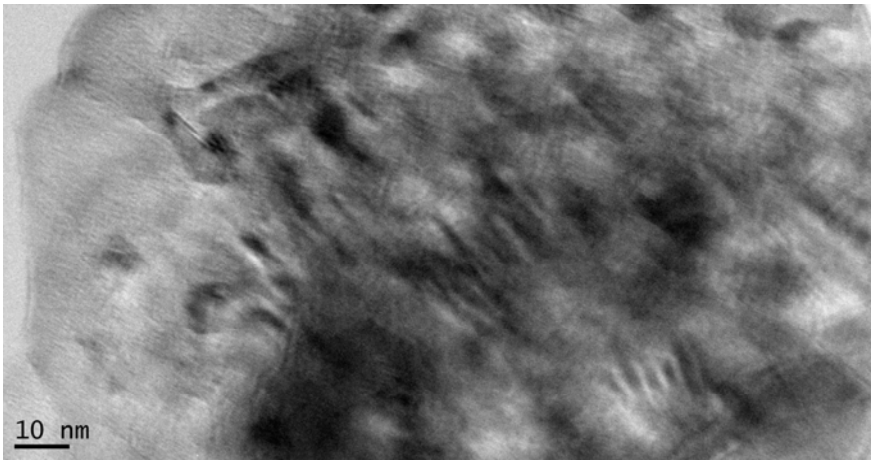

(b) 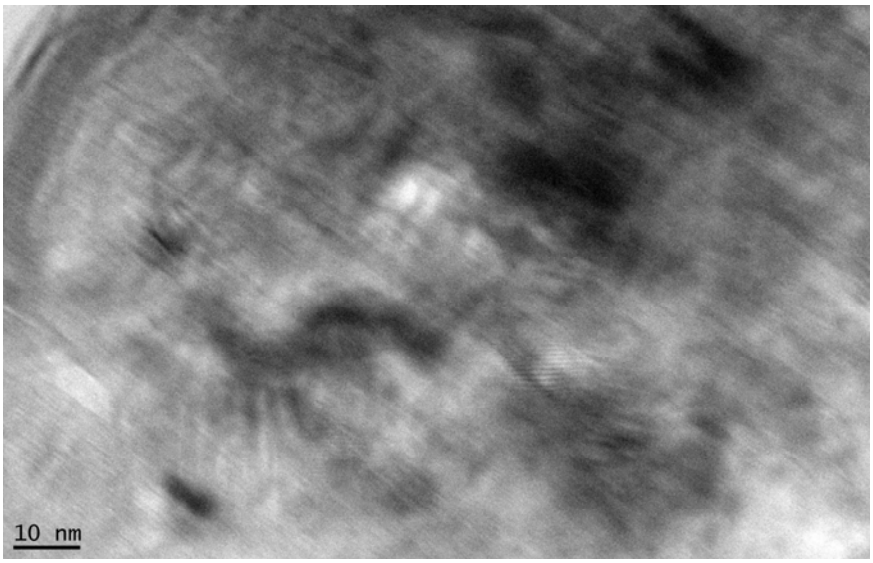

Figure **4-5**, $LuAlW_{11}O_{39}$ POM (compound **9**) sample tilting with goniometer in angle of +30 degree (a) and -30 degree (b).

We compared these lattice fringe values with d-spacing values generated from the single crystal structure of compound **9** shown in Figure **4-6**, and we found those two sets of values matched perfectly. The experimental results showed that the $LuAlW_{11}O_{39}$ POM compound had a molecular level layer in the nanoscale made by the Keggin crystal structure units.

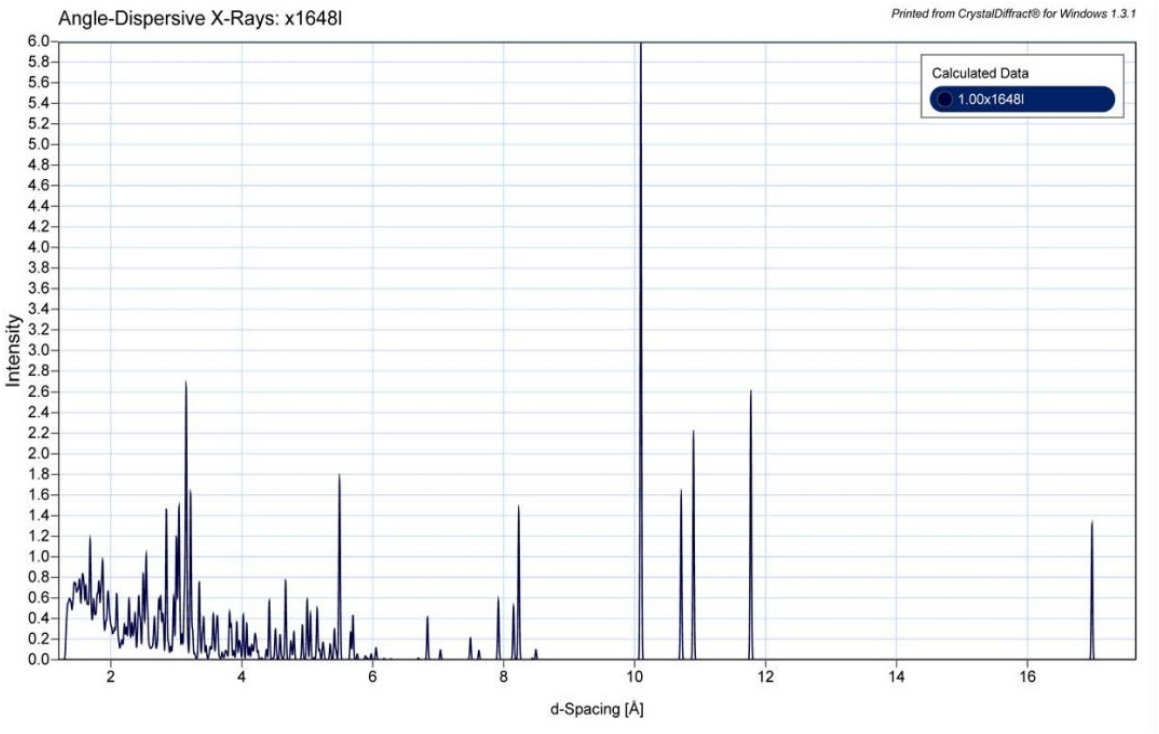

Figure **4-6** $LuAlW_{11}O_{39}$ POM lattice values calculated from X-ray single crystal data of $LuAlW_{11}O_{39}$ POM (compound **9**). These data show lattice spacing at 10 Å and 12 Å match the lattice fringe observed in the HRTEM.

Each single molecular level layer could potentially be utilized as a storage carrier if this layer could sustain itself on the substrate. Since different crystal phases are directionality dependent, the uniform order was maintained once the crystal phases began building on the same layer, which is indicative of how advantageous the magnetic material is, in terms of uniformity.

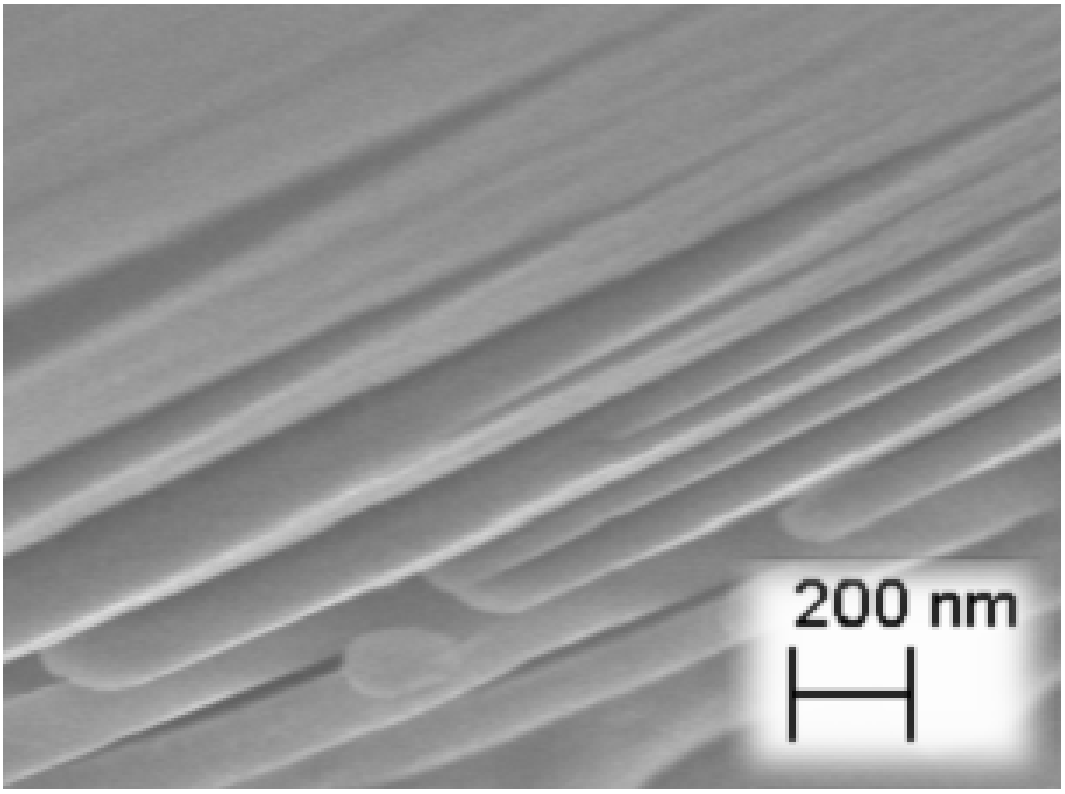

Figure **4-7**, SEM image of $LuAlW_{11}O_{39}$ POM show a layered morphology that is consistent with the crystal structure in Figure **3-14**.

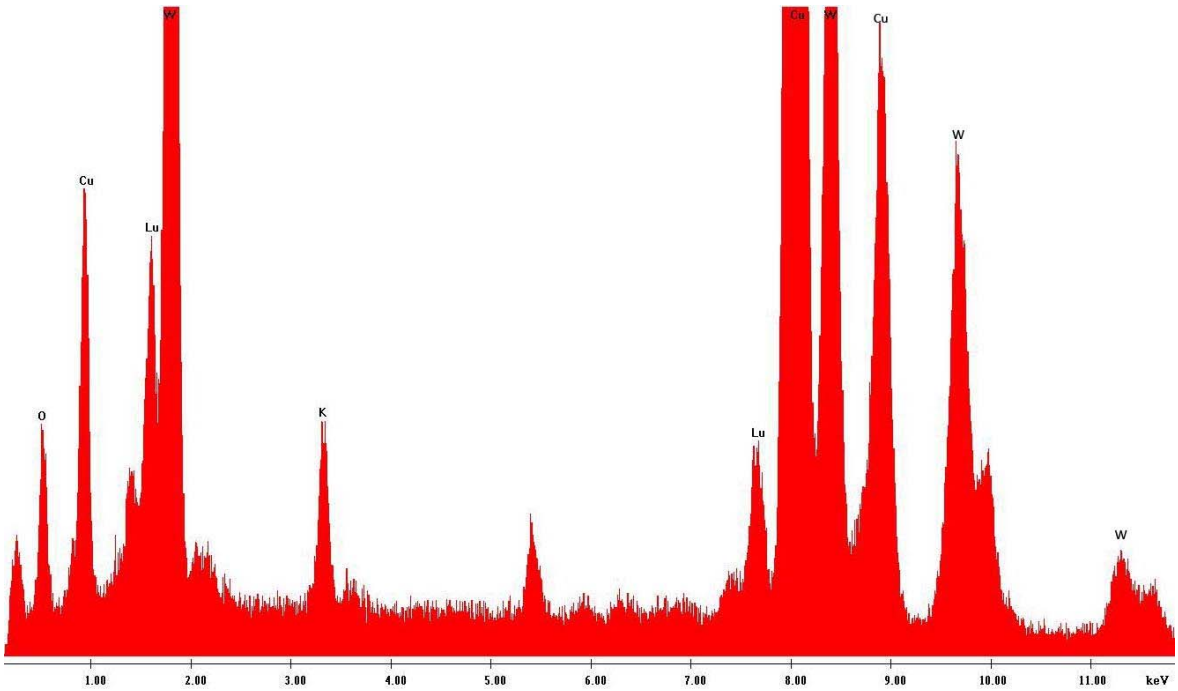

Figure **4-8** EDX spectrum of $LuAlW_{11}O_{39}$ POM (compound **9**) shows the elemental composition.

Encouraged by the results from the POM crystal in the Lu case, we tested the second POM compound $SmAlW_{11}O_{39}$ (compound **5**) by the same method. The HRTEM image (Figure **4-9**) indicates the main lattice fringe as 10.5 Å, existing in $SmAlW_{11}O_{39}$ POM crystals. After comparing this data with calculated X-ray single crystal data shown in Figure **4-10**, we found that these two sets also matched perfectly. The SEM image (Figure **4-11**) shows the layer-by-layer morphology as being very similar to the $LuAlW_{11}O_{39}$ POM case, with nanoscale molecular level layers 6 nm in thickness. The existence of Sm and W elements was proved by EDX spectrum as shown in Figure **4-12**.

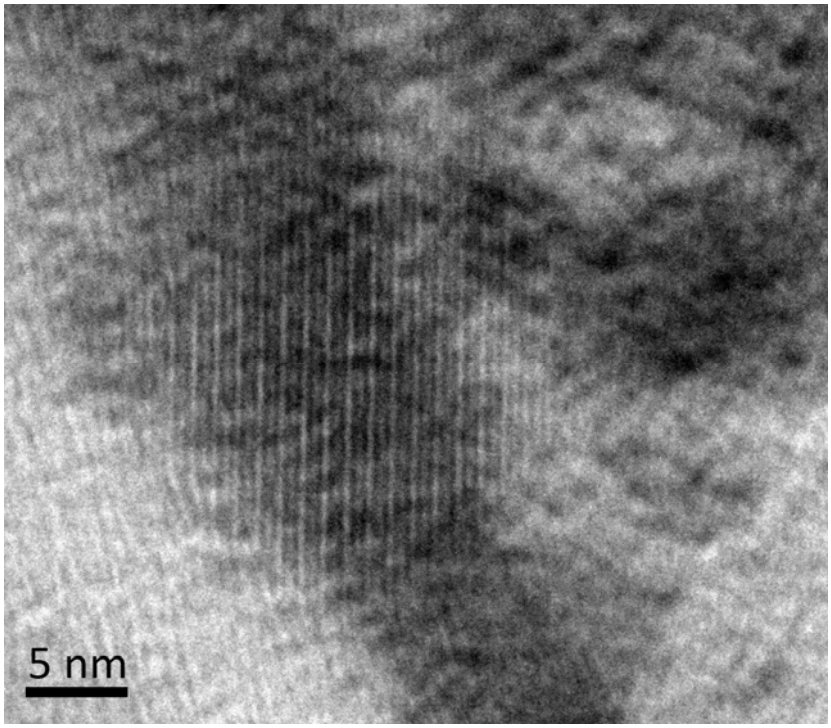

Figure **4-9** HRTEM of $SmAlW_{11}O_{39}$ POM (compound **5**). This shows the main lattice fringe is 10.5 Å. This lattice fringe compares well to the d-spacing data between layers of the $SmAlW11O_{39}$ POMs (Figure **4-13**).

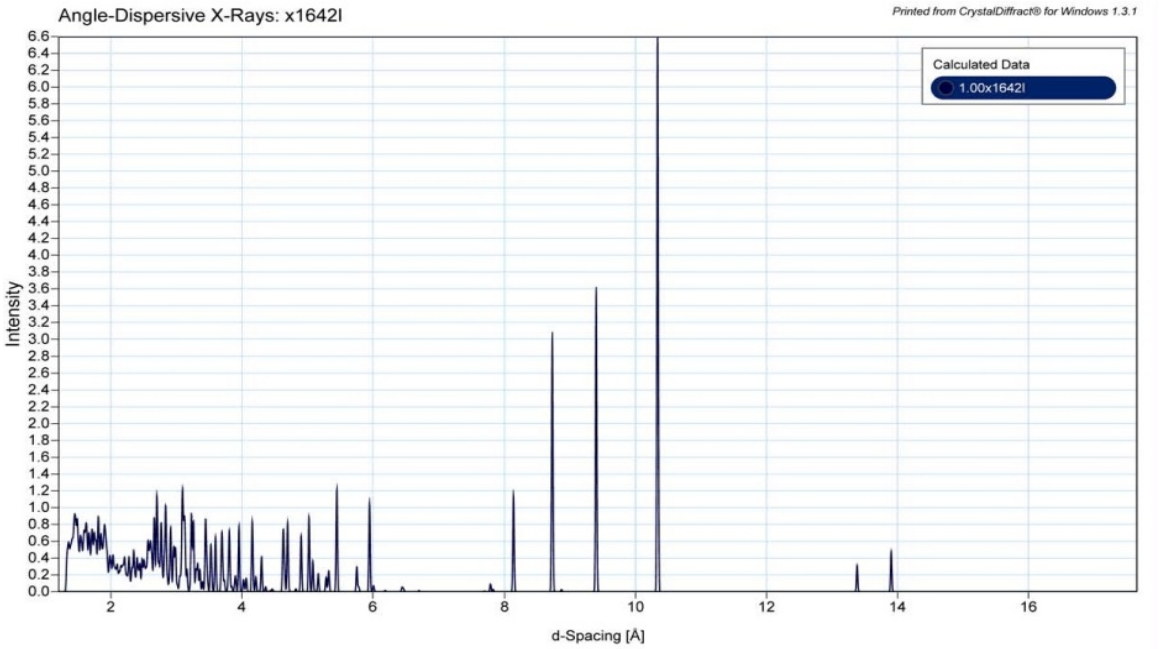

Figure **4-10** Lattice values calculated from X-ray single crystal data of the $SmAlW_{11}O_{39}$ POM compound. These data show lattice spacing at 10.5 Å matches the lattice fringe observed in the HRTEM.

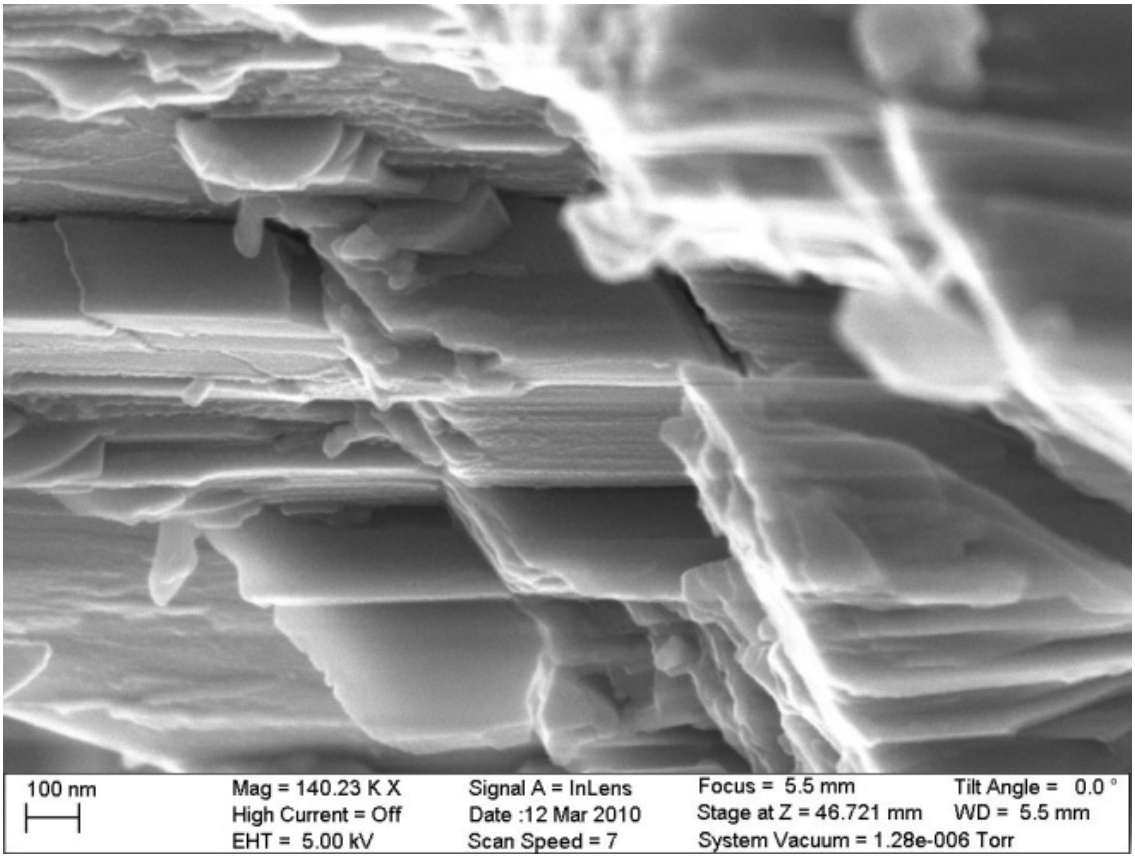

Figure **4-11** SEM image of $SmAlW_{11}O_{39}$ POM compound. These data show the layered morphology of the compound.

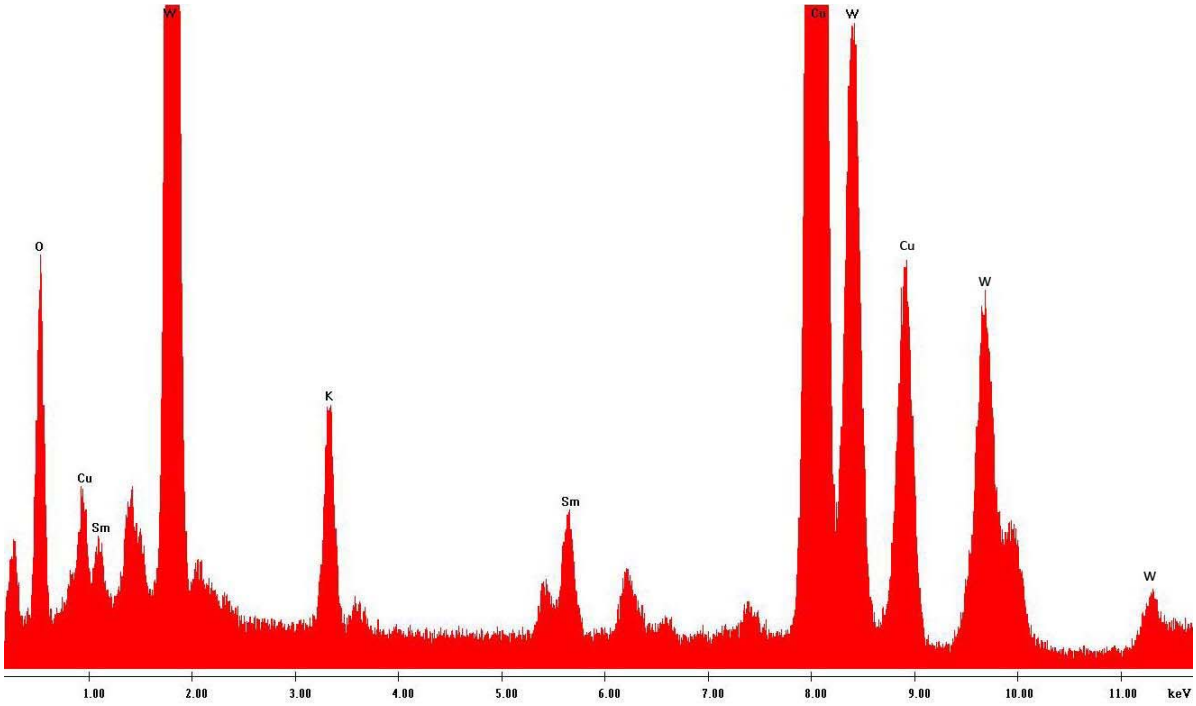

Figure **4-12** EDX spectrum of $SmAlW_{11}O_{39}$ POM compound shows the elemental composition.

4.4 Conclusion

In this chapter, SEM and HRTEM microscopy of compound **5** and **9** was studied, and compared to its crystal structure and lattice values calculated from their crystal structure. The result perfectly connected the molecule structure and nano grade morphology. More than 1nm size lattice was found from HRTEM image, which is very rare to be observed.

4.5 References

[1] http://itpro.nikkeibp.co.jp/members/NBY/techsquare/20030724/1

[2] http://www.geek.com/articles/chips/samsung-squeezes-667gb-per-platter-on-2tb-ecogreen-drive-2010084/

[3] Z. Bandić, E. Dobisz, T, Wu, T. Albrecht, *Solid State Technology Magazine*, **2006**, 9

[4] J. Gittleman, B. Abeles, and S. Bozowski, *Phys. Rev. B* **9**, **1974**, 3891–3897

[5] M. Kryder, *Magnetics Conference, 2000. INTERMAG 2000 Digest of Technical Papers. 2000 IEEE International* , 575–575

[6] M. Sadakane and E. Steckhan *Chem. Rev.*, **1998**, 98 (1), pp 219–238

[7] Y. Geletii, C. Hill, A. Bailey, K. Hardcastle, R. Atalla, and I. Weinstock, *Inorganic Chemistry,* **2005** *44* (24), 8955-8966

[8] B. Keita, L. Nadjo, *Electroanal. Chem*. **1985**, 191, 441.

[9] B. Keita, L. Nadjo, *J. Electroanal. Chem.* **1987**, 217, 287.

[10] B. Keita, L. Nadjo, *J. Electroanal. Chem.* **1987**, 227, 77.

[11] S. Liu, H. Möhwald, D. Volkmer, and D. G. Kurth, *Langmuir*, **2006**, 22 (5), pp 1949–1951

[12] S. Liu and Z. Tang, *nanotoday* Vol. 5, Issue 4, **2010**, 267-281

[13] M. Rindel, *African J. Sci.* **11** (1916), 362.

[14] C. Chang, K. Sun, S. Lee and L. Kan, *Biomaterials* Volume 28, Issue 11, April **2007**, 1941-1947

[15] T.. Niederhauser, Y. Lua, G. Jiang, S. Davis, D. Hess and M. Linford, *Angew Chem Int Ed*, 41 (2002), 2353–2356.

[16] Y. Lua, T. Niederhauser, B. Wacaser, I. Mowat, A. Woolley and R. Davis et al., *Langmuir,* **2002**, 18, 4840–4846.

[17] H. Bai, K. Xu, Y. Xu, H. Matsui, *Angew. Chem. Int. Ed.* **2007**, *46*, 3319.

[18] H. Bai, F. Xu, L. Anjia, H. Matsui, *Soft Matter* **2009**, *5*, 966.

Chapter 5. Polyoxometalate Application in Rhenium Chemistry: A Useful Tool for ^{99}Tc Research

5.1 Introduction

As one of the last naturally occurring element to be discovered, rhenium has several special properties and applications. [1]-[3] One of the important application of rhenium is making nickel-based alloys with high creep strength so that it can be used in jet engine. [4] For example, in F22 fighter engines, single-crystal alloys contain 6% rhenium. [5] Rhenium is also a very useful catalyst for catalytic reforming, olefin metathesis and hydrogenation reactions. [6]-[8] Rhenium isotopes ^{188}Re and ^{186}Re are liver cancer treatment. [9]

^{99}Tc is a major product of uranium-235 fission in nuclear reactors. Emitting soft beta rays, ^{99}Tc is the most significant long-lived fission product of uranium. Research about ^{99}Tc redox chemistry is a key step of nuclear waste stabilization and separation because ^{99}Tc will persist while other isotopes decay in nuclear waste tanks. To design separation and storage strategies, fundamental chemistry of ^{99}Tc must be understood. Rhenium and technetium have very similar chemistry properties, leading to the use of rhenium as a surrogate ^{99}Tc to perform a non-radioactive experiment, and then translate their works to technetium, especially, ^{99}Tc isotope. [9] [10]

Chemists are considering metal-oxide storage matrices to store ^{99}Tc. Polyoxometalate (POM), the polyatomic clusters composed of early transition metals are excellent models for metal-oxide materials [11]-[15].The research of polyoxometalate ^{99}Tc derivatives may provide useful information of the coordination chemistry and oxidation state speciation of Tc. By adjusting the pH of the solution, one of the M^{VI}

(M=Mo, W) unit on the POM structure can be lost and a vacancy is formed. There are alternating short-long O-M-O bonds in ring order in polyoxometalates.[12][13] Binding of counterions and protonation dynamics of the POMs may be analagous to dynamics found in solid-state metal oxide materials.

We concentrate on the mono-vacant defect Wells-Dawson ion $(\alpha_2\text{-}P_2W_{17}O_{61})^{10-}$ and $(\alpha_1\text{-}P_2W_{17}O_{61})^{10-}$ isomers shown in Figure **5-1**. These α_1 and α_2 defects impact redox properties as well as binding strength to transition metals. From previous lanthanides and transition metal POM speciation research, we know that high basicity of the α_1 vacancy requires high charge/size cations for stabilization.[16]-[28] The high basicity of the α_1 defect is ascribed by Contant[6] to the orientation of the PO_4^{3-} tetrahedron within the cavity of the W-O framework, positioning a basic oxygen atom near the α_1 site.

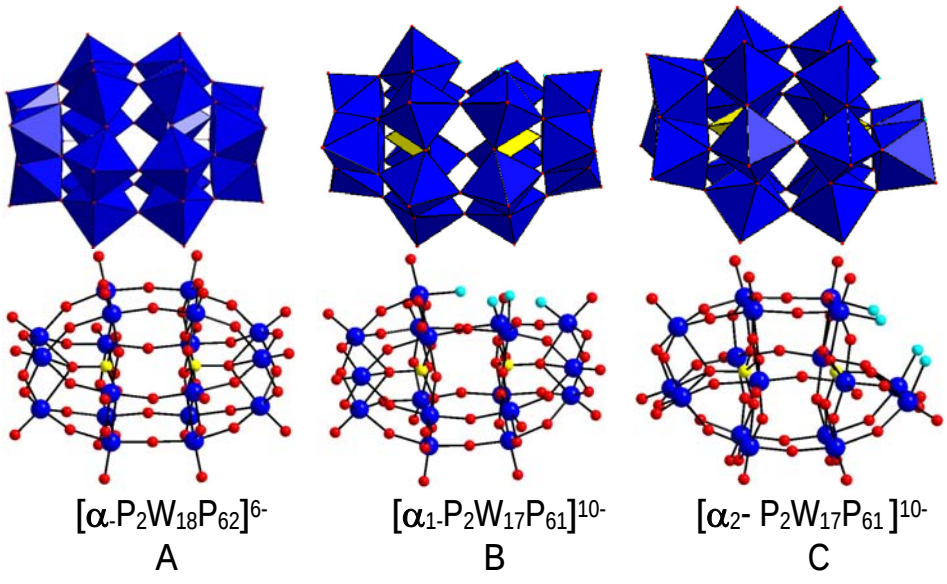

Figure 5-1 Wells-Dawson ion $(\alpha_2\text{-}P_2W_{17}O_{61})^{10-}$ and $(\alpha_1\text{-}P_2W_{17}O_{61})^{10-}$ isomers

In this study, rhenium complex of the $[\alpha_1\text{-}P_2W_{17}O_{61}]^{10-}$ isomer was prepared, characterized by multinuclear NMR, single crystal crystallography and preliminary electrochemical studies are reported. We also compared the electrochemical properties of rhenium $[\alpha_1\text{-}P_2W_{17}O_{61}]^{10-}$ complexes to rhenium $[\alpha_2\text{-}P_2W_{17}O_{61}]^{10-}$ complexes and ^{99}Tc $[\alpha_1\text{-}P_2W_{17}O_{61}]^{10-}$. We also prepared the rhenium complex of mono-vacant Keggin POM $[\alpha\text{-}AlW_{11}O_{39}]^{9-}$ and characterized it by multinuclear NMR, light scattering and Transmission Electron Microscopy (TEM).

5.2 Experimental Section

5.2.1 General.

Reagent grade chemicals were commercially available and used without further purification. Deionized water was used from a Millipore Reverse Osmosis Direct-Q System. Elemental analyses were carried out by Inductive Coupled Plasma Atomic Emission Spectrometry (ICP-AES, SEPCTROFLAME M120E). $\alpha_1\text{-}P_2W_{17}O_{61}^{10-}$ and $\alpha_2\text{-}P_2W_{17}O_{61}^{10-}$ ligands were prepared as described in the literature. [16] [29] and [30] . Pure water used throughout was obtained using a Millipore Direct Q5 system (conductivity =18 μΩ). Cyclic Voltammetry was performed on a BAS CV-50W Voltammetric Analyzer using glassy carbon electrode and standard Ag/AgCl reference electrode. Dynamic light scattering (DLS) were made on a CoolBatch Plus 90T Dynamic light Scattering Detector. α-Nonapotassium undecatungstoaluminate ($\alpha\text{-}K_9AlW_{11}O_{39}\cdot 12H_2O$) was prepared according to a published method and identified by infrared spectroscopy. [31]

5.2.2 Synthesis of compounds.

5.2.2.1 Synthesis of $[\alpha\text{-}Re^{V}OAlW_{11}O_{39}]^{6-}$, **10**

This synthesis was performed in a Schlenk tube under an atmosphere of nitrogen. α-$K_9AlW_{11}O_{39}$ (100 mg, 0.028 mmol) was dissolved in 5 ml warm degassed H_2O and stirred for 10 minutes. K_2ReCl_6 (20 mg, 0.028 mmol) was dissolved in 1 ml degassed water. Slowly added K_2ReCl_6 solution into $K_9AlW_{11}O_{39}$ slurry and kept stirring for 30 min. The color changed to dark purple. Saturated KCl solution was added to the reaction solution via a syringe. A dark purple powder appeared after cooling the Schlenk tube in refrigerator for two hours. The solution was filtered, and the dark purple residue was dried under nitrogen protection. ^{27}Al NMR spectra taken in D_2O under Oxygen free conditions. Chemical shift (Integration): 70.83 ppm (1), 69.11 ppm (2, Broad peak with Half width 0.86 ppm).

5.2.2.2 Synthesis of $[Re^{V}O(\alpha_1\text{-}P_2W_{17}O_{61})]^{7-}$ method 1, **11**

A solution of K_2ReCl_6 (40 mg, 0.08mmol) in H_2O (90 °C, 2 ml) was added into a scintillation vial containing a solution of $K_nH_{10-n}[\alpha\text{-}1\text{-}P_2W_{17}O_{61}]$ (20 mg, 0.04 mmol) in 2ml H_2O. The vial was heated for 30 min. The dark blue solution was tested by ^{31}P NMR spectroscopy to assess the purity and to identify substitution into the $1\text{-}P_2W_{17}O_{61}$ framework. For ^{183}W NMR studies, the solution was used in situ. For other studies, a dark blue solid was isolated by addition of 3 ml saturated KCl solution and left overnight. The product was filtered, washed by saturated KCl solution and dried in vacuum. Yield 60% to 70% based on K_2ReCl_6. IR (KBr, cm-1): 868 cm-1 (strong, broad), 937.61 cm-1 (weak), 1045 (strong, broad). 31P NMR (D_2O, ppm): -11.99 (1), -12,30 (1). 183W NMR (D2O, ppm): 35.17 (1), -108.55 (1), -111.43 (1), -157.35 (1), -167.90 (1), -179.63 (1), -

180.26 (1), -184,51 (1), -197.41 (1), -207.91 (1), -208.59 (1), -228.77 (1), -237.95 (1), -242.69 (1), -258.18 (1), -308.79 (1), -398.52 (1).

Column purification method of $[Re^{V}O(\alpha_1\text{-}P_2W_{17}O_{61})]^{7-}$ was developed by Dr. Benjamin P. Burton-Pye. 0.4 g of recrystallized product was dissolved in 5 mL distilled water and loaded onto a silica column (5.5 cm (diameter) x 60 cm filled to a height of 40 cm with silica) primed with methanol, and eluted with methanol. The dark blue fraction containing $[Re^{V}O(\alpha_1\text{-}P_2W_{17}O_{61})]^{7-}$ was reduced in volume by rotary evaporation and filtered to remove any silica. The solvent was then removed by rotary evaporation to yield pure $[Re^{V}O(\alpha_1\text{-}P_2W_{17}O_{61})]^{7-}$, free from $[Re^{V}O(\alpha_2\text{-}P_2W_{17}O_{61})]^{7-}$. ^{31}P NMR ($D_2O$, ppm): -12.02 (1) and -12.33 (1). ^{183}W NMR (D_2O, ppm): 35.17(1), -108.55(1), -111.43(1), -157.35(1), -167.90(1), -180.02(2), -184.51(1), -197.41(1), -208.1 (2), -228.77(1), -237.95(1), -242.69(1), -258.18(1), -308.79(1), -398.52(1).

The organic soluble TBA_4H_2 [α-1-$Re^{V}O$ $P_2W_{17}O_{61}$] was made by metathesis method and crystallized from CH_3CN solvent. Dissolve 0.09g (0.02mmol) K_7[α1-$Re(V)OP_2W_{17}O_{61}$] in 2ml water. Add 0.063g (0.02mmol) of Solid TBA·Br. Maintain pH at 4 to 5 by adding 1M HCl. After stirring for a few minutes, centrifuge it and get blue precipitate product. The blue solid was dissolved in CD_3CN to perform ^{31}P NMR experiment.

5.2.3 Analytical techniques

5.2.3.1 Collection of NMR Data

All NMR spectra were recorded on a JEOL GX-400 spectrometer with 5 or 10 mm tubes. Resonance frequencies are 104.224 MHz for ^{27}Al and 16.7 MHz for ^{183}W.

Chemical shifts are given with respect to 1M $AlCl_3$ for ^{27}Al and 1M Na_2WO_4 for ^{183}W. Typical acquisition parameters for ^{183}W spectra included the following spectral width, 10000Hz, acquisition time, 1.6 s, pulse delay, 1 s, pulse width, 50 μs. From 1000 to 60000 scans were acquired. Typical acquisition parameters for ^{27}Al spectra included the following spectral width 500 ppm, acquisition time, 0.31456 s, pulse delay, 1 s, pulse width, 5μs. From 1000 to 3000 scans were acquired. For both ^{27}Al and ^{183}W chemical shifts, the convention used is the more negative chemical shifts denote more upfield resonance.

(1) Single-Crystal X-ray structure Determination.

Crystals of **10** were collected under a thin layer of mineral oil using a polarizing microscope. Selected crystals were mounted on a glass fiber and quickly placed in a cold nitrogen stream on a Bruker SMART CCD diffractometer equipped with a sealed tube Mo anode (Kэ radiation, λ= 0.71073 Å) and graphite monochromatic or Nonius Kappa CCD diffractometer. Data collection, indexing, and initial cell refinements were collected at around 100 K. Data collection, indexing, and initial cell refinements were all handled using SHELXTL software. The SHELX package of software was used to solve and refine the restructures. [29] The heaviest atoms were located by direct methods, and the remaining atoms were found in subsequent Fourier difference syntheses. All refinements were fullsquares on F^2.

(3) Microscopy

Transmission Electron Microscope (TEM) images were taken with Zeiss EM 902 is a thermionic (tungsten) transmission electron microscope. Sample was made by dispersing sample solution on the TEM sample grid. The TEM sample was then dried in a 60˚C oven overnight.

(4) Dynamic Light Scattering (DLS)

Dynamic light scattering (DLS) measurement were made on a CoolBatch Plus 90T Dynamic light Scattering Detector.

(5) Electrochemical Data Collection

Electrochemical data were obtained using a BAS Voltammetric Analyzer System controlled by BAS CV-50W software (for PC). The cell used for cyclic voltammetry (CV) contained a glassy-carbon working electrode (BAS standard disk electrode, 3 mm OD), a Pt wire auxiliary electrode (0.5 mm), and a BAS Ag/AgCl (3M NaCl), reference electrode.

5.3 Result and discussion

5.3.1 ^{27}Al NMR and Oxidation of $[\alpha\text{-}Re^{V}OAlW_{11}O_{39}]^{6-}$ (10)

Shown on Figure 5-2, ^{27}Al NMR spectra of $[\alpha\text{-}Re^{V}OAlW_{11}O_{39}]^{6-}$ in oxygen free environment. Chemical shift (Integration): 70.83 ppm (1), 69.11 ppm (2, Broad peak with Half width 0.86 ppm). The probe signal has been removed from the spectra. The sharp peak in 70.83 ppm is free Keggin $K_5AlW_{12}O_{40}$. The broad peak at 69.11 ppm is attributed to $[\alpha\text{-}Re^{V}OAlW_{11}O_{39}]^{6-}$. Because there is equilibrium between $K_5AlW_{12}O_{40}$ and $K_9AlW_{11}O_{39}$ in solution (ratio is related to pH value), it is possible that there is excess

$K_5AlW_{12}O_{40}$ in the solution. Another possibility is that the product actually is a sandwich structure with two $[\alpha\text{-}Re^{V}OAlW_{11}O_{39}]^{6-}$ and one $K_5AlW_{12}O_{40}$ in the formula.

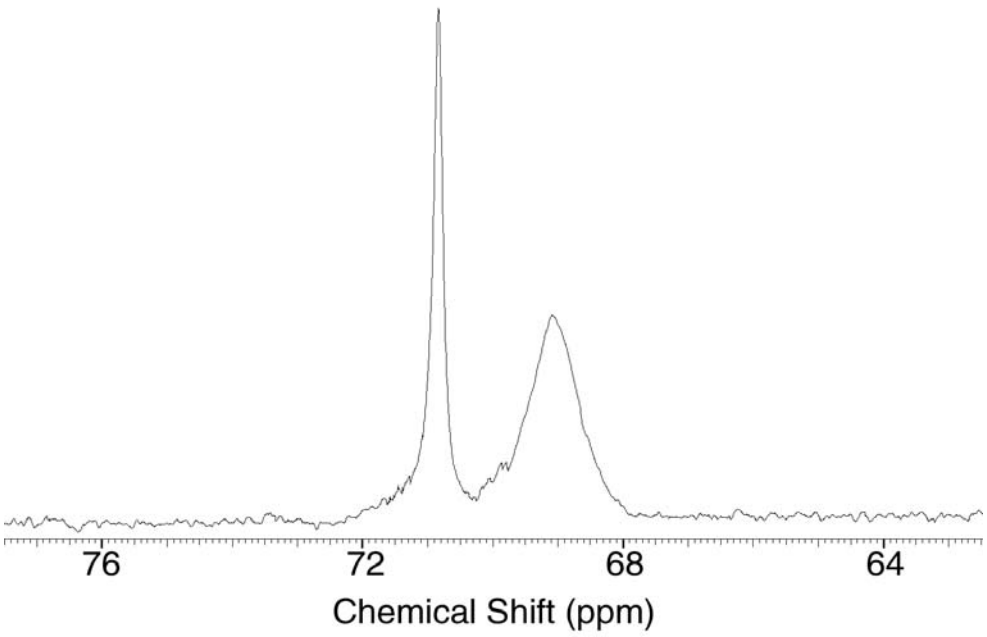

Figure 5-2. ^{27}Al NMR of $[\alpha\text{-}Re^{V}OAlW_{11}O_{39}]^{6-}$

Shown in Figure **5-3**, after leaving the purple solution (right) in the air for several hours, the color became pale yellow (left). If we seal the sample vial well, there is no color change for 30 days. To get further information about this color change, UV-vis spectra data were taken before and after the color change. From Figure **5-4**, after the color change from purple to pale yellow, rhenium (V) absorption at 500 nm becomes significantly smaller. In addition, there is absorption at 460 nm.

Because rhenium absorption disappeared but no precipitate was observed, we suspect that there are nanoparticles formation during the reaction in air. The light scattering experiment ensures a reliable representation of the actual size distribution is between 50

to 150 nm. We postulate that the reaction includes oxidation of the Re^{V} to Re^{VII} , but this needs to be studied further.

Figure **5-3** Compound **10** color changes from purple (right) to yellow (left) in air

After exposing the pale yellow solution sample in air for longer time, we will get colorless solution and black supernatant. The sample was centrifuged and the black powder was collected. A TEM sample was made by dispersing the black powder onto the sample grid. TEM pictures perfectly matched the light scattering data with respect to size of particles. Because the black powder is very stable and does not dissolve in water, we did EDX spectrum to study its elemental composition.

From the EDX spectrum shown in Figure **5-6** of black powder TEM sample, we observed the peaks of Re, Al and W in corresponding energy levels (K, L, M). From the EDX spectrum result, we believe this is a Rhenium aluminumtungstate POM can form a

nanoparticles that are very stable in the air. This new material should be further investigated for application of ^{99}Tc complexation.

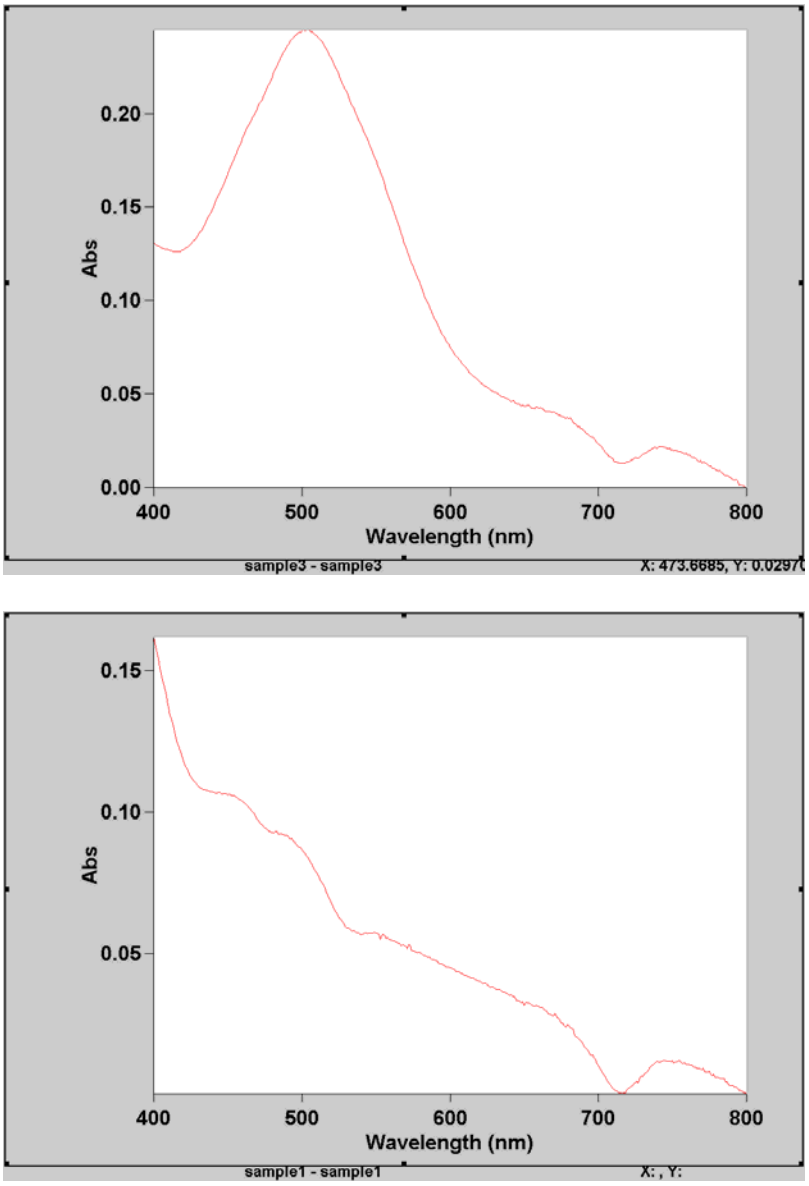

Figure **5-4**. UV-vis Spectra before (top) and after (bottom) the oxidation reaction in air

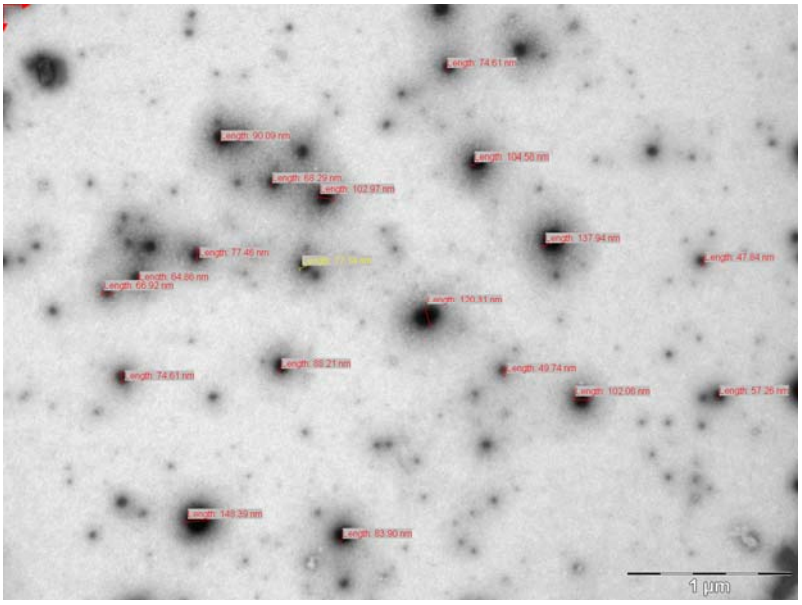

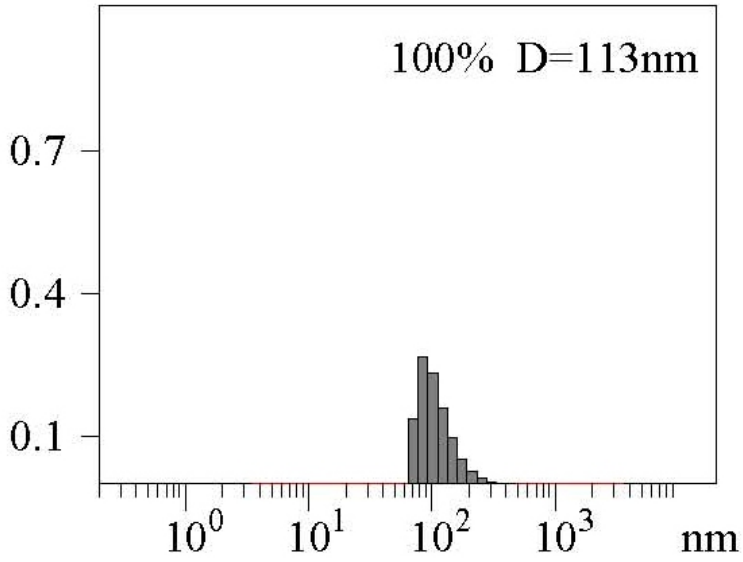

Figure **5-5**. TEM image (top) and Light Scattering Data (bottom) of the Re aluminotungstate exposed to air. These experiments show a uniform particle size of average 110 nm.

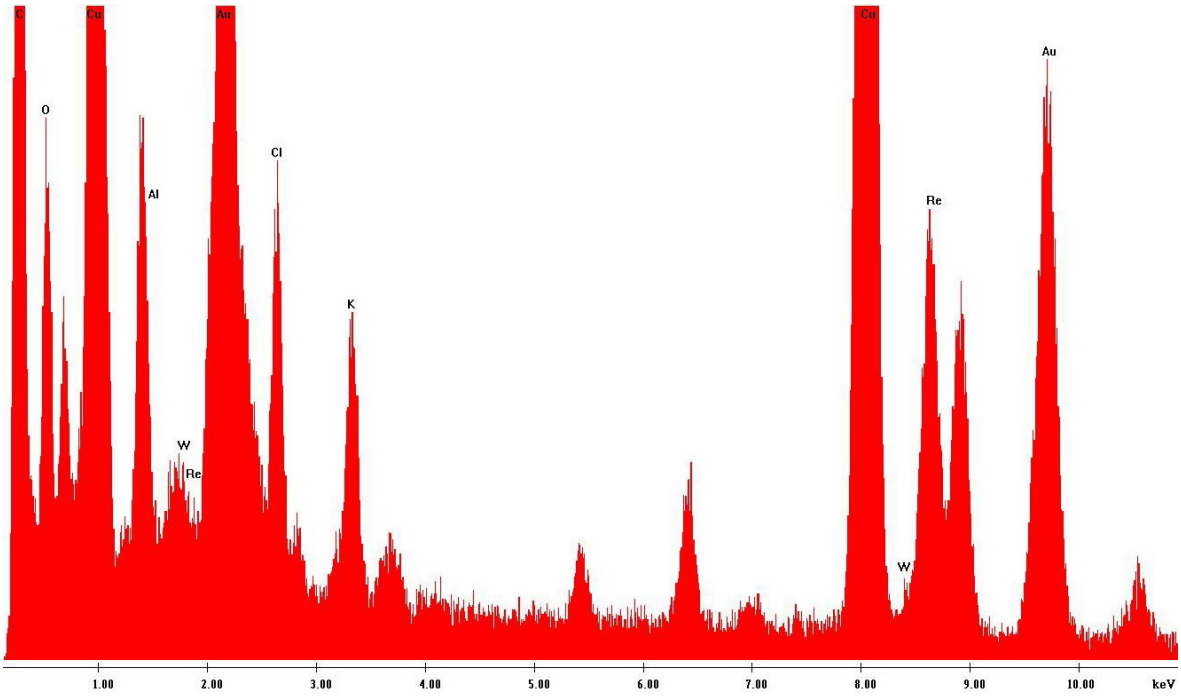

Figure **5-6** EDX spectrum of $ReAlW_{11}O_{39}$ POM compound show the elemental composition.

5.3.2 ^{31}P and ^{183}W NMR of [α-1-$Re^{V}O$ $P_2W_{17}O_{61}$]$^{6-}$

Shown in Figure **5-7**, ^{31}P NMR of [α1-$Re^{V}O$ $P_2W_{17}O_{61}$]$^{6-}$ potassium salt (D_2O) has two strong resonances at 12.0 ppm and 12.3 ppm. These two signals are the two P atoms in α1-$Re^{V}O$ $P_2W_{17}O_{61}$ cluster. Those two small resonances at 11.9 ppm and 12.9 ppm can be attributed to impurity by-product [α2-$Re^{V}O$ $P_2W_{17}O_{61}$]$^{6-}$. From the integration result, the purity of [α1-$Re^{V}O$ $P_2W_{17}O_{61}$]$^{6-}$ is about 93%. The phosphorous atom close to the Re^{V} center and the remote phosphorous is assigned to the downfield resonance. Figure **5-8** showes the ^{31}P NMR of [α1-$Re^{V}O$ $P_2W_{17}O_{61}$]$^{6-}$ TBA salt in CD_3CN solvent. TBA salt of [α1-$Re^{V}O$ $P_2W_{17}O_{61}$] $^{6-}$ has more than 50% [α-$P_2W_{18}O_{62}$]$^{6-}$ impurity. ^{183}W NMR

is used for structural identification of compound **11** in solution. Each tungsten atom presents one resonance.

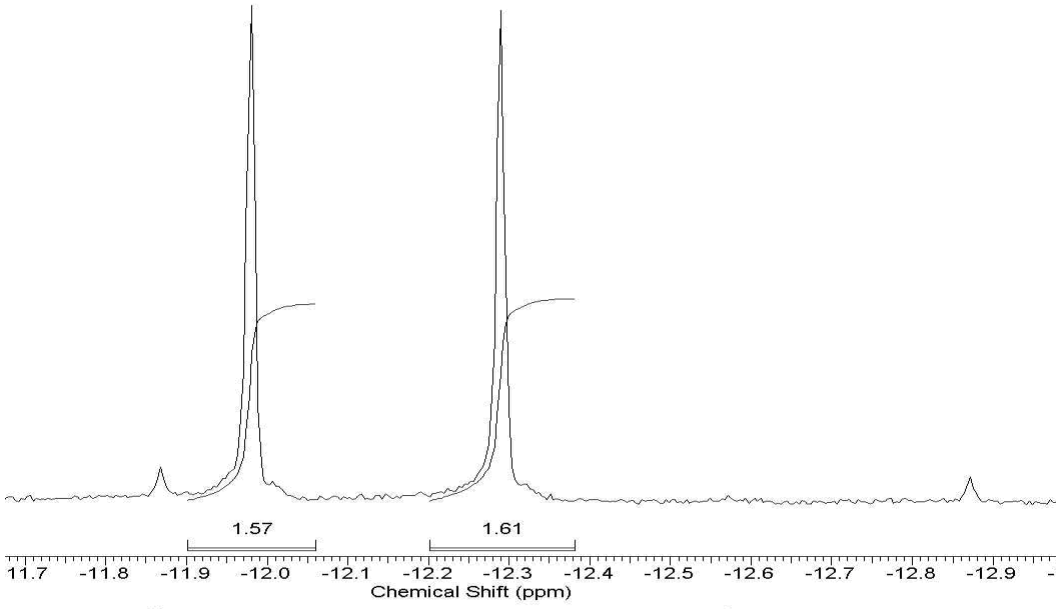

Figure **5-7** ^{31}P NMR of [α1-Re^{V}O $P_2W_{17}O_{61}$]$^{6-}$ Potassium salt.

Shown in Figure **5-9,** the Re^{V}O complex of α_1-$P_2W_{17}O_{61}^{10-}$ potassium salt clearly shows 17 well-resolved resonances with appropriate integrations for incorporation of the Re^{V}O center into the belt region of the α_1-$P_2W_{17}O_{61}^{10-}$ lacunary polyoxometalate. There are 17 signals with similar integration because α_1-$P_2W_{17}O_{61}^{10-}$ is C_1 symmetry (Figure **5-1**) so that all W atoms are inequivalent. The pattern observed in Figure **5-9** is clearly different from the Tc^{V}O(α_1-$P_2W_{17}O_{61}$)$^{7-}$ species in Figure **5-10**, [32] and from free α_1-$P_2W_{17}O_{61}^{10-}$ ligands. [33] We can not assign each signal to specific tungsten atoms.

However, the upfield resonance is likely attributed to a W atom close to the vacancy. With 16 resonances, the ^{183}W NMR spectra of $[\alpha 1\text{-}Re^{V}O\ P_2W_{17}O_{61}]^{6-}$ TBA salt (CD_3CN) salt is very similar to $[\alpha 1\text{-}Re^{V}O\ P_2W_{17}O_{61}]^{6-}$ Potassium salt, but its quality is not as good (Figure **5-11**).

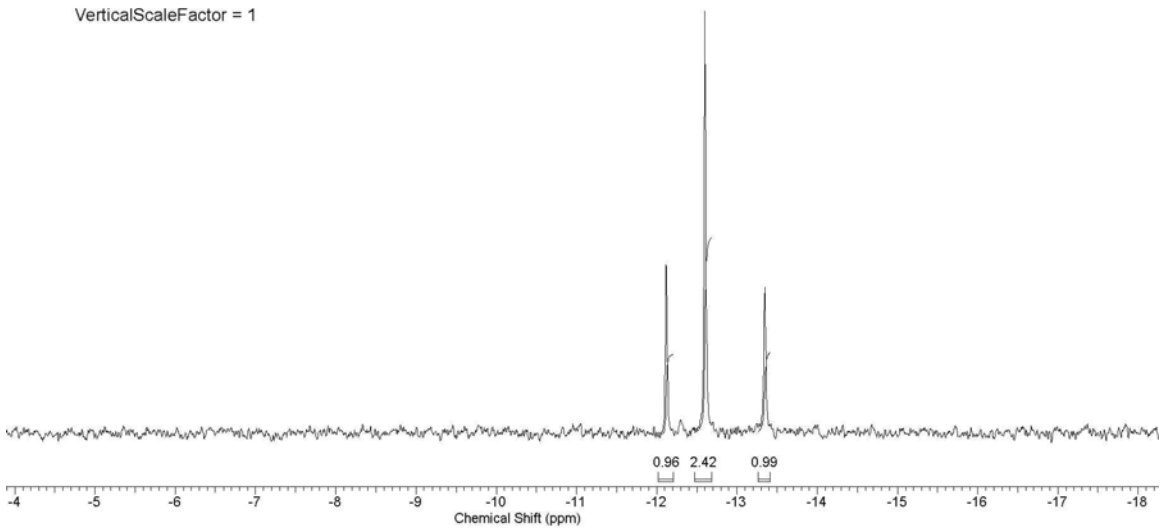

Figure **5-8** ^{31}P NMR of $[\alpha 1\text{-}Re^{V}O\ P_2W_{17}O_{61}]^{6-}$ TBA salt. This shows a significant $\alpha_1\text{-}P_2W_{18}O_{62}^{6-}$ impurity.

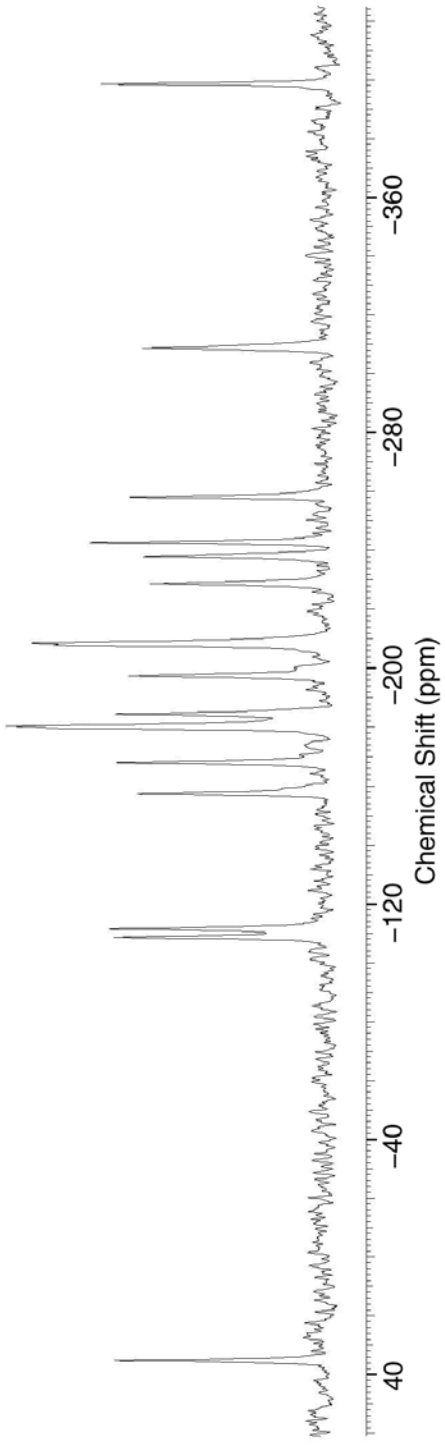

Figure **5-9** ^{183}W NMR of $[\alpha 1\text{-}Re^{V}O\ P_2W_{17}O_{61}\ ]^{6-}$ Potassium salt

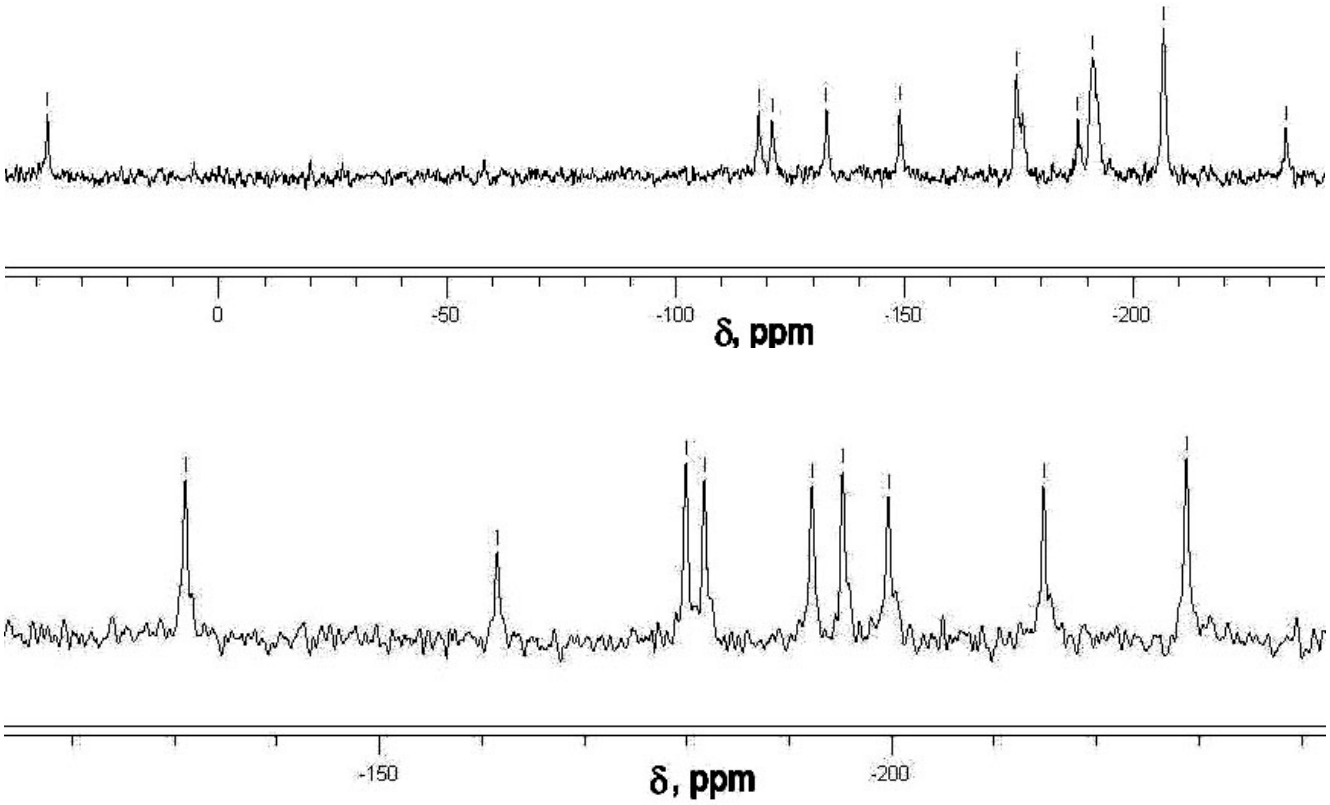

Figure **5-10** ^{183}W NMR of [α1-Tc^{V}O $P_2W_{17}O_{61}$]$^{6-}$ (top) and [α1-Tc^{V}O $P_2W_{17}O_{61}$]$^{6-}$ (bottom) in D_2O

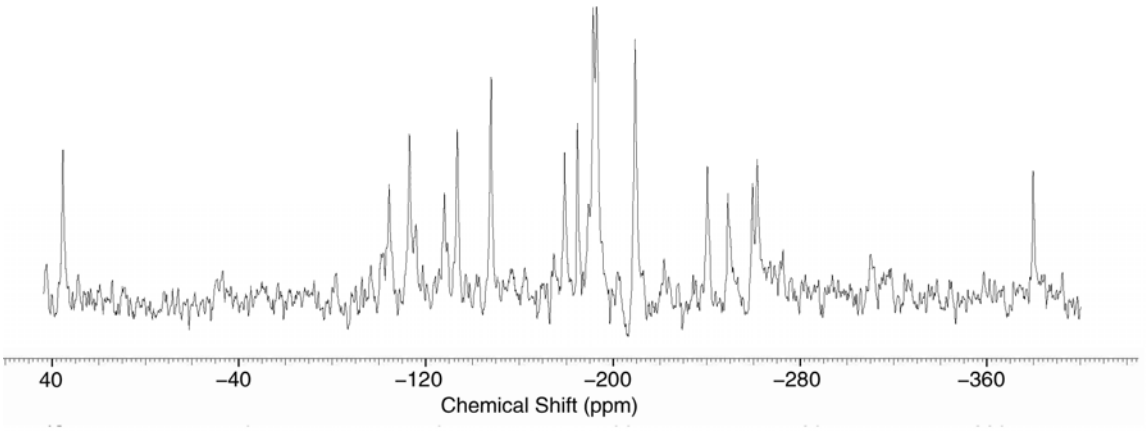

Figure **5-11** ^{183}W NMR of [α1-$Re^{V}O$ $P_2W_{17}O_{61}$]$^{6-}$ TBA salt

5.3.3 Crystal Structure and CV of [α-1-$Re^{V}O$ $P_2W_{17}O_{61}$]

The organic soluble TBA_5 H_2 [α-1-$Re^{V}O$ $P_2W_{17}O_{61}$] was made by a metathesis method and crystallized from CH_3CN solvent. In the crystal structure shown in Figure **5-12**, we can not tell the difference between W and Re atoms because rhenium and tungsten are next to each other on the periodic table. The model used is that the Re atom delocalizes on 11 tungsten atoms. In each unit there are one α-1-$Re^{V}O$ $P_2W_{17}O_{61}$ POM unit, five tetra-butylammonium ions and four CH_3CN solvent molecules.

Electrochemistry of the aqueous soluble K_7[α-1- $Re^{V}O$ $P_2W_{17}O_{61}$] compound were conducted at a concentration of 0.2mM in pH=5 buffer (0.5 M Na_2SO_4 in 0.01 M NaOAc). The working electrode is glassy carbon, the auxiliary was platinum wire and the reference was Ag/AgCl. All spectra present were ran at a scan rate of 10 mV/S.

We did the comparison between $K_7[\alpha\text{-}1\text{-}Re^{V}O\ P_2W_{17}O_{61}]$ and $K_7[\alpha\text{-}1\text{-}Tc^{V}O\ P_2W_{17}O_{61}]$ CV spectra in Figure **5-13** . The Re (V/VI) wave occurs at c.a. 420 mV and The Tc (V/VI) wave occurs at c.a. 1 V, with a 600 mV difference. This showed that ReO(V) is much easier to be oxidized than TcO(V) center. From CV we also know that $K_7[\alpha\text{-}1\text{-}Re^{V}O\ P_2W_{17}O_{61}]$ sample is not pure because its curve is not as smooth as $K_7[\alpha\text{-}1\text{-}Tc^{V}O\ P_2W_{17}O_{61}]$ in the 0 mv to 400 mv area. There are signals attribute to K_6 ($\alpha\text{-}P_2W_{18}O_{62}$) impurity.

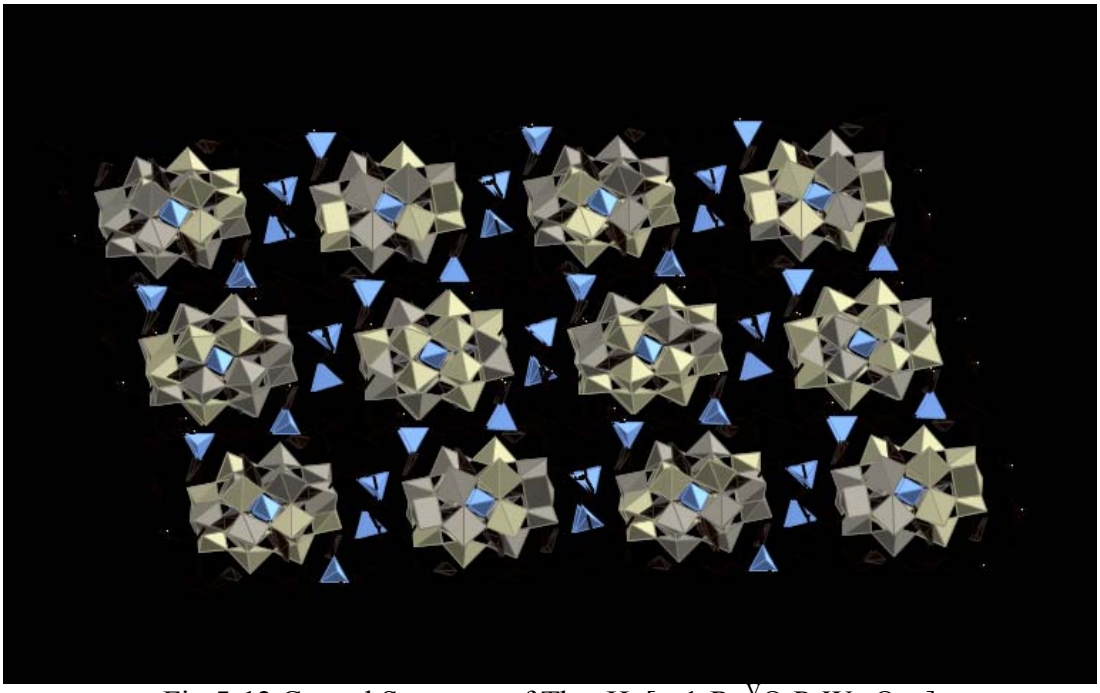

Fig **5-12** Crystal Structure of $Tba_5H_4[\alpha\text{-}1\text{-}Re^{V}O\ P_2W_{17}O_{61}]$

Table 5-1 Selected crystallographic data for compound 11

	11
Empirical Formula	$(CH_3CN)_4[(C_4H_9)_4N]_5ReOP_2W_{17}O_{61}$
MW	5560.57
Crystal System	Monoclinic
Space Group	C2yc
a / Å	25.957(5)
b / Å	15.445(3)
c / Å	36.085(7)
α / º	90
β / º	105.77(3)
ɣ / º	90
V / $Å^3$	13922(5)
Z	4
Crystal Size / mm	0.46×0.30×0.16
R indices [I >2 σ (I)]	R1 = 0.0809
	wR2 = 0.2071
Final R (all data)	R1 = 0.0743
	wR2 = 0.2015

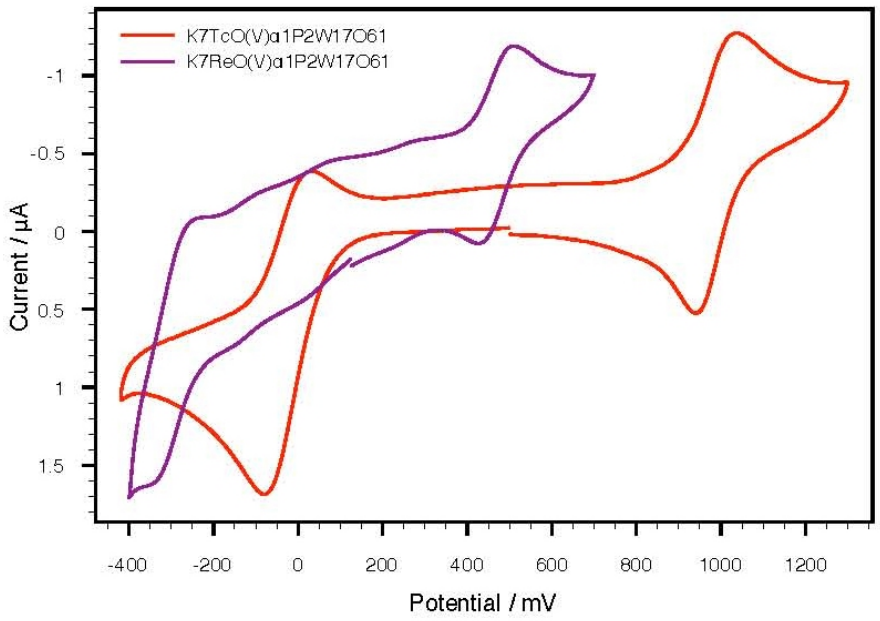

Figure **5-13** Compare $K_7[\alpha\text{-}1\text{-}\ Re^{V}O\ P_2W_{17}O_{61}]$ and $K_7[\alpha\text{-}1\text{-}\ Tc^{V}O\ P_2W_{17}O_{61}]$

5.4 Conclusion

Rhenium derivative of $[\alpha\text{-}\ AlW_{11}O_{39}]$ POM **10** was synthesized and studied its ^{27}Al NMR characterization was accomplished. We also reported that it is easy to be oxidized by oxygen and form nano particles. We also did synthesis and characterization of $[Re^{V}O(\alpha_1\text{-}P_2W_{17}O_{61})]^{7-}$. We studied the ^{31}P and ^{183}W NMR of $[Re^{V}O(\alpha_1\text{-}P_2W_{17}O_{61})]$ **11**. We also reported the crystal structure of organic soluble $TBA_5H_2[Re^{V}O(\alpha_1\text{-}P_2W_{17}O_{61})]$ **11**.

5.5 Reference

[1] H. Moseley, *Philosophical Magazine*, **1914**, 703–713.

[2] W. Noddack, I. Tacke, O. Berg, *Naturwissenschaften*, **1925**, **13** (26): 567–574

[3] W. Noddack, I. Noddack,,*Zeitschrift für anorganische und allgemeine Chemie*, **1929**, 183 (1): 353–375.

[4] H. Bhadeshia, *Nickel Based Superalloys*, University of Cambridge.

[5] B. Cantor, P. Grant, *Aerospace Materials: An Oxford-Kobe Materials Text*. CRC Press., 2001, 82–83.

[6] M. Ryashentseva, *Russian Chemical Reviews*, 1998, **67**: 157–177.

[7] J. Mol, *Catalysis Today*, **1999**, 51 (2), 289–299.

[8] T. Angelidis, D. Rosopoulou, V. Tzitzios, *Ind. Eng. Chem. Res.* **1999**, 38 (5): 1830–1836.

[9] a. J. Dilworth, S. Parrott. *Chemical Society Reviews*, **1998**, 27: 43–55.

b. P. Dyson and G. Sava, *Dalton Trans*, **2006**, 1929-1933

[10] R. Colton, R. Peacock, *Quarterly Reviews Chemical Society* , **1962**, 16, 299–315.

[11] V. Day, W. Klemperer, *Science* **1985**, *228*, 533-541.

[12] N. Leclerc-Laronze, M. Haouas, J. Marrot, F. Taulelle, G. Herve, *Angew. Chem. Int. Ed.* **2006**, *45*, 139-142.

[13] X. Fang, C. Hill, *Angew. Chem. Int. Ed.* **2007**, *46*, 3877-3880.

[14] V. Day, W. Klemperer, C. Schwartz, R. Wang, *Surface Organometallic Chemistry: Molecular Approaches to Surface Catalysis*; Kluwer Academic Publishers: New York, **1988**, 173.

[15] D. Long, E. Burkholder, L. Cronin, *Chem. Soc. Rev.* **2007**, *36*, 105-121.

[16] M. Abbessi, R. Contant, R. Thouvenot, G. Herve, *Inorg. Chem.* **1991**, *30*, 1695-1702.

[17) C. Zhang, R. Howell, Q. Luo, H. Fieselmann, L. Todaro, L. Francesconi, *Inorg. Chem.* **2005**, *44*, 3569-3578.

[18] C. Boglio, G. Lenoble, C. Duhayon, B. Hasenknopf, R. Thouvenot, C. Zhang, R. Howell, B. Burton-Pye, L. Francesconi, E. Lacote, S. Thorimbert, M. Malacria, C. Afonso, J. Tabet, *Inorg. Chem.* **2006**, *45*, 1389-1398.

[19] M. Kozik, C. Hammer, L. Baker, *J. Am. Chem. Soc.* **1986**, *108*, 2748-2749.

[20] M. Kozik, L. Baker, *J. Am. Chem. Soc.* **1990**, *112*, 7604-7611.

[21] R. Acerete, S. Harmalker, C. Hammer, M. Pope, L. Baker, , *J. C. S. Chem. Commun.* **1979**, 777-9.

[22] J. Ciabrini, R. Contant, J. Fruchart, *Polyhedron* **1983**, *2*, 1229-33.

[23] X. Lopez, C. Bo, J. Poblet, *J.Am. Chem. Soc.* **2002**, *124*, 12574-12582.

[24] B. Keita, B. Levy, L. Nadjo, R. Contant, *New. J. Chem.* **2002**, *26*, 1314-1319.

[25] R. Contant, G. Herve, *Reviews in Inorganic Chemistry* **2002**, *22*, 63-111.

[26] J. VanderHeyden, M. Heeg, E. Deutsch, *Inorganic Chemistry* **1985**, *24*, 1666-1673.

[27] K. Libson, M. Woods, J. Sullivan, J. Watkins II, R. Elder, E. Deutsch, *Inorganic Chemistry* **1988**, *27*, 999-1003.

[28] E. Deutsch, K. Libson, J. Vanderheyden, *The inorganic chemistry of technetium and rhenium as relevant to nuclear medicine*Cortina International: Verona, **1990**; Vol. 3.

[29] *SHELXTL*, Brucker AXS, Inc., Bruker Advanced X-ray Solutions, **1999**

[30] R. Contant, R. *Inorg. Synth.* **1990**, *27*, 71-111.

[31] J. Bartis, S. Sukal, M. Dankova, E. Kraft, R. Kronzon, M. Blumenstein, L. Francesconi, *J. Chem. Soc., Dalton Trans,* **1997**, 1937-1944.

[32] J. Cowan, C. Hill; R. Reiner and I. Weinstock, Inorg. Synth Vol 33.

[33] From Donna, Ben and Fang's pending paper

[34] J. Bartis, Y. Kunina, M. Blumenstein, L. Francesconi, *Inorg. Chem.* **1996**, *35*, 1497-1501.

REFERENCES

Chapter 1

[1] R. Kurzweil**,** *Exponential Growth of Computing for 110 Years*, From http://www.kurzweilai.net/exponential-growth-of-computing

[2] Indiana University (**2000**, March 27). Several New Single-Molecule Magnets Discovered. *ScienceDaily*. Retrieved March 16, 2011, from http://www.sciencedaily.com/releases/2000/03/000327084104.htm

[3] B. Xu, X. Xiao, X. Yang, L. Zang, and N. Tao; *J. Am. Chem. Soc.*, **2005**, 127 (8), 2386–2387

[4] L. Brousseau, III, *J. Am. Chem. Soc.*, **2006**, 128 (35), pp 11346–11347

[5] P. Solomon and N. Lang, *ACS Nano*, **2008**, 2 (3), pp 435–440

[6] H. Li, X. Yan, G. Luo, R. Qin, Q. Liu, L. Yu, C. Xu, J. Zheng, J. Zhou, J. Lu, Z. Gao, S. Nagase, and W. Mei, *J. Phys. Chem. C*, **2010**, 114 (37), 15816–15822

[7] S. Klokishner, S. Ostrovsky, O. Reu and A. Palii, P. Tregenna-Piggott, T. Brock-Nannestad and J. Bendix, H. Mutka, *J. Phys. Chem. C*, **2009**, *113* (20), 8573–8582

[8] K. Stokbro, *J. Phys. Chem. C*, **2010**, 114 (48), 20461–20465

[9] T. Lis, *Acta Crystallogr.* **1980**, B36, 2042

[10] A. Caneschi, D. Gatteschi, R. Sessoli, A. Barra, L. Brunel, M. Guillot, *J. Am. Chem. Soc.*, **1991**, 113(15), 5873-5874.

[11] S. Aubin,.; M. Wemple; D. Adams,; H. Tsai; G. Christou; D. Hendrickson, *J. Am. Chem. Soc.*,**1996**, 118(33), 7746-7754.

[12] L., Beltran; J. Long, *Acc. Chem. Res.*, **2005**, 38(4); 325-334.

[13] S. Aubin, D. Hendrickson, S. Spagna, H. Eppley, R. Sager, H. Eppley, G. Christou, *Chem. Commun.*, **1998**, (7),803-804

[14] M. Soler, P. Artus, K. Folting, J. Huffman, D. Hendrickson, G. Christou, *Inorg. Chem.*, **2001**, 40(**19**), 4902-4912.

[15] R. Sessoli, H. Tsai, A. Schake, S. Wang, J. Vincent, K. Folting, D. Gatteschi, G. Christou, D. Hendrickson, *J. Am. Chem. Soc.* **1993**, *115*, 1804

[16] M. Pope, A. Muller, *Polyoxometalates: From Platonic solid to Anti-Retroviral Activity*; Kluwer Academic Publishers: Dordrecht, The Nederlands, **1994**.

[17] M. Sadakane, M. Dickman, M. Pope, Angew. Chem. Int. Ed. **2000**, 39, No.16 2914

[18] P. Mialane, L. Lisnard, A. Mallard, J. Marrot, E. Antic-Fidancev, P. Aschehoug, D. Vivien, and F. Sécheresse, Inorg Chem. **2003**, 42, 2102-2108

[19] T. Yamase, M. Pope, *Polyoxometalate Chemistry for Nano-Composite Design*; Kluwer: Academic Publishers: Dordrecht, The Netherlands, **2002**

[20] R. Peacock and T. Weakley, *J. Chem. Soc. A***, 1971**, 1836 - 1839

[21] J. Wang, J. Zhao, X. Duan, and J. Niu, *Crystal Growth & Design*, **2006**, vol.6, No. 2, 507-513

[22] F. Li, L. Xu, Y. Wei, G. Gao, L. Fan, Z. Li, *Inorg Chim Acta,* 359, 3795

[23] J. Wang, X. Duan, X. Du, and J. Niu, *Crystal Growth & Design*, **2006**, vol6, No. 2, 2266-2270

[24] J. Cowan, A. Bailey, R. Heintz, B. Do, K. Hardcastle, C. Hill, and I. Weinstock, *Inorg. Chem.,* **40** (26), 6666 -6675, 2001

[25] E. Coronado, A. Forment-Aliaga, F. Romero, V. Corradini, R. Biagi, V. Renzi, A. Gambardella, U. Pennino, *Inorg. Chem.*; (Communication); **2005**; 44(22); 7693-7695.

[26] R. Robson; B. Abrahams, S. Batten, R. Gable, B. Hoskins, J. Liu, *ACS Symp. Ser.* **1992**, *499*, 256−273.

[27] B. Abrahams, B, Hoskins, R. Robson, *J. Am. Chem. Soc.* **1991**, *113*, 3606−3607.

[28] M. Fujita, Y. Kwon, S. Washizu, K. Ogura, *Am. Chem. Soc.* **1994**, *116*, 1151−1152.

[29] B. Abrahams, B. Hoskins, J. Liu, R. Robson, *J. Am. Chem. Soc.* **1991**, *113*, 3045−3051.

[30] S. Batten, B. Hoskins, R. Robson, *Chem. Commun.* **1991**, 445−447.

[31] R. Gable, B. Hoskins, R. Robson, *Chem. Commun.* **1990**, 762−763.

[32] B. Hoskins, R. Robson, *J. Am. Chem. Soc.* **1990**, *112*, 1546−1554.

[33] B. Abrahams, B. Hoskins, R. Robson, *Chem. Commun.* **1990**, 60−61.

[34] B. Moulton and M. Zaworotko, *Chem. Rev.*, **2001**, 101 (**6**), 1629–1658

[35] X. Kong, Y. Ren, P. Zheng, Y. Long, L. Long, R. Huang, L. Zheng, *Inorg. Chem.*; **2006**; 45(26); 10702-10711.

[36] C. Zhang, R. Howell, K. Scotland, F. Perez, L. Todaro, and L. Francesconi, *Inorg. Chem.*, **2004**, 43 (24), pp 7691–7701

[37] S. Liu, H. Möhwald, D. Volkmer, and D. Kurth, *Langmuir*, **2006**, 22 (5), 1949–1951

[38] S. Liu and Z. Tang, *Nanotoday* Volume 5, Issue 4, August **2010**, 267-281

Chapter 2

[1] N. Greenwood; A. Earnshaw., **1997**. *Chemistry of the Elements*, 2nd Edition, Oxford:Butterworth-Heinemann. ISBN 0-7506-3365-4

[2] A. Searle, **1913**, *the Silicates in Chemistry and Commerce*

[3] G. Kauffman, *Coordination Chemistry A Century of Progress*, **1994**, Volume 565

[4] J. Bailar, Jr. *The Chemistry of the Coordination Compounds,* Reinhold Publishing Corporation, **1956**, 472-482

[5] L. Baker, J. Figgis, *J.Am. Chem. Soc*, **1970**, 92(12), 3794-3797

[6] N. Greenwood; A. Earnshaw, **1997**, *Chemistry of the Elements* (2nd ed.), Oxford: Butterworth-Heinemann, ISBN 0080379419

[7] S. Bradley, R. Kydd and R. Yamdagni *J. Chem. Soc., Dalton Trans.*, **1990**, 413 – 417

[8] J. Cowan, A. Bailey, R. Heintz, B. Do, K Hardcastle, C. Hill, and I. Weinstock, *Inorg. Chem.*, **2001**, 40 (26), 6666–6675

[9] D. Smith and M. Pope, Inorg. Chem. 12, 331 (1973).

[10] I. Weinstock, R. Atalla, R. Reiner, M. Moen, K. Hammel, C. Hill, and M. Harrup, *J. Mol. Catal. A, Chemical*, **116**, 59 (1997).

[11] M. Sadakane and E. Steckhan, *Chem. Rev.*, **1998**, 98 (1), pp 219–238

[12] B. Keita, L. Nadjo, *J. Electroanal. Chem*. **1987**, *217*, 287

[13] Y. Geletii, C. Hill, A. Bailey, K. Hardcastle, R. Atalla, and I. Weinstock, *Inorg. Chem.*, 2005, 44 (24), pp 8955–8966

[14] S. Liu, D. Kurth, H. Mohwald, D. Volkmer, *Adv. Mater.* **2002**, 14, 225.

[15] SHELXTL,Brucker AXS, Inc., Bruker Advanced X-ray Solutions, **1999**

[16] J. Mason, *Multinuclear NMR*, 1987

[17] N. Nuraje, K.Su, A. Haboosheh, J. Samson, *et al.*, *Adv. Mater.* 2006, *18*, 807.

[18] N. Nuraje, S. Mohammed, L. Yang, Matsui, H., *Angew. Chem. Int. Ed.* 2009, *121*, 1.

Chapter 3

[1] D. Parker, R. Dickins, H. Puschmann, C. Crossland, and J. Howard, *Chem. Rev.*, **2002**, 102 (6), 1977–2010

[2] J. Kido and Y. Okamoto, *Chem. Rev.*, **2002**, 102 (6), 2357–2368

[3] T. Yamase, and H. Naruke, *Coordination Chemistry Reviews*, Vol. 111, **1991**, 83-90

[4] J. Bünzli and C. Piguet, *Chem. Rev.*, **2002**, 102 (6), 1897–1928

[5] U. Kortz, A. Müller, J. Slageren, J. Schnack, N. Dalal and M. Dressel, *Coordination Chemistry Reviews*, Vol. 253, Issues 19-20, **2009**, 2315-2327

[6] T. Akutagawa, D. Endo, S. Noro, L. Cronin and T. Nakamura, *Coordination Chemistry Reviews*, Vol 251, Issues 21-24, **2007**, 2547-2561

[7] N. Kaltsoyannis, P. Scott, *The f-Elements*; Oxford University, **1999**.

[8] M. Drew, *Coord. Chem. Rev.* **1977**, *24*, 179.

[9] J. Cowan, A. Bailey, R. Heintz, B. Do, K. Hardcastle, C. Hill, and I. Weinstock, *Inorg. Chem.,* **2001**, 40 (26), 6666 -6675.

[10] P. Mialane, L. Lisnard, A. Mallard, J. Marrot, E. Antic-Fidancev, P. Aschehoug, D. Vivien, and F. Sécheresse, *Inorg Chem.* **2003**, 42, 2102-2108

[11] M. Sadakane, M. Dickman, M. Pope, *Angrew. Chem. Int. Ed*. **2000**, 39, No.16 2914

[12] J. Wang, J. Zhao, X. Duan, and J. Niu, *Crystal Growth & Design*, **2006**, Vol. 6, No. 2, 507-513

[13] F. Li, L. Xu, Y. Wei, G.Gao, L. Fan, Z. Li, *Inorg. Chim Acta.,* 359, 3795

[14] J, Wang, X, Duan, X, Du, and J, Niu, *Crystal Growth & Design*, **2006**, Vol. 6, No. 2, 2266-2270

[15] J. Cowan; C. Hill; R. Reiner and I. Weinstock., *Inorg. Synth*, Vol. 33

[16] *SHELXTL*, Brucker AXS, Inc., Bruker Advanced X-ray Solutions, **1999**

[17] J. Mason, *Multinuclear NMR*, **1987**

[18] M. Zimmermann , N. Frøystein, A. Fischbach, P. Sirsch, H. Dietrich, K. Törnroos, E. Herdtweck, R. Anwander, *Chem. Eur. J.* **2007**, 13, 8784-8800

[19] C. Zhang, R. Howell, K. Scotland, F. Perez, L. Todaro, L. Francesconi, *Inorg Chem.* **2004**. 43, 7691-7701

[20] T. Yamase, M. Pope, *Polyoxometalate Chemistry for Nano-Composite Design*; Kluwer: Academic Publishers: Dordrecht, The Netherlands, **2002**.

[21] B. Moulton and M. Zaworotko *Chem. Rev.*, **2001**, 101 (6),1629–1658,

Chapter 4

[1] http://itpro.nikkeibp.co.jp/members/NBY/techsquare/20030724/1

[2] http://www.geek.com/articles/chips/samsung-squeezes-667gb-per-platter-on-2tb-ecogreen-drive-2010084/

[3] Z. Bandić, E. Dobisz, T, Wu, T. Albrecht, *Solid State Technology Magazine*, **2006**, 9

[4] J. Gittleman, B. Abeles, and S. Bozowski, *Phys. Rev. B* **9**, **1974**, 3891–3897

[5] M. Kryder, *Magnetics Conference, 2000. INTERMAG 2000 Digest of Technical Papers. 2000 IEEE International* , 575–575

[6] M. Sadakane and E. Steckhan *Chem. Rev.*, **1998**, 98 (1), pp 219–238

[7] Y. Geletii, C. Hill, A. Bailey, K. Hardcastle, R. Atalla, and I. Weinstock, *Inorganic Chemistry,* **2005** *44* (24), 8955-8966

[8] B. Keita, L. Nadjo, *Electroanal. Chem*. **1985**, 191, 441.

[9] B. Keita, L. Nadjo, *J. Electroanal. Chem.* **1987**, 217, 287.

[10] B. Keita, L. Nadjo, *J. Electroanal. Chem.* **1987**, 227, 77.

[11] S. Liu, H. Möhwald, D. Volkmer, and D. G. Kurth, *Langmuir*, **2006**, 22 (5), pp 1949–1951

[12] S. Liu and Z. Tang, *nanotoday* Vol. 5, Issue 4, **2010**, 267-281

[13] M. Rindel, *African J. Sci.* **11** (1916), 362.

[14] C. Chang, K. Sun, S. Lee and L. Kan, *Biomaterials* Volume 28, Issue 11, April **2007**, 1941-1947

[15] T.. Niederhauser, Y. Lua, G. Jiang, S. Davis, D. Hess and M. Linford, *Angew Chem Int Ed*, 41 (2002), 2353–2356.

[16] Y. Lua, T. Niederhauser, B. Wacaser, I. Mowat, A. Woolley and R. Davis et al., *Langmuir,* **2002**, 18, 4840–4846.

[17] H. Bai, K. Xu, Y. Xu, H. Matsui, *Angew. Chem. Int. Ed.* **2007**, *46*, 3319.

[18] H. Bai, F. Xu, L. Anjia, H. Matsui, *Soft Matter* **2009**, *5*, 966.

Chapter 5

[1] H. Moseley, *Philosophical Magazine*, **1914**, 703–713.

[2] W. Noddack, I. Tacke, O. Berg, *Naturwissenschaften*, **1925**, **13** (26): 567–574

[3] W. Noddack, I. Noddack,,*Zeitschrift für anorganische und allgemeine Chemie*, **1929**, 183 (1): 353–375.

[4] H. Bhadeshia, *Nickel Based Superalloys*, University of Cambridge.

[5] B. Cantor, P. Grant, *Aerospace Materials: An Oxford-Kobe Materials Text*. CRC Press., 2001, 82–83.

[6] M. Ryashentseva, *Russian Chemical Reviews*, 1998, **67**: 157–177.

[7] J. Mol, *Catalysis Today*, **1999**, 51 (2), 289–299.

[8] T. Angelidis, D. Rosopoulou, V. Tzitzios, *Ind. Eng. Chem. Res.* **1999**, 38 (5): 1830–1836.

[9] a. J. Dilworth, S. Parrott. *Chemical Society Reviews*, **1998**, 27: 43–55.

b. P. Dyson and G. Sava, *Dalton Trans*, **2006**, 1929-1933

[10] R. Colton, R. Peacock, *Quarterly Reviews Chemical Society* , **1962**, 16, 299–315.

[11] V. Day, W. Klemperer, *Science* **1985**, *228*, 533-541.

[12] N. Leclerc-Laronze, M. Haouas, J. Marrot, F. Taulelle, G. Herve, *Angew. Chem. Int. Ed.* **2006**, *45*, 139-142.

[13] X. Fang, C. Hill, *Angew. Chem. Int. Ed.* **2007**, *46*, 3877-3880.

[14] V. Day, W. Klemperer, C. Schwartz, R. Wang, *Surface Organometallic Chemistry: Molecular Approaches to Surface Catalysis*; Kluwer Academic Publishers: New York, **1988**, 173.

[15] D. Long, E. Burkholder, L. Cronin, *Chem. Soc. Rev.* **2007**, *36*, 105-121.

[16] M. Abbessi, R. Contant, R. Thouvenot, G. Herve, *Inorg. Chem.* **1991**, *30*, 1695-1702.

[17) C. Zhang, R. Howell, Q. Luo, H. Fieselmann, L. Todaro, L. Francesconi, *Inorg. Chem.* **2005**, *44*, 3569-3578.

[18] C. Boglio, G. Lenoble, C. Duhayon, B. Hasenknopf, R. Thouvenot, C. Zhang, R. Howell, B. Burton-Pye, L. Francesconi, E. Lacote, S. Thorimbert, M. Malacria, C. Afonso, J. Tabet, *Inorg. Chem.* **2006**, *45*, 1389-1398.

[19] M. Kozik, C. Hammer, L. Baker, *J. Am. Chem. Soc.* **1986**, *108*, 2748-2749.

[20] M. Kozik, L. Baker, *J. Am. Chem. Soc.* **1990**, *112*, 7604-7611.

[21] R. Acerete, S. Harmalker, C. Hammer, M. Pope, L. Baker, , *J. C. S. Chem. Commun.* **1979**, 777-9.

[22] J. Ciabrini, R. Contant, J. Fruchart, *Polyhedron* **1983**, *2*, 1229-33.

[23] X. Lopez, C. Bo, J. Poblet, *J.Am. Chem. Soc.* **2002**, *124*, 12574-12582.

[24] B. Keita, B. Levy, L. Nadjo, R. Contant, *New. J. Chem.* **2002**, *26*, 1314-1319.

[25] R. Contant, G. Herve, *Reviews in Inorganic Chemistry* **2002**, *22*, 63-111.

[26] J. VanderHeyden, M. Heeg, E. Deutsch, *Inorganic Chemistry* **1985**, *24*, 1666-1673.

[27] K. Libson, M. Woods, J. Sullivan, J. Watkins II, R. Elder, E. Deutsch, *Inorganic Chemistry* **1988**, *27*, 999-1003.

[28] E. Deutsch, K. Libson, J. Vanderheyden, *The inorganic chemistry of technetium and rhenium as relevant to nuclear medicine*Cortina International: Verona, **1990**; Vol. 3.

[29] *SHELXTL*, Brucker AXS, Inc., Bruker Advanced X-ray Solutions, **1999**

[30] R. Contant, R. *Inorg. Synth.* **1990**, *27*, 71-111.

[31] J. Bartis, S. Sukal, M. Dankova, E. Kraft, R. Kronzon, M. Blumenstein, L. Francesconi, *J. Chem. Soc., Dalton Trans,* **1997**, 1937-1944.

[32] J. Cowan, C. Hill; R. Reiner and I. Weinstock, Inorg. Synth Vol 33.

[33] From Donna, Ben and Fang's pending paper

[34] J. Bartis, Y. Kunina, M. Blumenstein, L. Francesconi, *Inorg. Chem.* **1996**, *35*, 1497-1501.